

# Sheffield Hallam University

*The morphological characterisation of grains and grain boundaries.*

MUIRHEAD, John J.

Available from the Sheffield Hallam University Research Archive (SHURA) at:

<http://shura.shu.ac.uk/20099/>

## A Sheffield Hallam University thesis

This thesis is protected by copyright which belongs to the author.

The content must not be changed in any way or sold commercially in any format or medium without the formal permission of the author.

When referring to this work, full bibliographic details including the author, title, awarding institution and date of the thesis must be given.

Please visit <http://shura.shu.ac.uk/20099/> and <http://shura.shu.ac.uk/information.html> for further details about copyright and re-use permissions.

CITY CAMPUS, HOWARD STREET  
SHEFFIELD S1 1WB



19773

**REFERENCE**

ProQuest Number: 10697406

All rights reserved

INFORMATION TO ALL USERS

The quality of this reproduction is dependent upon the quality of the copy submitted.

In the unlikely event that the author did not send a complete manuscript and there are missing pages, these will be noted. Also, if material had to be removed, a note will indicate the deletion.



ProQuest 10697406

Published by ProQuest LLC (2017). Copyright of the Dissertation is held by the Author.

All rights reserved.

This work is protected against unauthorized copying under Title 17, United States Code  
Microform Edition © ProQuest LLC.

ProQuest LLC.  
789 East Eisenhower Parkway  
P.O. Box 1346  
Ann Arbor, MI 48106 – 1346

The Morphological Characterisation of Grains and  
Grain Boundaries

John Muirhead

A thesis submitted in partial fulfilment of the  
requirement of Sheffield Hallam University for the  
degree of Doctor of Philosophy

July 2001



## Declaration

The work described in this thesis was carried out by the author in the Materials Research Institute, Sheffield Hallam University, between October 1997 and October 2000. The author declares that this work has not been submitted for any other degree. The work is original except where acknowledged by reference.

Author:

John Muirhead

Supervisor:

Dr. Jess Cawley

## Abstract

It is well reported that the grain size of polycrystalline materials is important in determining mechanical properties. Within this thesis investigations are reported from an inter-comparison of grain size methods, the impact of an incomplete network of grain boundaries after chemical etching (missing boundaries) on grain size measurements and finally the relationship between grain size and the misorientation of grains. The experimental techniques used are manual grain size measurement methods, automatic image analysis and Electron Backscatter Diffraction (EBSD). The materials used are a ferritic, single phased, equi-axed steel (mild steel) and a ferrite/pearlite steel. The relative simplicity of the mild steel microstructure effectively removes complicating factors such as multi-phases or grain elongation allowing a more focused investigation into grain size methods. The ferrite/pearlite steel can be found more readily in industrial applications where impact toughness is an important property. Manual measurement methods and automatic image analysis are used for the inter-comparison of grain size methods. The manual methods are described in the standard ASTM E112, and are the lineal, planimetric, single circle and three circle methods. It is shown that there is a difference across the methods in the number of measurements required to obtain a specified accuracy. Also that sampling is critical to ensure that the measurements made are representative of the microstructure in that it is more important to measure more specimens than more fields of view within one specimen or many grains within one field of view. Automatic image analysis can provide a substantial database and thus is a useful grain sizing method. It is demonstrated that the number of pixels in a digital image forming a grain boundary, determined by the pixel resolution, will influence the measurements. Also from using digital images a specific number of grain boundaries are removed thus artificially creating missing boundaries making their impact on grain size measurements quantifiable. Manual and automatic measurements are conducted and it is shown that the mean grain size is relatively less affected by missing boundaries than might be perceived from a visual inspection. An EBSD map provides a complete network of grain boundaries since a boundary is formed from the orientation of one grain to another (misorientation), compared to standard metallographic techniques, e.g. chemical etching. EBSD maps are compared with optical images of the same fields of view and missing boundaries are then located. From this it is shown that there is a significant difference between two operators in determining the location of boundaries. EBSD is also used to investigate the correlation between the location of missing boundaries and the misorientation of the grains at that boundary and shows a trend of higher misorientation for boundaries not chemically etched up. The final section of this thesis is concerned with the relationship between the misorientation of small/small, small/large and large/large grains and the size of grains of the ferrite phase from the ferrite/pearlite steel. EBSD maps provide the misorientation data and are also used for grain sizing conducted on the automatic image analysis system. From the misorientation data the boundaries can be categorised as low or high angle and it is found that there are more low angle boundaries between small/small grains and small/large grains than between large/large grains.

This work is dedicated to my girlfriend Rebecca Metcalfe and to my parents  
John and Rita Muirhead

## ACKNOWLEDGEMENTS

To my supervisory team, Dr Jess Cawley, Dr Colin English, Prof John Titchmarsh and Prof Andrew Strang, I would like to extend my gratitude for allowing me to tap into their wisdom. I would particularly like to acknowledge the support, unfaltering advice and constant concern to get me through this PhD from Jess, my director of studies. Also to Colin, my first industrial supervisor, for his encouragement and for showing confidence in me.

Steve Porter, once a technician at Sheffield Hallam University who played an important part in creating this thesis, was a friend with an invaluable level head at times of 'crisis' and a great many thanks go to him. To the rest of the technicians, Paul Slingsby and Cheryl Shaw and the IT manager Terry Hudson, thanks for the support and good sense of humour.

A special thanks go to my parents, for once again backing me up 100% for what I want to do, for pushing me to the end and especially for always being there to listen. To the rest of my family I thank for their encouragement and for helping me to enjoy the good times.

Last but by no means least I would like to acknowledge the constant support and love of my girlfriend, Bex, for making the 'downs' 'ups' and especially for her unique ability to 'gently' persuade me to keep going and get this thesis finished.

## Table of contents

<u>1.INTRODUCTION</u>	<u>1</u>
1.1.General introduction	1
1.2.The nature of polycrystalline materials	2
1.3.The objectives of the programme	3
1.4.The experimental approach	5
1.4.1. Specimen preparation	5
1.4.2. Manual methods.	6
1.4.3. Automatic image analysis.	6
1.4.4. Electron Back Scatter Diffraction	7
<u>2.LITERATURE SURVEY</u>	<u>8</u>
2.1.Introduction	8
2.2.Microscopy	8
2.2.1. Automatic image analysis	8
2.2.2. Electron Backscattered Diffraction	11
2.2.2.1.Introduction	11
2.2.2.2.A description of the technique	13
2.2.2.3.Resolution	14
2.2.2.4.Lattice strain	18
2.2.2.5.Further limitations of EBSD	19
2.2.2.6.A comparison of other techniques	20
2.3.The nature of polycrystalline materials	23
2.3.1. Complex microstructures	23
2.3.1.1.Introduction	23
2.3.2. Grain boundaries	23
2.3.2.3.Coincident site lattice	24
2.3.2.4.The influence of grain boundaries on microstructure	25
2.3.2.5.High and low angle boundaries	29
2.3.2.6.The influence of grain boundaries on mechanical properties	30

2.3.2.7.Special boundaries	35
2.4.Specimen preparation techniques	37
2.4.1. Etching	37
2.5.Grain size measurement methods	39
2.5.1. Comparison of ASTM E112 methodologies	39
2.5.1.1.Intercept methods against planimetric	39
2.5.1.2.Intercept against comparison	40
2.5.1.3.An overall comparison	41
2.5.2. Comparison of standards	41
2.5.2.1.Summary	46
2.5.3. ASTM E112	47
2.5.4. Problems with grain size measurement	49
2.5.4.1.Distributions	50
2.5.4.2.Twinning	51
2.6.Summary	51
<u>3.EXPERIMENTAL</u>	<u>52</u>
3.1.Introduction	52
3.2.Specimen preparation	52
3.2.1.The mild steel	52
3.2.2.Why specimen preparation was so important	58
3.2.3.Techniques investigated	61
3.2.3.1.Etching	62
3.2.4.Summary of preparation techniques	64
3.2.5.Mixed pearlite ferrite material	67
3.3.Methods of grain size measurement	68
3.3.1.The ASTM grain size number	68
3.3.2.Manual methods	70
3.3.2.1.Comparison chart method	70
3.3.2.2.The planimetric method	71
3.3.2.3.Intercept methods	72
3.4.Automatic image analysis	75
3.4.1.Pixel resolution	77
3.4.2.Grain boundary reconstruction	79

3.4.2.1. Image convolution processes	79
3.4.2.2. Edge detection	80
3.4.2.3. Thresholding	83
3.4.3. Grain size measurement methods	88
3.5 Missing boundaries and grain size measurements	89
3.5.1. The impact of missing boundaries on grain size measurements	90
3.5.2. The location of missing boundaries	92
3.5.2.1. Magnification selection	92
3.6. Electron Back Scatter Diffraction (EBSD)	94
3.6.1. System set up	94
3.6.2. Formation of EBSD patterns	96
3.6.3. Interpretation of EBSD Patterns	99
3.6.3.1. Automatic pattern indexing	100
3.6.4. Crystal orientations	104
3.6.4.1. Misorientations	105
3.6.5. EBSD examination procedure	106
3.6.5.1. Calibration	106
3.6.5.1. Collection of electron backscatter patterns	110
3.6.5.3. Resolution and mapping times	111
3.6.6. Sources of error	114
3.6.6.1. Orientation measurement	114
3.7. Image distortion on the SEM	116
<b>4. RESULTS</b>	<b>118</b>
4.1. Specimen preparation	118
4.1.1. Results	120
4.2. Grain size measurements	128
4.2.1. Inter-comparison of manual methodologies	129
4.2.1.1. Effect of increasing fields	132
4.2.2. Sampling	135
4.2.2.1. The number of specimens	135
4.2.2.2. The number of fields per specimen	138

4.2.2.3.Number of counts per field	141
4.2.3.The impact of missing boundaries on grain size measurements	142
4.2.3.1.Manual measurements	143
4.2.3.2.Automatic image analysis	146
4.2.4.Comparison of automatic image analysis grain size measurements with EBSD	149
4.2.4.1.Comparison of results with boundaries removed	171
4.2.5.Comparison of two optical grain size measurements	176
4.2.6.The impact of not including the boundary into the measurement using the automatic image analysis system	180
4.2.7.The grain shape and misorientation of missing boundaries	185
4.2.8.Comparison of manual and automatic grain size measurements with optical and EBSD imaging	189
4.2.8.1.A comparison of results from optical and EBSD imaging using manual methods	192
4.2.8.2.A comparison of results from using manual and automatic methods	193
4.3.Assessment of boundaries with misorientation	194
4.3.1.Assessment with the location of boundaries on EBSD but not reconstructed on optical	194
4.4.The misorientation of grains and grain size	197
4.4.1.Misorientation data for grain boundaries between large/large, large/small and small/small grains	200
4.4.2.Misorientation and grain size for specimen 3 and 4	201

5.DISCUSSION	205
5.1.Introduction	205
5.2.Grain size methodology	206
5.2.1.Inter-comparison of manual methodologies	206
5.2.2.Sampling	211
5.2.2.1.Summary	212
5.3 The impact of missing boundaries on grain size measurements	214
5.3.1.Summary	217
5.4.Assessment of the impact of image resolution on grain size measurements using automatic image analysis.	218
5.4.1.Differences between the EBSD images of different resolutions	219
5.4.1.1.Summary	221
5.4.2.Differences between the optical and the lower pixel resolution EBSD images for grain size	222
5.5.Comparison of the results from the two operators	229
5.5.1.Assumptions made in the reconstructing of the optical images by two different operators	233
5.5.2.Boundaries found in one image form but not in the other	235
5.5.2.1.Boundaries that existed in the optical images but not in the EBSD images	236
5.5.2.2.Boundaries that existed in the EBSD images but not in the optical images (missing boundaries)	237
5.6.Missing boundaries and misorientation	240
5.6.1.A summary of the results from using automatic image analysis	241
5.7.Comparison of manual and automatic grain size measurements with optical and EBSD imaging	243
5.7.1.Differences between manual measurements of	

the EBSD and optical images	244
5.7.2.Differences between manual and automatic measurements of the EBSD and optical images	246
5.7.2.1.Summary	250
5.8.Misorientation data for grain boundaries between large/large, large/small and small/small grains	252
5.8.1.The association of misorientation and grain size	252
<b>6.CONCLUSIONS</b>	<b>254</b>
6.1.Grain size methodology	254
6.1.1.Inter-comparison of manual methodologies	254
6.1.2.Sampling for grain size measurements	254
6.1.3.The choice of manual grain size measurement methods	255
6.2.The impact of missing boundaries on grain size measurements	256
6.3.The impact of pixel resolution on grain size measurements using automatic image analysis	257
6.3.1.Grain sizes of EBSD images of different pixel resolutions	257
6.3.2.Grain sizes of optical images and lower pixel resolution EBSD images	258
6.4.The decisions regarding reconstructing grain boundaries	259
6.4.1.Boundaries reconstructed in one image form but not in the other	259
6.5.Manual measurements of EBSD and optical images	260
6.5.1.Manual and automatic measurements of EBSD and optical images	260
6.6.Missing boundaries and misorientation angles	262
6.7.Misorientation angles of grain boundaries between large/large, large/small and small/small grains	263
6.7.1.The association of misorientation and grain size	263

7.	<u>FUTURE WORK</u>	264
	7.1. Grain size measurements	264
	7.2. Automatic image analysis	265
	7.3. Electron back scatter diffraction	267
8	<u>POSTERS, PUBLICATIONS AND REFERENCES</u>	268
	8.1 posters	268
	8.2 publications	268
	8.3 references	269

## List of figures

Figure 1	A schematic of the location of the areas measured in the cross-section of the mild steel	55
Figure 2	A schematic of the location of the areas measured in the longitudinal section of the mild steel	57
Figure 3	Images of EBSD maps without using a suspension in the specimen preparation (left image) with using a suspension (right image).	60
Figure 4	A plot showing the conversion from the number of grains per mm squared and mean linear intercept values to G grain size units.	68
Figure 5	Images demonstrating the error imposed from adding a boundary to an object	77
Figure 6	The Sobel Convolution Filters	82
Figure 7	A digital image of the mild steel and the same image after the Sobel filter has been passed through	83
Figure 8	Image demonstrating how grain boundary reconstruction can produce grains that are too large (left) and too small (right)	87
Figure 9	Binary Images showing 0% (left) and 20% (right) missing boundaries.	91
Figure 10	The hardness indentations providing markers for four segments to be montaged.	93
Figure 11	Components of an EBSD system	94
Figure 12	A schematic showing the formation of one pair of Kikuchi lines from the diffraction of the electron beam with one family of lattice planes.	97
Figure 13	EBSD pattern from the mild steel	99
Figure 14	A plot demonstrating how lines are defined in Hough space.	101
Figure 15	A plot showing all the vectors representing a line in Hough Space	102

Figure 16	A comparison of the distances between indentations between images taken at specimen at zero tilt and images at 70 tilt	116
Figure 17	An image of the specimen after polishing with Buehler's Gamma Micropolish No 3 Alumina B and etching using a 2% nital solution.	120
Figure 18	An image of the specimen after polishing with Struers' OP, an Acidic Alumina, made up with 50% water and then etched with ferric chloride.	122
Figure 19	An image of the specimen after polishing using Struer's Colloidal Silica and etching using a 2% nital solution	123
Figure 20	An image of the specimen after using the Buelher's Gamma Micropolish No 3 Alumina B and 20% volume ferric chloride mixture.	124
Figure 21	An image of the specimen after using Buehler's Gamma Micropolish No 3 Alumina B and a 5% nital polish/etch mixture	125
Figure 22	An image of the specimen after using the Buehler's Gamma Micropolish No 3 Alumina B and a 10% nital polish/etch mixture	126
Figure 23	An image of 2 specimens after using the Buehler's Gamma micropolish No 3 Alumina B and a 7% nital polish/etch mixture.	127
Figure 24	A plot of the ASTM grain size numbers for each specimen and for each method	130
Figure 25	A plot showing the effect of increasing the number of fields measured on the grain size number	132
Figure 26	A plot of the percentage relative accuracy against the number of grains measured for all methods	134

Figure 27	A plot of the ASTM G number from each specimen from using the lineal and planimetric methods	136
Figure 28	A plot of the ASTM G numbers of the lineal method against the planimetric method	137
Figure 29	A plot of the individual ASTM G numbers from each field of view in each specimen using the lineal method	139
Figure 30	A plot of the individual ASTM G numbers from each field of view in each specimen using the planimetric method	139
Figure 31	A histogram of the mean ASTM G numbers from measuring 1,2 and 3 fields of view using the lineal method	139
Figure 32	A histogram of the mean ASTM G numbers from measuring 1,2 and 3 fields of view using the planimetric method	139
Figure 33	A plot of the ASTM G number measured on images with 0,5,10,15 and 20% boundaries removed using all the manual methods	143
Figure 34	A plot of the mean of the manual methods measuring the ASTM G number on images with 0,5,10,15 and 20% boundaries removed	145
Figure 35	A plot of the ASTM G number measured on images with 0,5,10,15 and 20% boundaries removed measuring with the single circle, lineal and 3 circle method using the automatic image analysis system	146
Figure 36	A plot of the mean ASTM G number from measuring with the single circle, three circle and lineal methods using the automatic image analysis system on images with 0,5,10,15 and 20% boundaries removed	147
Figure 37	Colour Code for Grain Sizes	151

Figure 38	An Optical image of specimen 1 with the measured grains colour coded according to their size	152
Figure 39	An EBSD image of the smaller pixel resolution of specimen 1 with the grains measured colour coded according to their size	152
Figure 40	An EBSD image of the greater pixel resolution of specimen 1 with the grains measured colour coded according to their size	153
Figure 41	A histogram of the grain area distributions measured on the optical and EBSD images of both pixel resolutions using the automatic image analysis system for specimen 1	154
Figure 42	An Optical image of specimen 2 with the measured grains colour coded according to their size	156
Figure 43	An EBSD image of the smaller pixel resolution of specimen 2 with the grains measured colour coded according to their size	156
Figure 44	An EBSD image of the greater pixel resolution of specimen 2 with the grains measured colour coded according to their size	157
Figure 45	A histogram of the grain area distributions measured on the optical and EBSD images of both pixel resolutions using the automatic image analysis system for specimen 2	158
Figure 46	An Optical image of specimen 3 with the measured grains colour coded according to their size	160
Figure 47	An EBSD image of the smaller pixel resolution of specimen 3 with the grains measured colour coded according to their size	160
Figure 48	An EBSD image of the greater pixel resolution of specimen 3 with the grains measured colour coded according to their size	161

Figure 49	A histogram of the grain area distributions measured on the optical and EBSD images of both pixel resolutions using the automatic image analysis system for specimen 3	162
Figure 50	An Optical image of specimen 4 with the measured grains colour coded according to their size	164
Figure 51	An EBSD image of the smaller pixel resolution of specimen 4 with the grains measured colour coded according to their size	165
Figure 52	An EBSD image of the greater pixel resolution of specimen 4 with the grains measured colour coded according to their size	166
Figure 53	A histogram of the grain area distributions measured on the optical and EBSD images of both pixel resolutions using the automatic image analysis system for specimen 4	167
Figure 54	A histogram of the grain area distributions measured on the optical and EBSD images of both pixel resolutions using the automatic image analysis system for all specimens	169
Figure 55	Histograms of grain area distributions of each individual specimen comparing measurements on the optical images, the EBSD images of greater pixel resolution and the optical images with those boundaries not on the EBSD images removed	172
Figure 56	Comparison of the grain size distribution from the optical image, the optical image with the boundaries that did not exist in the EBSD removed, and the greater pixel resolution EBSD images for all specimens	174

Figure 57	Histograms of grain area distributions of each individual specimen comparing measurements on the optical images reconstructed by two operators (operator 1 & operator 2) and the EBSD images of greater pixel resolution.	178
Figure 58	Histograms of grain area distributions of all specimens comparing measurements on the optical images reconstructed by two operators (operator 1 & operator 2) and the EBSD images of greater pixel resolution.	179
Figure 59	The ratios of perimeter/area plotted against the aspect ratios of minor/major axes of ellipses of the same area	181
Figure 60	The ratios of perimeter/area plotted against the area of the ellipses	183
Figure 61	A plot of the ASTM grain sizes measured on the optical and the greater pixel resolution EBSD images of each specimen using the planimetric, single circle, three circle and lineal manual methods and also by automatic image analysis	191
Figure 62	A histogram of the boundaries not reconstructed by Operator 1 categorised according to their misorientation angles	194
Figure 63	A histogram of the boundaries not reconstructed by Operator 2 categorised according to their misorientation angles	196
Figure 64	An example of a true grain identification map showing a more refined grain structure	198
Figure 65	Examples of EBSD images with, from left to right, small grains, small and large grains and large grains colour coded according to the scale shown above	199
Figure 66	A plot of the misorientation data for grain boundaries between small/small, small/large and large/large grains	200

- Figure 67 Plots of the percentage of grain boundaries between small/small, small/large and large/large grains with misorientation angles for specimens 3 and 4. 202
- Figure 68 A schematic demonstrating the location and directions grain size measurements were conducted during the initial characterisation of the mild steel sample 208

## List of tables

Table 1	The elemental composition of the mild steel reference material	65
Table 2	The mean linear intercept results from measuring along the transverse cross sectional plane. The specific location of the measurement fields are shown in Figure 1.	66
Table 3	The number of intercepts measured across a longitudinal section of the mild steel	68
Table 4	The etches and their compositions investigated in determining the ideal specimen preparation technique.	75
Table 5	The microscope settings for each manual grain size methodology	85
Table 6	The compositions of the etches tested for the sample preparation of the mild steel.	131
Table 7	The sample mean calculated from all fields of view across all specimens and methods.	143
Table 8	Showing the mean linear intercept values and the equivalent ASTM G numbers from measuring along 1 and 2 lines using the lineal method	154
Table 9	The image pixel sizes of the optical and the two EBSD images for all four specimens	163
Table 10	Grain shape and misorientation data of boundaries in the EBSD images but not in the optical images (missing boundaries )for operator 1	198
Table 11	Grain shape and misorientation data of boundaries in the EBSD images but not in the optical images (missing boundaries) for operator 2	199

Table 12	The mean sphericities and aspect ratios of the optical and the EBSD images of both pixel resolutions for all specimens	201
Table 13	Showing the percentages of the total number of boundaries measured in specimens 3 and 4 that are smaller than 15° and greater/equal to 15° misorientation for each grain size category	216
Table 14	Showing the percentages of the total number of boundaries measured in specimens 3 and 4 that are smaller than 15° and greater/equal to 15° misorientation	216

# **1. INTRODUCTION**

## **1.1. General Introduction**

This thesis is concerned with some of the methods currently available for measuring the grain size in polycrystalline, metallic materials.

To be able to measure the size of grains with some confidence is important for quality assurance and material property determination purposes and at the time of writing there were four quantitative manual grain size measurement methods prescribed in various industrial standards. Also, within the last few years with the advent of faster and more economical computers the use of automatic image analysis has played a more prominent role. All these techniques are investigated within this thesis.

The metallographic preparation of specimens to reveal the microstructure is important for subsequent grain size determination and involves many variables, such as an incomplete network of grain boundaries. The impact of these variables to the final grain size measurement is also investigated.

Electron back scatter diffraction (EBSD) is a technique that provides crystal orientation information. This technique was adopted for this work to provide a complete network of grain boundaries against which the location of missing boundaries using optical imaging could be achieved. It was also used to

provide the misorientation data of boundaries allowing a relationship with grain size to be investigated.

## **1.2. The Nature of Polycrystalline Materials**

Most metallic materials are made up of crystals (polycrystalline), otherwise known as grains, which are formed from conventional methods of metal production. It is the mechanical working and thermal treatments through these metal production methods that are responsible for the microstructures developed. Each grain contains atoms, which are arranged in a systematic manner and are defined by the Bravais lattice system. The planes and directions of these atoms are described by using Miller Indices and stereographic projections. The grains are often orientated differently to one another and between them grain boundaries are formed, which define the transition zone where the atoms rearrange from one grain orientation to another. The orientation of the planes can influence certain properties of the material [1].

It is also the size of the grain that is important when predicting certain material properties, for example the Hall-Petch equation describes the relationship between grain size and yield stress. This relationship can be described as the yield stress being inversely proportional to the square root of the grain size.

Specifically the Hall-Petch relationship for steels is:

$$\sigma_{lys} = A + B d^{-1/2} \quad \text{Equation 1}$$

where  $\sigma_{lys}$  is the lower yield stress, A is the friction stress opposing the dislocation motion, B is a material constant which represents the ease of generating dislocations, and d is the average grain diameter. [2,3,4]

### **1.3. The Objectives of the programme**

The underlying objective of the programme was to establish better practice in grain size measurements through a study of the methods that were in use at the time of writing. There were various aspects considered and the specific objectives were as follows:

1. To assess current practice of modern manual grain size measurement methods through an inter comparison of those prescribed in the relevant industrial standards. This was achieved by considering accuracy, e.g. the number of grains, fields of view and specimens to reach a specific accuracy level, and efficiency with respect to reaching this accuracy level by minimising time and errors.

2. To assess the impact of missing boundaries on grain size measurements by comparing the difference in the measured grain size of microstructures with various percentages of boundaries removed against a specific accuracy level. The location of grain boundaries is of course important when grain size measurements are to be conducted since they define the shape and size of the grains. However, locating a grain boundary using optical microscopy is not always straightforward since they are often difficult to etch using traditional chemical etching techniques. Often a reconstruction of so called 'missing boundaries' is required prior to grain size measurement to ensure that the microstructure is representative of the material. Determining where a boundary might or might not have been etched is often conducted visually by the operator and hence is subject to an individual's judgement. However, with the use of the EBSD technique a complete network of boundaries was provided due to their location being determined from the orientation of one grain relative to another (misorientation). Thus by comparing a specimen area where images have been created via optical microscopy and by EBSD the actual location of missing boundaries became possible.
3. The use of automatic image analysis and digital images in grain size measurements by considering the importance of pixel resolution and by comparing with manual measurements.

4. The relationship between grain size and misorientation angles through the use of EBSD to provide a complete network of grain boundaries and the misorientation data for each boundary.

## **1.4. The experimental Approach**

### **1.4.1. Specimen preparation**

A sample material was provided by Corus\* being a mild steel with a fully ferritic, equi-axed microstructure. The relative simplicity of this microstructure allowed an investigation that is focused on grain size methods without complicating factors such as multi-phases and directionality and it is relatively convenient for etching and distinguishing boundaries.

The preparation of the material was important in terms of ensuring the surface finish was representative of the bulk material. Etching of the surface was also important in order to reveal the grain boundaries for subsequent reconstruction using the automatic image analysis system and for measurement of grain size. Specimen preparation was also important for the use of EBSD since the information this technique provides came from very close to the surface. Therefore, the residual stresses induced from specimen preparation had to be eliminated and etching became important to this end.

Various specimen preparation techniques were investigated, including electro chemical methods, until the optimum was developed.

#### 1.4.2. Manual methods.

This material was extensively characterised for grain size using all the methods prescribed in the standards BS4490 [5], ISO643 [6] and ASTM E112 [7] and by using an automatic image analyser. Where appropriate a highly accurate grain size measurement was established together with a substantial data set.

By characterising the sample material and from investigating the application of grain size measurements within industry a critique of the standards was conducted to investigate their suitability to meet the requirements within industry.

#### 1.4.3. Automatic image analysis.

An automatic image analysis system can conduct measurements on a digital format and provide a large amount of data relatively efficiently compared to manual measurements. A system was used to measure grain size, which involved firstly capturing and digitising images of the microstructure. Thus the use of digital imaging was incorporated within the work, specifically the importance of pixel resolution. Grain size measurements using this technique

firstly involved reconstructing the boundaries by using standard image processes and also by operator interfacing using digital editing.

#### 1.4.4. Electron Back Scatter Diffraction

Electron back scatter diffraction is a scanning electron microscope (SEM) based diffraction technique and the electron back scatter patterns produced are used to determine crystal orientations. From the orientation of one grain with respect to another, known as misorientation, the location of a grain boundary was established. This provided a complete network of grain boundaries compared to the uncertainty in the location of all the boundaries from etching specimens and using optical imaging.

## **2. LITERATURE SURVEY**

### **2.1. Introduction**

The literature survey reported in this chapter is concerned with the current situation regarding microscopy and material properties. The chapter begins with a survey of microscopy, particularly involving automatic image analysis and Electron Back Scatter Diffraction (EBSD). The use of automatic image analysis for quantitative analysis of microstructures is assessed. The use of EBSD as a tool for understanding complex material properties and their microstructure is assessed in the next section. This is followed by a survey of the specimen preparation techniques for the specific steels used in this thesis. The final section provides a survey of grain size measurement methods, including a critique of the most common standards in use within industry.

### **2.2. Microscopy**

#### **2.2.1. Automatic Image analysis**

Vander Voort described the use of image analysis systems for grain size measurement in [8]. 'With the current drive to improve product quality, which has fostered development of statistical databases, control charts, and so forth, only image analysis can provide the necessary data with the required precision

and in the required volume.' Consequently ASTM devised a standard, namely ASTM E1382, 'Standard Test Methods for Determining Average Grain Size Using Semi - Automatic and Automatic Image Analysis' [9], which was introduced in 1990 [8].

Leithner detailed the limitations of image analysis in grain size measurement based upon the importance of specimen preparation [10]. The example given was that a scratch could be counted as a boundary. Indeed automatic image analysis of microstructure necessitates the most optimum specimen preparation possible, e.g. no scratches from mechanical polishing [11,12].

As a comparison with manual image analysis Le Pennec et al set out to measure grain size in a low carbon steel using image analysis [13]. It was found that the 'questionable reproducibility of manual methods is overcome.' In addition to this a relative error of the mean intercept of 1% or 2% was gained allowing mechanical properties to be predicted with a level of accuracy 'never before reached'.

Another limitation of image analysis was defined by the resolution of the camera and microscope, both limiting the overall imaging resolution. For example, the measurement of a grain can be influenced by the number of pixels making up a boundary, where fewer pixels result in a less accurate measurement. Thus image analysis is more 'sensitive to magnification effects'[14,15] than manual methods.

Mishima conducted a more critical assessment [16], where an attempt was made to determine how consistent results were if several different image analysis systems were used to measure the grain size of a common sample. Essentially the investigation involved creating binary images by thinning an input image, repairing the grain network, and finally measuring. Thinning was required before measurements could be undertaken to maximise the grain area by minimising the grain boundary. Several specimen preparation methods were used to assess the systems' abilities further. The conclusion drawn was that for microstructures containing complexities such as precipitate dispersion input images 'cannot go through the grain boundary thinning process'. Therefore the optimum accuracy in grain sizing was not achieved.

## 2.2.2. Electron Back Scattered Diffraction

### 2.2.2.1. Introduction

EBSD has been described as a “powerful experimental tool for the measurement of local textures” [17], where advantages of EBSD over other systems are that “orientations can be measured from operator-selected regions of 0.5 $\mu$ m or less, specimens are the typical bulk SEM type, therefore specimen preparation is straightforward, and orientations can be measured semi-automatically in about thirty seconds each” [17]. Also, diffraction patterns provide a considerable amount of information regarding the crystal phase, lattice parameters and the orientation of crystals [17]. The misorientation distribution information is very important, for example in the analysis of micromechanisms of superplastic deformation as it provides a clear picture of the distribution of the subgrain formation and their contribution in the final texture evolution [18]. According to Ralph the ease at which data is accumulated and their relatively simplicity to interpret was demonstrated by how rapidly academic and industrial research laboratories have adopted the EBSD technique [19].

Also EBSD can overcome the problems associated with grain size measurements particularly due to all the grain boundaries being visible [20,21].

For example, a mean grain size may be larger from measuring with an optical technique than from using EBSD since fewer boundaries visible will cause grains to be perceived as larger [20].

Historically there was the orientation distribution function (o.d.f.) and the misorientation distribution function (m.d.f.). The former described the probability density for the occurrence of specified crystallographic orientations and the latter the probability density for the occurrence of specified intercrystalline misorientation between adjacent grains [22]. These techniques have essentially been absorbed into EBSD, which is concerned primarily with the measurement of macrotexture and mesotexture, the former being a measure of the texture averaged over many thousands of grains, and the latter being a measure of populations of misorientations. It also includes the measurement of microtexture, which is a texture measurement on an individual orientation basis, i.e. on the scale of the microstructure. [17,23]

#### 2.2.2.2. A Description of the Technique

The orientation of grains can be referenced to a set of external axes relating to the macroscopic specimen geometry (absolute orientation) but also with reference to the neighbouring grain (misorientation). Misorientation can be expressed as a 3 x 3 matrix that relates the crystal co-ordinate frame to the chosen reference frame in the specimen.[17,24]

$$M_{12} = A_1^{-1}A_2 \quad \text{Equation 2}$$

Where  $A_1$  and  $A_2$  are two contiguous grains and  $M_{12}$  defines the misorientation between them.

However, this matrix overdefines the misorientation since there are nine numbers describing 3 degrees of freedom. Alternatively there is the axis of misorientation and angle of misorientation. The former is a "direction which is common to both grain  $A_1$  and  $A_2$ " whereas the latter is "an angle which rotates the lattice of grain  $A_2$  onto grain  $A_1$  about the misorientation axis".[17,24]

From this comes the angle/axis parameter ( $\theta/l$ ), or misorientation parameter, which is used to describe misorientation geometry between grains [25]. This is a useful parameter since it allows immediate recognition of low angle boundaries.

### 2.2.2.3. Resolution

It is important that the system geometry is first calibrated adequately and secondly reproduced faithfully from the calibration set up when using EBSD for quantitative investigations. For example, unless the system is calibrated well at the specimen working height “errors of 2-3° could results in a boundary being wrongly categorised” [17].

#### Angular Resolution

Angular resolution depends on calibration of the EBSD system and subsequent specimen alignment [26]. Bowen points out that care must be taken in specimen preparation, including specimen mounting in the microscope, where absolute orientation is required [27].

EBSD pattern indexing is achieved through the use of recognition algorithms such as the Hough Transform. Therefore the number of pixels applied to a digitised pattern will determine, in part, the angular resolution, i.e. a higher pixel resolution giving a higher angular resolution [20]. For correct indexing it is important that the widths of the Kikuchi bands in an EBSD pattern are measured accurately since, via the Bragg angles, they represent the lattice parameters of the material under analysis. Generally a Hough Transform will

convert bright linear features into bright peaks in parameter space and dark linear features into dark peaks, therefore giving a band as a bright peak surrounded by two dark peaks. If there is poor resolution in the digitised pattern, e.g.. a bright line spans 10 pixels, then the exact location of the band is not so defined. This can be overcome by performing a convolution of the Hough Transform with a mask whose shape resembles the general peak generated by a typical band in order to locate the centre of the peaks [28]. One such convolution was described by Lassen and is named the butterfly mask [29]. Experiments have shown that the majority of Kikuchi bands could be located with high precision although this precision was significantly reduced when the bands were very wide.

Ultimately the angular resolution will be limited by the image quality from the camera or phosphor screen. This limitation can be illustrated from a study of nickel aluminide by Ubhi [30]. The investigation was to include verification that both the  $\beta$ -NiAl,  $\alpha$ -Cr and  $\gamma'$ -Ni<sub>3</sub>Al phases were present. However, since their lattice parameters are similar ( $\beta$ -NiAl = 0.2887nm,  $\alpha$ -Cr = 0.2880nm) the Kikuchi patterns produced were indistinguishable. This limitation is also important for misorientations. For example, a study by Tirschler and Blochwitz concerned texture stability during fatigue testing under room temperatures at medium amplitudes [31]. However, the reported angular accuracy of the EBSD system used was  $\pm 0.5^\circ$ , which was insufficiently sensitive to detect any changes in texture at the medium amplitudes utilised.

Specific work was carried out by Prior to assess the magnitude of errors associated with the calculation of misorientation axes associated with small misorientations [32]. It was pointed out that the misorientation axes of grain and subgrain boundaries provide constraints upon the slip systems potentially active during deformation and recovery. EBSD measurements were made on the same grains after certain rotations around the normal to the specimen surface. It was concluded, and corroborated by Wilkinson from a similar study [33], that the errors on misorientation axes decreased as the misorientation increased where magnitudes of 20° or more misorientation measurements will be within 5° of the true value.

#### Spatial Resolution

Spatial resolution was defined by Humphreys as the distance across a boundary which the patterns cannot be solved [26] and has been estimated to be 50 to 150nm for aluminium parallel to the tilt axis and 150 to 500nm perpendicular to the tilt axis [34]. It is also affected by the atomic number of the specimen with light materials having a worse spatial resolution due to greater penetration of the electron beam, and also affected by the beam current and accelerating voltage.

It is important to set the beam current to the optimum condition to gain maximum spatial resolution. With low currents the resulting Kikuchi lines are not so well defined and the recognition algorithm may not index, or incorrectly

index the pattern. With high currents the spatial resolution is limited by the beam size and the depth of penetration into the specimen. The optimum is found between these two settings. However, poor definition of Kikuchi lines can be overcome by integrating several images of the same pattern before indexing. However, this does result in an increase to indexing time, which is significant when large areas are being mapped. Also, there is more scope for optimum spatial resolution with an increased beam current when a field emission gun is utilised since the beam diameter is not as sensitive to beam current as a W filament [34]. Also, a field emission gun is more stable and provides a more reproducible current allowing orientation maps over a large area of the specimen to be performed. [26]

The diffusion of a Kikuchi band results from local bending of the lattice planes by dislocations, which cause electrons to be scattered away from the Bragg condition [35]. Lattice strain also affects the definition of Kikuchi lines and so only a small amount of cold work in a material can be tolerated for subsequent analysis using EBSD [23].

#### 2.2.2.4. Lattice Strain

Attempts have been made to use the diffusion of a Kikuchi pattern to determine the extent of lattice strain within a crystal. Specific work by Buchanan et al described a procedure to assess plastic strain using EBSD patterns obtained from a type 316 austenitic stainless steel [36]. Traditionally hardness measurements are used to assess the extent of residual strain and it was proposed in this work that EBSD could provide a spatial resolution approximately three orders of magnitude better for such assessments. The method reported involved the assessment of the pixel grey level changes across a band, ensuring first that there were no surface defects by polishing extensively, and then to create a calibration with a scale of pattern sharpness using the same material prior to straining. Subsequent assessments could then be made by comparing with the calibration scale. The limitation of this method with this material was concluded to be 15% strain beyond which the rate of change in the pixel grey level was too low.

Another method developed by Wilkinson involving pattern diffusion was related to elastic strains [37]. This involved increasing the distance between the specimen and the detector resulting in the angular resolution being increased whilst forsaking the angular range obtainable with the detector closer to the specimen. The increase in angular resolution was described where the same 1mm distance on the detector screen, which previously translated to 2°, then translated to 0.4° with the increase in distance between the detector and

specimen. The elastic strains were then related to the changes in interzonal angles from those expected from unstrained crystals. Among the conclusions it is significant to note that the results obtained were in excellent agreement with X-ray measurements.

The use of diffuseness of EBSD patterns of various creep strains in nickel based superalloys specimens stressed parallel to the direction of solidification was examined and reported by Quested et al [38]. Again calibration of strain versus pattern diffuseness was used to estimate the strain accumulated by individual grains by comparing these with the diffuseness of the subsequent patterns. Calibration was determined by selecting a magnification above which no improvement in pattern quality was obtainable thus eliminating variables from surface deformation and microscope operating conditions. One of the conclusions drawn from this work was that grains close to  $\langle 100 \rangle$  gave less diffuse patterns than those near  $\langle 110 \rangle$  indicating that there was less creep strain for the former.

#### 2.2.2.5. Further Limitations of EBSD

There is one particular failing of the EBSD system for indexing Kikuchi patterns well and this was demonstrated for ferritic structures. This error occurred when the pattern mainly consisted of bands having a common intersection, in this case a  $\langle 111 \rangle$  or a  $\langle 001 \rangle$  zone axis. The problem arose from the fact that the

indexing procedure required another band that does not share the same intersection. For example, when a  $\langle 111 \rangle$  zone axis is found in the middle of a pattern, and because of the particular features of the body centred cubic (bcc) structure of the ferrite crystal, one needs a very high quality pattern to find and correctly index such a band. If this is not the case, the software may wrongly index the bands sharing the common  $\langle 111 \rangle$  zone axis, and owing to the geometric properties of the pattern, the resulting (wrong) orientation is always  $30^\circ$ ,  $\langle 111 \rangle$  rotated from the correct orientation. [39]

#### 2.2.2.6. A Comparison of other Techniques

Diffraction techniques in a scanning electron microscope became widely available during the 1970's, namely Selected Area Channelling, Kossel X-Ray Diffraction and Electron Back Scatter Diffraction (EBSD) [17]. EBSD showed the greatest potential and much research was conducted into its application to crystal phase identification and crystal phase orientation.

X-rays methods: these include back reflection Laue using microbeam X-rays and micro Kossel X-ray diffraction. The former requires comparatively large concentrations of phases and grain sizes of at least 1mm and the latter is inconvenient to use although provides a spatial resolution of less than  $10\mu\text{m}$  [17,40].

Selected Area Channeling (SAC): EBSD has superseded this technique since EBSD provides a greater spatial resolution of 200-500nm compared to 10 $\mu$ m. Also the specimen preparation required for SAC is more difficult than for EBSD. Finally the angular field of view is up to 80° for EBSD but only 16° for SAC. [17]

Transmission Electron Microscopy (TEM) and Scanning Transmission Electron Microscopy (STEM): Although with convergent beam electron diffraction in a TEM and electron energy loss spectroscopy (EELS) in a STEM offers a better spatial resolution (1nm) and better accuracy (0.1 to 0.2°) than EBSD the specimen preparation required is much more involved. Therefore EBSD is the preferred technique unless resolutions better than 200-500nm are required.[17,41]

Electron Channelling Contrast Imaging (ECCI): there is a small but recordable change in BSE intensity when an electron beam is rocked over a specimen in a SEM. Generally ECCI is more sensitive, with greater angular resolution, and is faster than EBSD but does not provide the quantification found with EBSD [42].

Generally the advantages of EBSD over other techniques are the angular resolution and the use of bulk specimens rather than thin foils allowing for a greater area to be investigated, e.g. boundary orientations relative to both the specimen and the crystal geometry [43]. Also, with modern computers it is possible to produce, acquire and automatically analyse a diffraction pattern with 0.1 to 0.5s. Spatial resolution has been improved within recent years with the

introduction of a field emission gun within the SEM allowing some investigations that were traditionally done using the TEM now being done using the EBSD [26].

## 2.3. The Nature of Polycrystalline Materials

### 2.3.1. Complex Microstructures

#### 2.3.1.1. Introduction

There are many factors concerning the properties of a metallic material. Most commercial materials are of a polycrystalline form and it is well established that the physical, mechanical and chemical properties of materials of this form differ markedly from those of a single crystal form [44].

### 2.3.2. Grain Boundaries

Grain boundaries play an important role in influencing material properties [45,46]. Not least they play an important part in how a microstructure develops

during the processing of a material. Considering grain boundaries, a polycrystalline material can be defined as “a collection of grains assembled such that the system of grain boundary junctions constitutes a network with connectivity both in terms of topology and orientation.”[24]

#### 2.3.2.1. Coincident Site Lattice

The coincident site lattice (CSL) was first recognised by Kronberg and Wilson and subsequently developed by Frank and Brandon amongst others [47]. It refers to the lattice points of two grains that are superimposed [25]. Since the CSL is common to both grains it provides useful information regarding the grain boundary between them. It implies a magnitude of an ordered structure hence such a boundary fits together better than a non-CSL boundary, i.e. one that is totally disordered. Hence it provides a “measure of the match between the lattices of neighbouring grains.” [17]. Where there is a good match there is also low volume free energy, which is central in determining thermodynamic properties of an interface [24].

The formulation of a misorientation allows for CSL classification [23]. For example a misorientation parameter  $36.87^\circ/(100)$ , gives a CSL of 5 when the second grain is rotated  $36.87^\circ$  about a origin fixed in both grains [25]. The

number 5 is the reciprocal density of coinciding sites, hence one in five lattice points result, and is given by the notation  $\Sigma = 5$  CSL.

As a representation of grain boundary structure the CSL can be over simplified [45,48]. It fails to unanimously predict the correlation between boundary geometry and material properties because only the orientation relationship between neighbouring lattices is specified rather than the actual relationship at the boundary surface. It also only represents three of the five degrees of freedom where the other two are obtained from boundary plane orientation. Here the interface plane scheme has been developed which, as the name indicates, describes the boundaries in terms of their planes.

#### 2.3.2.2. The Influence of Grain Boundaries on Microstructure

The phenomenon of dynamic recrystallisation influences the evolution of a microstructure. It has scientific and engineering importance as it plays an important role in the evolution of microstructure and the control of bulk properties [49]. This phenomenon takes place by the nucleation and growth of new grains at the expense of the deformed matrix during annealing. There are many factors determining the sites of recrystallisation nuclei and deformation bands, large inclusions, second phase particles, grain interfaces are some of the preferential sites [50]. Duggan et al conducted a study of the dependence of the original grain size and their orientation on the recrystallisation behaviour

of a coarse grained copper after rolling reductions [51]. It was concluded that for rolling reductions of less than around 90% there was dependence whereas at higher rolling strains cube orientated nuclei began to dominate the recrystallisation process.

Migration was stated to be the predominant process as it controls the kinetics of recrystallisation and grain growth and affects the resulting grain size and the evolution of crystallographic textures [52]. There are various factors dictating the migration rate and generally low angle boundaries will migrate slower than high angle boundaries. The total energy associated with boundaries is reduced if the total area of the grain boundary population is reduced. This provides the driving force for grain growth, which, if prevented, may instigate rotation of the boundaries. This will somewhat reduce the free energy resulting in a lower energy boundary type. A highly symmetrical arrangement of atoms at boundaries occurs with relaxation [45].

Specific work conducted by Jensen et al investigated annealing temperatures and the resulting microstructure for Al-SiC composites [53]. The recrystallised grain size was seen to decrease with an increase in temperature implying that more nuclei had become active. Using EBSD it was also found that, at the lower annealing temperature 40% of the grains were close to the  $\{100\}\langle 013\rangle$  orientation with the remaining 60% being of all other orientations. The percentage of the latter was found to increase with an increase in the temperature, reducing the preferred orientation, and the grain size distribution

of these grains contained around 27% of very small grains. The sizes of the preferred orientated grains were evenly distributed and therefore the conclusion drawn was that the grains with all orientations only grew slightly in this higher temperature range.

Small additions of solute have significant effects on the recrystallisation, grain growth and kinetics of phase transformation in metals. Specifically the solute atoms influence the recrystallisation from a direct interaction between moving boundaries [54]. For example, impurities give rise to a change in the recrystallisation texture of steels and eventually of their mechanical, electrical and magnetic properties [55].

EBSID has been utilised by Skjervold et al to characterise the local texture in an Al-1.2wt% Si-alloy heat treated to contain large Si-particles approximately  $4.5\mu\text{m}$  and then deformed in compression [56]. Among other conclusions it was found that large misorientations can accumulate within local regions and they preferentially develop in constrained regions, e.g. grain boundaries and large second phase particles where clusters of particles seemed to increase the misorientation more effectively.

Hayakawa et al disputed the theory of the development of the secondary recrystallisation  $\{110\}\langle 001\rangle$  Goss texture where the CSL boundaries, having both lower grain boundary energies and higher migration mobilities, surround the Goss grains [57]. The theory in dispute was based on the study of pure

materials where high mobility of CSL boundaries was observed at low temperatures whereas for this study the temperature needed for secondary recrystallisation was higher than for normal grain growth. It was concluded that there was no unique and special configuration of CSL boundaries around the Goss grains in the electrical steel studied.

An experiment was conducted by Randle [58] to investigate how strain-induced grain growth was influenced by the heating rate. Two nickel blocks of 99.5% purity were annealed under different conditions, one heated faster than the other, after being subjected to a compressive strain. Orientations of each block were measured using EBSD. The results showed that there was a higher concentration of poles near  $\langle 111 \rangle$  and  $\langle 100 \rangle$  for the faster block. Consequently twinning occurred more in the faster specimen during grain growth and more anomalous grain growth with a slower temperature increase.

Further studies using EBSD showed that twinning did not play an important role in the nucleation process of a cold rolled titanium alloy where the heating treatment was between 520 and 620°C [59]. The process of recovery was investigated by examining specimens after annealing from 1 minute to 60 minutes. It was concluded that the twins were consumed by their parent grains and the last twin was annealed out after about 40 minutes.

### 2.3.2.3. High and Low Angle Boundaries

In molybdenum polycrystals it has been demonstrated that low angle boundaries are replaced or modified with high angle boundaries during recrystallisation [50].

Grain boundaries influence the control and development of microstructure during thermochemical processing [47]. For example, an annealed aluminium sample was found to have a coarse grain structure with a high number of low angle  $\Sigma 1$  boundaries. The general results for an aluminium sample were different in that there was normally expected coarse grains surrounded by random boundaries with small grains with low angle boundaries and low  $\Sigma$  CSL boundaries. It was postulated that the different formation of this microstructure was due to heavy rolling at the final processing step. More recently it has been realised that the design and control of grain boundaries can be manipulated to give better properties [50].

Dislocation boundaries during plastic deformation also play an important role in determining microstructures and Hughes et al investigated this phenomena on Al, Ni and Ta deformed to large strains by rolling or in torsion [60]. From using transmission electron microscopy, convergent beam diffraction and determining crystal orientations from the convergent beam Kikuchi patterns it was found

that a lamellar structure of dislocation boundaries of small and medium angles mixed with large angle boundaries were formed. It was also concluded that the formation of high angle boundaries led to a deformation induced reduction in grain size.

#### 2.3.2.4. The Influence of Grain Boundaries on Mechanical Properties

The measurement of grain misorientations over large sample regions is of great interest since it provides “a direct measure of part of the grain boundary geometry, which can be related to physical properties associated with the boundary itself” [17].

Grain boundaries also play an important role in limiting material properties, e.g. segregation is often a limiting factor [61]. In general solute atoms in grain boundaries increase the strength of the material [50]. For example, small additions of boron can change the properties of austenitic steels considerably as boron atoms segregate to boundaries rendering an increase in hardenability. For example, Zhang et al have demonstrated that segregation of boron to boundaries in Fe-3% ( $\alpha$ -Fe) was stronger than in  $\gamma$ -Fe and that the binding energy of boron segregation in Fe-3%Si was also greater than that of carbon segregation in  $\alpha$ -Fe. Ultimately this indicated that boron was a very strong adhesion element in  $\alpha$ -Fe [62]. Ductility at low deformation temperatures for a

coarse recrystallised microstructure was reduced by the interaction of solute atoms with moving dislocations. Specifically, Ni<sub>3</sub>Al without boron in the boundaries displayed a much higher ductility. Also, sulphur was found not to segregate to {111}  $\Sigma$ 3 boundaries and only to a limited extent at boundaries with two low index planes [63]. In fact, if special properties were induced then this was more a result from the orientation of the grain boundary planes than from other material preparation factors [64].

Special mechanical properties are induced in a material when a CSL relationship exists [64],[47]. For example, twin boundaries ( $\Sigma = 3$  CSL) in High Nitrogen Stainless Steels do not favour the formation of Cr<sub>2</sub>N precipitates [64].

EBSD allows for a more detailed investigation into grain boundaries and their relationships with materials properties. For example, the distributions on sub-grain sizes and misorientations are features that can be used to characterise the stored energy from deformation [65]. Also, for a variety of fcc materials, susceptibility to creep cavitation damage depends in part upon the intercrystalline misorientation when these materials are subjected to temperatures above one-third their absolute melting point [22]. Finally, it was found using EBSD that “nearly all boundaries between acicular ferrite plates were found to be high angle boundaries with misorientation angles greater than 45°.” [39,66]

There has been much discussion whether metals could deform by diffusional creep. Thorsen et al conducted an experiment to investigate this specifically by using a Cu-2wt.%Ni material that was subjected to creep for 46.3 days with an applied stress of 1.14 MPa. An aluminium grid was deposited onto the material allowing displacements to be measured at the boundaries, and misorientations were measured using EBSD. It was concluded that material was deposited at grain boundaries and, for this particular experiment, that diffusional creep can occur. This was because there was a displacement of the aluminium grid from one grain with respect to an adjacent one and that grain boundary dislocations implied that the deposition of material at a boundary was coupled to grain boundary sliding and migration [67].

A comprehensive use of EBSD in the study of quasi-cleavage and hydrogen induced fractures in titanium alloys was conducted by Bache et al [68]. The technique was used to confirm that, in dwell and cyclic fatigue fractures and at high hydrogen levels, basal plane deformation and slip localisation were important factors.

Further work concerning fatigue was conducted by Hu et al where the focus was on fatigue cracking behaviour of a metastable beta titanium, Ti-6.8 Mo-4.5 Fe-1.5 Al (in wt%), particularly on the influence of grain misorientations and grain boundary geometry [69]. Here it was found that high angle boundaries were favourable for intergranular fatigue crack initiation, implying the existence

of larger internal stresses. Also, among other factors, that for a short crack to initiate into a contiguous grain a low angle boundary was required.

Ubhi et al reported that EBSD was a suitable technique for the study of diffusion-bonded interfaces [70]. Using this technique it was shown that microtextures of solid state diffusion bonded interfaces could be different because of different starting textures of different recrystallisation processes.

Generally it has been stated that there is some direct evidence that links specific intergranular phenomena with boundary geometry in polycrystals, e.g. segregation, precipitation and cracking [63,24]. For example, intergranular stress corrosion cracking and correlations with the geometrical structure of grain boundaries was studied by Pan et al [71]. It was concluded the general high angle boundaries were most susceptible to cracking and that  $\Sigma 3$  grain boundaries were observed to crack. It was further stated that the key factors controlling the crystallography of grain boundary planes were a combination of the material, twinning, microtexture, CSL and the boundary plane. Further use of EBSD contributed to obtaining a more complete picture of the microstructure including probing the surfaces which bound crystals where these surfaces contained cracks, fractures and grain or phase boundaries. Knowing the crystallography of such surfaces provided a key to understanding their physical properties [72].

Another experiment utilising EBSD involved two nickel spheres, which were compressed to a height of 6mm [17]. One was then annealed at 1000°C for 1 hour and water quenched (fast) and the other slowly ramped to 1000°C over three hours, held for one hour, then slowly cooled to room temperature (slow). From an EBSD analysis it was seen that the 'slow' specimen contained almost double the CSLs than the 'fast' specimen. Also half of the CSLs in the 'slow' specimen were tilt or twist boundaries compared to less than a quarter in the 'fast' specimen. From this analysis it was concluded that "the kinetics factors associated with the heat treatment cycle had a strong effect on the populations of special boundaries" and that EBSD "was an efficient and convenient tool for the measurement of grain boundary geometry".

Tamm and Skrotzki investigated deformation and recrystallisation behaviours of NiAl where local textures of deformed and recrystallised areas using EBSD [73]. One of their main conclusions was that the recrystallisation mechanism involved an increase in misorientation due to dislocations incorporated in subgrains. The diffusion of Kikuchi patterns offered a means of identifying active slip systems and so provided insights into the mechanisms of plastic deformation in polycrystals [35].

With regards to Al-Li alloys, grain boundary types developed after recrystallisation of the 8090 alloy tested in tension at high temperature were studied by Eddahbi et al. The microstructures of the annealed and deformed states were compared and, among other conclusions, it was stated that the

deformation behaviour was dramatically different from that of most aluminium alloys. The dynamic recrystallisation behaviour was characterised by an increase of  $\Sigma 3$  and  $\Sigma 13$  boundaries and it was generally believed that an increase in these type of boundaries was associated to the recrystallisation of new grains [74].

Lopes stated that the Grain Boundary Character Distribution (GBCD) was a key factor for reducing intergranular cracking in iron aluminide [75]. Although this alloy possessed excellent oxidation resistance, had relative low density, high Young's modulus and was low in cost, it was brittle and had a strong tendency to intergranular fracture. It was shown from the study that there was little preferred misorientation textures and no interface with [111] misorientation was found. Since random boundaries were intrinsically weak the intergranular weakness could be reduced by increasing the proportions of low angle boundaries and low  $\Sigma$  CSL boundaries.

#### 2.3.2.5. Special Boundaries

Some high angle grain boundaries behave differently from other high angle boundaries [76]. Their distinguishing feature is that they do not change continuously with misorientation and that physical quantities, e.g. diffusion and corrosion, are not monotonically dependent on misorientation but instead demonstrate energy cusps of various depths. For example, a study reported by

Rabkin et al included a plot of temperature against grain boundary tilt angle and it was demonstrated that the region representing special boundaries decreased as the  $\Sigma$  value increased [77]. Above a specific temperature there existed a maximal  $\Sigma$  value above which the boundary properties vary monotonically with the tilt angle. These so called 'special' boundaries were described as those 'which have markedly different values for properties than an average boundary' [63]. Special boundaries were often preferred since they could improve the performance of a material in service. The CSL can fail in predicting material properties for special boundaries as they do not always have CSL's. However, according to Randle, the precise nature of special boundaries is unclear although it is thought that they are determined by the crystallography, chemistry and electronic state of the boundary [23].

Gottstein et al conducted work to investigate the segregation effects and the activation energy for the mobility of  $\langle 100 \rangle$  tilt grain boundaries on misorientation in aluminium specimens with various degrees of purity [78]. They concluded that special grain boundaries segregate less and thus move faster than random boundaries. However, this was limited to a small interval of total impurity where at the higher (99.99995%) or lower (99.98%) levels the mobility of high angle grain boundaries did not depend on misorientation but did for the intermediate 99.992% level.

Specific work conducted by Aust et al related special boundaries and properties of a Nickel based alloy 600 (Ni-16Cr-9Fe) [79]. Generally it was stated that low

$\Sigma$  boundaries could provide obstacles to the propagation of cracks, so that the intergranular fracture will stop at these boundaries. The experiments from this work demonstrated that an increase in special boundaries reduced the susceptibility of the alloy to intergranular attack and this was attributed to the well-ordered structural characteristics of the boundaries rendering them less sensitive to precipitation and segregation.

## **2.4. Specimen Preparation Techniques**

### **2.4.1. Etching**

Specimen preparation is an important step before analysis of a microstructure can be conducted well. For the purposes of this thesis it was important that the grain boundaries were revealed to the greatest extent for characterisation using the automatic image analysis technique. For this technique, and for EBSD, it was important that any mechanical deformation from grinding and polishing was removed from the specimen.

The techniques used to reveal the grain boundaries vary fully with the type of grain structure being examined. For example, there are standard etchants utilised to reveal austenitic and ferritic grain structures [80].

The austenitic Alloy, L605, illustrates a common problem, as it is difficult to etch so that all of the grain boundaries are visible. This makes it very difficult to measure the grain size with a high degree of precision [81]. Also, in low carbon steels, such as sheet steels, parent austenite grain boundaries can be revealed only in rare cases [80]. The method to be used for measurement is also an important factor to consider in materials preparation. For example a twinned grain structure of cartridge brass is etched producing grains with different contrasts in black and white. All the grains are revealed but because of this contrast 'it is virtually impossible to measure by automatic image analysis' [81]. Also, the nital etch commonly used to reveal ferrite grain boundaries is sensitive to crystallographic orientation and will not clearly reveal all the grain boundaries. This is a serious problem if image analysis is performed. The use of Marshall's reagent will generally produce a very high degree of boundary delineation in ferritic low-carbon steels [80]. In general 'etchants that produce grain contrast attack may be quite suitable for comparison-chart grain size ratings'. However, they 'are less satisfactory for manual measurements and useless for image analysis' [80]. 'Greater attention must be given to specimen preparation (for image analysis) than is necessary for manual analysis; that is the quality of grain boundary delineation must be very high' [80].

Also the etch time is important, that is the time a specimen is etched to reveal the microstructure. An experiment was conducted to determine what effect the etch time has on grain size measurements using nital [14] and concluded that as the etch time increased the ASTM grain size unit changed from 4.5 to 8.5.

## **2.5. Grain Size Measurement Methods**

### **2.5.1. Comparison of ASTM E112 Methodologies**

The ASTM grain size measurement methodologies form the standard methods widely adopted. They were therefore adopted for the experimental work reported in this thesis.

#### **2.5.1.1. Intercept Methods against Planimetric**

An experiment was conducted to assess the effectiveness of the three circle method [82]. It included a uniform and non-uniform microstructure, the latter giving a substandard polish to represent a worse case scenario. Five observers did a total of three independent measurements on twenty micrographs, representing these microstructures. In the conclusions drawn it was noted that, for the uniform microstructure, 'there was some systematic variation associated with the observers' interpretation of what constituted an intercept.' 'Although these variations were statistically significant, from a practical point of view the method transcends these observer variations, since the average measured grain size ranged from 26.6 to 30.9 $\mu\text{m}$ '. What was stated here was that the variations were consistent with the grain size

distribution and hence the interpretations were accurate. For the non-uniform microstructure it was concluded that 'even though there was a statistically significant variation associated with each observers' interpretation of what constituted an intercept, the large number of intercepts provided by the method minimised this effect.' Finally the effectiveness of this method was confirmed from timing the observers as they measured to conclude that 'a quantitative value for the grain size could be obtained within 15 to 30 minutes.' Vander Voort confirmed these findings by saying that 'The three-circle intercept method provides a more precise estimate of the grain size in much less time than required by the planimetric method' [81].

Vander Voort continued to state that for a single measurement field, the planimetric method produces a lower standard deviation than the intercept method. However, because the planimetric method is much slower, for equal measurement accuracy, about 60% more time is required for this method than the intercept method. Consequently the intercept method is more efficient than the planimetric [80].

#### 2.5.1.2. Intercept against Comparison

Vander Voort is of the opinion that 'a good grain size measurement can be made with this method (Heyn Intercept Method) in slightly more time than is required for a comparison chart rating, but with much greater accuracy' [80].

Anon comments that the comparison chart method is quicker and provides an easier assessment of grain size than is possible by counting [83]. However agreement is reached with the former statement as Anon confirmed that 'comparison of specimens with (the) standard charts gave only a descriptive finding' [83].

#### 2.5.1.3. An Overall Comparison

ASTM Committee E4 conducted an inter-laboratory exercise to develop data for precision and bias statements in ASTM E112 [8]. For the comparison chart ratings it was concluded that 'the estimated grain size number was consistently 0.5 to 1G unit lower than the true grain size', (a G unit referring to the ASTM grain size indexing system), otherwise 'there was no difference in the grain size estimates by the planimetric and intercepts methods'.

#### 2.5.2. Comparison of Standards

The following points were used to compare ASTM E112 [7], BS4490 [5] and ISO643 [6], the three main standards identified for grain size measurements. Generally the criteria adopted in comparing the standards involved investigating the differences, consistencies and inter-dependencies.

The comparison was conducted by examining each standard at face value and also by assessing each one as they were used in practice. The latter approach allowed characterisation of the mild steel to be conducted thoroughly and efficiently since good measurements practice was developed from the studying the standards. It also allowed for a subjective appraisal of standards and this has also been included within the following sections.

1. Accuracy:

- a) Is it clear which method will provide the highest accuracy for a given number of measurements?

E112 claimed that for both the planimetric and intercepts methods repeatability and reproducibility were less than  $\pm 0.5$  grain size number. This was an indication that a precision of greater than half a unit was possible. However, ISO643 and BS4490 both stated that an accuracy of greater than half a unit is not possible for any given method and BS4490 went on to stipulate that no reporting should be given to a precision greater than half a unit.

For determining which method should be adopted for a given level of accuracy, E112 stated that the comparison method was sufficiently accurate for most commercial purposes but for greater accuracy either the planimetric or intercept method should be used. Finally it stated that the lineal method will be the referee in all cases. In comparison, BS4490 claimed that "since no greater

precision is obtained by the count method (intercept), the comparison method is likely to be used in most cases”.

- b) Is it clear how many fields of view/measurements are required to obtain the desired level of accuracy?

Only E112 gave any statistics that would allow the operator to find confidence in the precision in the results obtained. It goes further than this by providing charts that relate relative accuracy of measurements with the 3 circle, intercept and planimetric methods. These charts were derived from an inter-laboratory exercise conducted to determine precision and bias estimates for grain size measurements. They were placed in an appendix but, in the author’s opinion, a more obvious place would be preferable where they could be used by an operator to determine, before measuring, how many measurements would be required to obtain the desired accuracy. However, it did state that if the relative accuracy was not satisfactory then further measurements were required and that the “frequency of measurements should be based upon agreement between the manufacturers and users.”

This was substantially more informative than ISO643 and BS4490 where there was no mention of statistics to aid the operator in obtaining a desired accuracy. However, ISO643 did state that there should be an “adequate number of fields to have a valid count”.

## 2. Counting:

### a) How is counting for each method dealt with?

All three standards were consistent for the planimetric method, e.g. count whole grains within the circle as one and those intersected by the circle as half. For the lineal intercept method all the rules regarding counting were consistent also. However, for circular intercepts only ISO643 dealt with intercepts being lower than they would be for the lineal method, by stating that an intercept with a triple junction should be counted as 2, not 1.5 as stated in E112. Only E112 stated that a count of 2 should be given only when a manual tally counter was being used.

### b) How is an ideal magnification determined for each measurement method?

Selection of magnification: all three were consistent regarding the planimetric method, e.g. there should be around 50 grains within the circle. However inconsistencies existed between the three regarding the intercepts methods. For the single circle method E112 claimed that if the circle was smaller than about three times the mean lineal intercept then the distribution was not Gaussian, and recommended around 35 counts per circle. Both ISO643 and BS4490 simply stated that at least 25 counts should be obtained. For the three circle method all stated that around 50 intercepts were required but E112 went

on to explain that "some metallographers feel more comfortable counting 10 fields with about 40 to 50 counts per field." This provided an ideal counting situation to minimise errors in counting and to obtain enough counts for good precision. Finally, both ISO643 and E112 stated that at least 50 counts should be obtained per straight line for the lineal method but BS4490 did not make any reference to magnification for this particular method.

3. How is the selection of fields of view dealt with, i.e. is bias emphasised?

All stated that it should be done randomly but they differ there after. E112 stated more specifically that in selecting randomly it should be done blindly, e.g. with the light out, or the shutter closed, or with the eye turned away. ISO643 simply stated that measurements shall only be done once per field examined.

4. How are different microstructures dealt with regarding:

a) Preparation of specimens.

All three standards dealt with preparing steels of different microstructures, including heat treatments, tempering and etching. E112 went on to refer to other standards for both material preparation and etching. However, only BS4490 stated that the specimen should be polished "to a finish that will clearly reveal the grains during microscopical examination".

b) Measurement of specimens.

All gave instructions as to how to deal with structures of more than one phase. However, only E112 mentioned which methods would be best for different structures, e.g. intercept for non-equiaxed structures. ISO643 dealt with twinning and grains of different grain size indices. BS4490 included measuring when there was an obvious directionality to the grain flow.

5. Reporting – how is the measurement expressed and how clear is the associated statistical accuracy.

E112 was significantly more comprehensive in what it stated should be reported. Specifically ISO643 and BS4490 had no mention of anything regarding statistics that would indicate the accuracy of the measurements.

2.5.2.1. Summary

- BS4490 and ISO643 were very similar and show very few inconsistencies.
- Where BS4490 and ISO643 succeed over E112 was their relative simplicity. E112 purported to deal with many parameters that required some working through in order to obtain only the information that was relevant to the operator. For example, it is possible to remove the information deemed

necessary for grain size measurements and place this information on one sheet of paper and use it for all similar grain size measurements and remain in compliance with the standard. If so much information is required then a clearer layout is required, especially regarding customer specifications.

- All the information given in all three standards regarding specimen preparation could be brought together for one comprehensive section.
- There is constructive information to be given from each standard but they are not as informative individually as they are collectively.

### 2.5.3. ASTM E112

Vander Voort claimed that ASTM E112 is 'one of the most widely cited' [81] standards. This was substantiated by Horalek who stated that the majority of national grain size measurement standards were based on ASTM E112 [84].

In 1963 all the grain size methods were incorporated into E112 [80]. Wyman stated that the purpose of the writing up of this standard was to provide a means whereby all metallic and materials could be measured for grain size using a consistent method of representing this measurement, e.g. the 'ASTM grain size system' [85]. Previously there were various methods, including the number of grains per unit area or average grain diameter. Wyman felt that there was a 'lack of uniform nomenclature'. According to Vander Voort 'It is

now common practise to express grain sizes in terms of the simple exponential equation:

$$n = 2^{G-1} \quad \text{Equation 3}$$

where:

n = the number of grains per square inch at 100X magnification, and

G = the ASTM grain size number.' [81]

With the formation of this standard came new comparison charts. The first comparison charts were for copper and were introduced in 1930 in a revision of ASTM E2 [81]. ASTM E2 was first proposed in 1917 and it included both the planimetric and intercept measurement methods. Use of these methods, particularly the planimetric method, prompted requests for a similar grain size rating. Consequently, a comparison chart was added in the 1930 revision of ASTM Method E2 [80]. Further developments brought about E19 for austenitic grains and E89 for ferritic materials [83]. In researching previous practices using comparison charts Wyman concluded that 'if the standards (the charts) are not realistic then they will not be used' and 'if they (the charts) do not reasonably well resemble the "unknown" operator errors are prone to occur' [85]. For example the hexagonal networks were once used for comparison were abandoned because they were not realistic. Hence the comparison charts developed with E112 comprise of microstructures that are realistic.

Another important factor, according to Wyman, approached by the committee E4 was that of counting. They recognised the importance of having a sufficient number of grains counted to acquire a statistical level of confidence but also that a high level of counting incurred greater errors. Included within this was the fact that often it is impractical to require that many grains are counted and hence they set 'certain reasonable minima' [85].

#### 2.5.4. Problems with grain size measurement

Three sources of errors in grain size measurement have been recognised by Vander Voort [80]. The first arise from experimental limitations, for example poor grain boundary delineation, over-etching, miscounting, etc. The second is from improper sampling where fields should be chosen blindly to avoid operator bias. The last is found in how representative these fields are of the entire material. In a further study [86] it was stated that the stereological relationships between two-dimensional and three-dimensional microstructural parameters 'are known, but not often recognised or appreciated'. However, it was also found that, for cold-rolled materials, measurements on a single longitudinal plane are sufficient to estimate the grain size.

#### 2.5.4.1. Distributions

One of the main problems with grain size measurement is the fact that the grains are not uniform. When an operator cuts through a material along a specific plane and then reveals the microstructure on a cross section a range of sizes not larger than the cross section of the largest grain sampled is observed [81]. The sectioning plane can produce an apparent spread of grain areas that will cover the average areas of three to four ASTM grain size numbers [80]. Hence there is a grain size distribution from which a mean is often reported. These distributions can have more complicated effects on the material properties than are average grain size dependent [87]. 'This is not an average of the maximum cross-sectional area of each grain because the sectioning plane does not intersect each grain at its maximum width' [81]. This is often further complicated by the grain size distribution not being normal but bimodal. To deal with this ASTM E930 'Test Methods for Estimating the Largest Grain Observed in a Metallographic Section (ALA Grain Size)' was developed [88]. Other problems include different product shapes or different processes producing non equi-axed grains, e.g. elongated grains. This further complicates matters and influences the ability to measure the grain size [81].

#### 2.5.4.2. Twinning

Generally twinning is ignored in grain size measurement. However Vander Voort points out that 'if we are trying to establish a relationship between microstructure and properties, for example strength, we must consider twin boundaries as they influence dislocation movement' [81]. Twinning refines the grain size and gives additional Hall-Petch strengthening [89].

### **2.6. Summary**

Generally microstructures of polycrystalline materials and their relationship with material properties have been examined to provide the most recent developments. Within this the influence of grain boundaries on the formation of microstructure and also on material properties has also been assessed. Finally modern techniques for quantitative analysis of such analyses have been investigated.

### **3. EXPERIMENTAL**

#### **3.1. Introduction**

This chapter describes how the materials used for this research work were evaluated. The materials were characterised for grain size using manual methods, automatic image analysis and Electron Back-Scattered Diffraction (EBSD) and each of these techniques is described. The EBSD also provided crystallographic information pertinent to the investigations of this thesis. This chapter also describes how important specimen preparation was in using these techniques and how an optimum specimen preparation procedure was developed.

#### **3.2. Specimen Preparation**

##### **3.2.1. The Mild Steel**

The material was hot-rolled and subsequently air cooled to room temperature and was produced in the form of a 6mm round bar. Specimens approximately 20mm

long were prepared from the material. The elemental composition of the sample is given in Table 1 below.

element	% mass
carbon	0.0030
silicon	0.0100
manganese	0.1700
phosphor	0.0120
sulphur	0.0110
aluminium	0.0410
nickel	0.0020
niobium	0.0050
titanium	0.0600
oxygen	0.0025

**Table 1 The elemental composition of the mild steel reference material**

Ideally the mild steel should have been equi-axed with a homogenous grain size therefore allowing a more direct correlation between sampling and missing boundaries with grain size, i.e. the investigations described in this thesis. However, from linear intercept counts (see section 3.3.2) along a transverse cross-

section a change in the average grain size in the radial direction was found. The results from these counts are shown in Table 2 and the locations of the measurement fields with respect to the cross sectional plane in Figure 1. It can be seen that the outer edge of the specimen had a smaller grain size than the inner section.

Field	Intercepts	Field	Intercepts	Field	Intercepts
A1	37.5	B1	26.5	C	23.5
A2	20.5	B2	21.5		
A3	24.0	B3	20.5		
A4	29.0	B4	22.5		
A5	24.0	B5	22.0		
A6	31.5	B6	27.5		
A7	32.0	mean	23.4		
A8	20.0				
Mean	29.8				

**Table 2 The mean linear intercept results from measuring along the transverse cross sectional plane. The specific location of the measurement fields are shown in Figure 1.**

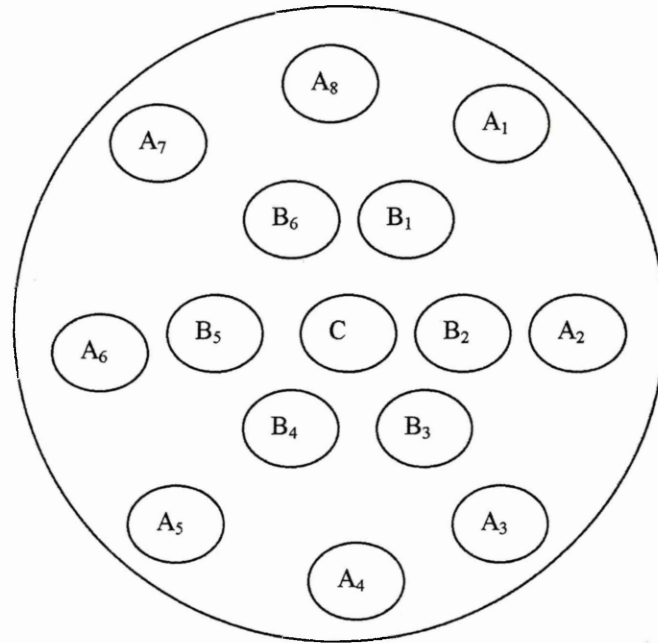


**Figure 1 A schematic of the location of the areas measured in the cross-section of the mild steel.**

Additionally a specimen was prepared with a section cut close to the diametric plane in the longitudinal direction. Again linear intercepts were counted along the longitudinal and transverse directions. The results are shown in Table 3 with the corresponding locations in figure 2 and demonstrated that, since the aspect ratio varied across the diametric plane from 1.01 to 0.91, there was some grain elongation present.

Intercepts			Intercepts			Intercepts		
Field	X <sub>(long)</sub>	Y <sub>(trans)</sub>	Field	X <sub>(long)</sub>	Y <sub>(trans)</sub>	Field	X <sub>(long)</sub>	Y <sub>(trans)</sub>
A1	21.5	23.5	B1	20.0	24.5	C1	25.5	26.5
A2	22.0	22.0	B2	20.0	23.5	C2	22.5	24.0
A3	22.0	25.0	B3	23.0	24.5	C3	23.0	24.0
A4	21.0	25.0	B4	19.5	22.5	C4	27.5	23.0
Aspect ratios	0.91 (0.04)	Aspect ratios	0.87 (0.03)	Aspect ratios	1.01 (0.07)			

**Table 3 The number of intercepts measured across a longitudinal section of the mild steel**

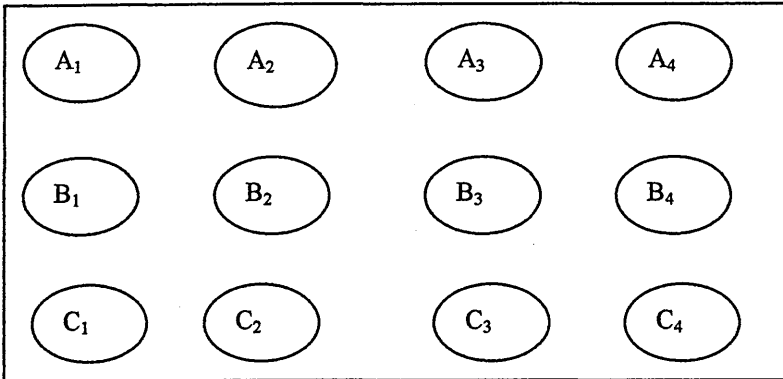


**Figure 2 A schematic of the location of the areas measured in the longitudinal section of the mild steel**

Therefore the results with respect to grain size methodology, missing boundaries and sampling analysed and discussed for this material were from measurements taken longitudinally as close to the diametric plane as possible, approximately 0.1mm, in order to maximise homogeneity of the grain size in the region where measurements were taken.

### 3.2.2. Why Specimen Preparation was so Important

The mild steel had to be prepared to allow for grain size measurements using optical and image analysis techniques. Throughout the investigation the Electron Back Scattering Diffraction (EBSD) technique was also used. Since each analysis technique would be used to compare results a specimen preparation technique was established that would allow each analysis technique to be applied to a specimen in the same condition.

The material was soft, approximately 97Hv<sub>20</sub>, and therefore easily deformed with extensive mechanical grinding and polishing. Therefore it was difficult to ensure that the resulting surface integrity was high, i.e. that it was representative of the bulk material by removing damage from grinding and polishing, whilst also ensuring that the surface was scratch-free [90]. For example, examination of specimens after initial grinding and polishing exhibited many scratches. It was then found that an oxide coating was breaking up during grinding and hence particles from the coating were able to scratch the material. It was therefore imperative that each specimen was thoroughly cleaned using an ultra-sonic bath to ensure that no particles were carried over to the polishing stages. Also, it was found that cutting up specimens was best done manually using a hack-saw since this would induce

less deformation into the soft material than a more convenient rotating silicon/carbide cut off wheel. From the same principle the underside of each mounted specimen was passed across each grinding paper to remove the coarser particles before grinding the specimen.

Within the image analyser there was a means of reconstructing the grain boundary network. However, the ability for the reconstruction to provide the most complete network of boundaries was dependent on how well specimens were prepared. Specifically the system was unable to distinguish between an etched up boundary and a scratch formed from mechanical deformation. It was important therefore that specimens were prepared to a mirror finish where a minimum number of scratches existed [12].

Surface integrity was important for EBSD since this analysis technique was sensitive to residual stress caused by mechanical polishing and from any oxide deposition. Since the penetration depth of back-scatter electrons was approximately 20nm, even small levels of surface deformation could cause diffusion in the EBSD pattern rendering it impossible to solve automatically, or at least reducing confidence in the automatic solving [26].

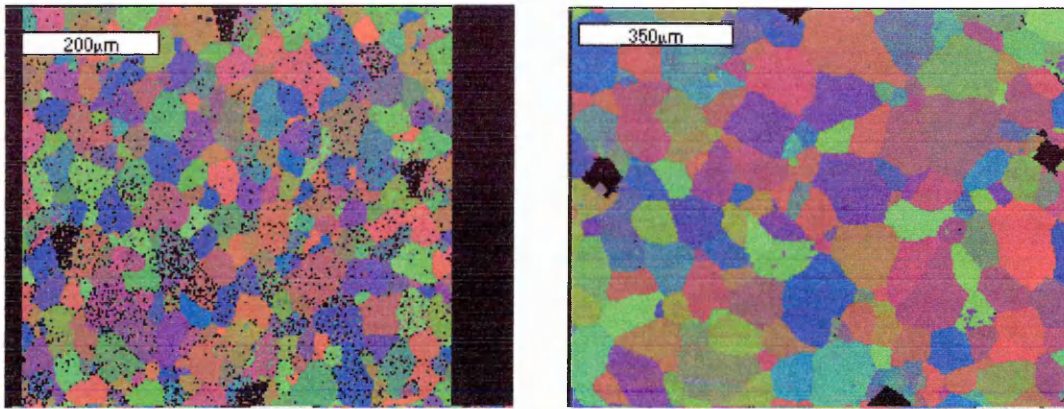


**Figure 3 Images of EBSD maps without using a suspension in the specimen preparation (left image) with using a suspension (right image).**

By comparing the two images in Figure 3 it can be seen that simply to finish polishing with a 1µm diamond polish was insufficient. The number of unsolved EBSD patterns, shown as black dots, was greater in the left image than the right. This was due to diffusion in the EBSD pattern from stress induced in the specimen from preparation. Consequently attempts were made to determine whether an effective electro-polishing technique could be developed. However, this was abandoned since ideal polishing conditions for the material were elusive. The next stage proposed was to find a suspension that would remove 1µm scratches satisfactorily.

### 3.2.3. Techniques Investigated

Once the techniques for grinding and polishing up to 1 $\mu$ m diamond paste were established several combinations of different suspensions and etches were investigated. This also included mixing etches with the suspension during polishing to determine whether this would improve the removal of scratches. It potentially could have also provided an efficient means of partially pre-etching the specimen.

The suspensions were:

- Struers' OP - A Acidic Alumina made up with 50% water.
- Buehler's Gamma Micropolish No 3 Alumina B.
- Struers' OP - A Colloidal Silica.

The polishing cloth used throughout was Buehler's 1 $\mu$ m cloth.

### 3.2.3.1. Etching

Etching was also an important part of material preparation. For image analysis it was a means of delineating the grain boundaries allowing for grain boundary reconstruction [90]. Also, for EBSD it was a means of relieving the specimen of any residual stress imposed during polishing [91]. An attempt was made to establish electro etching parameters, e.g. the chemicals, voltage, current and time, but as with electro polishing the ideal conditions were elusive. The focus was then chemical etching and from a study of the relevant literature the etches considered are detailed in Table 4.

Etch	Composition
Nital (2% solution)	40cm <sup>3</sup> nitric acid, 1960 cm <sup>3</sup> alcohol
Marshall's Reagent	5mL sulphuric acid, 8g oxalic acid, 100mL mixed with 30% volume hydrogen peroxide
Ferric Chloride	60g anhydrous ferric chloride, 100 cm <sup>3</sup> hydrochloric acid and making up to 2000 cm <sup>3</sup> with alcohol

**Table 4 The etches and their compositions investigated in determining the ideal specimen preparation technique.**

Essentially nital and ferric chloride provided contrast between the grains as the lattice orientation of each determined the rate of attack. Marshall's reagent, on the other hand, attacked the boundaries and hence provided contrast between boundary and grain.

Three specimens of the mild steel were used throughout, one for each suspension. Each specimen was re-polished using a 1 $\mu$ m diamond paste except when excessive relief was evident where upon the specimen was re-ground using

1200 grit paper, then polished with 6 $\mu$ m diamond paste followed by 1 $\mu$ m polish. Relief was determined to be excessive when it became impossible to have the entire specimen area in focus at one time using an optical microscope.

Assessment of the results from each stage were based on how well 1 $\mu$ m scratches were removed and if any remaining scratches could be tolerated. This assessment was done after etching the specimens since etching could exacerbate the visible effect of scratches. The results from each combination of etch/suspension are reported in section 4.1.

#### 3.2.4. Summary of preparation techniques

Although using a mixture of suspension and etch could have provided an efficient means of preparing the specimen for etching with Marshall's it was not adopted. Finding the right mixture that would remove enough scratches and etch to a level allowing further etching with Marshall's within a time that would not induce relief was very difficult to find. Since the results produced with the suspension were sufficient and that a good etching technique had been established, using a suspension alone was the route finally chosen. This was easily reproduced across different specimens since it was relatively easy to monitor how much

polishing time was required with frequent examinations under an optical microscope.

The suspension chosen was Buehler's Gamma Micropolish No 3 Alumina B. This provided better surface integrity than Struers' OP - A Acidic Alumina made up with 50% water. Struers' OP - A Colloidal Silica provided equally sufficient results as for Buehler's Gamma Micropolish No 3 Alumina B but the former required more polishing time thus increased the amount of relief.

Nital was chosen over ferric chloride because it was a better pre-etch for Marshall's reagent to provide good grain boundary contrast. The etching technique established involved a pre-etch on the polished specimen with a 2% nital solution followed with an etch using Marshall's reagent. Using nital alone was unsatisfactory since the preferential etching made subsequent grain boundary reconstruction using automatic image analysis difficult [80]. The grains in a grey level image produced from a specimen etched with nital were of various intensities but the boundaries were not so clearly defined. Thresholding for the boundaries alone was difficult to achieve without thresholding for the grains also (see section 3.4.2.3). Marshall's reagent provided sufficient contrast between grain and boundary allowing the grain boundaries to be thresholded. Finally the combined

etch of nital and Marshall's reagent was used because scratches were less exacerbated than from using nital alone.

Overall the final preparation procedure adopted was:

- Sand blast to remove the oxide coating.
- Cut the material into 20mm sections using a hacksaw.
- Slit each specimen longitudinally to within 1mm of the diametric plane, therefore allowing for subsequent material removal down to the diametric plane.
- Mount in a conductive compound, allowing for analysis using a Scanning Electron Microscope.
- Grind using papers with particle sizes from 240 grit down to 800 grit.
- Clean thoroughly in an ultra-sonic bath.
- Polish first using a 6 $\mu$ m and then a 1 $\mu$ m diamond paste for a 'mirror' finish, cleaning in an ultra-sonic bath between polishes.
- Polish using Buehler's Gamma Micropolish No 3 Alumina B on a microcloth.
- Etch using a 2% nital solution for approximately 2-5 seconds at room temperature, followed by Marshall's reagent for approximately 60 seconds at room temperature.

### 3.2.5. Mixed Pearlite Ferrite material

This material was used to investigate the relationship between the misorientation angles of small/small, small/large and large/large grains and to assess their importance to impact toughness. The experience gained from preparing the mild steel allowed for a preparation technique to be developed for this material. The focus of the investigation was on the ferrite phase and so essentially the same technique could be applied. The only main difference was that etching with 2% nital was sufficient for the subsequent investigation using EBSD mapping and image analysis. The Marshall's etch had a detrimental effect on the pearlite phase and this made defining the phase boundaries difficult. Since grain size measurements were not conducted using optical microscopy, as was the case in characterising the mild steel nital was sufficient as the final specimen preparation stage.

### 3.3. Methods of Grain Size Measurement

#### 3.3.1. The ASTM Grain Size Number

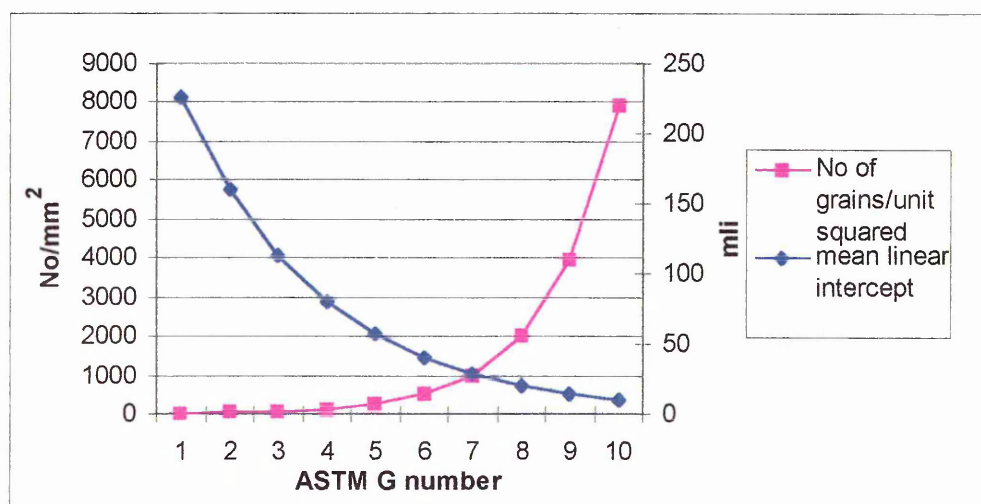


**Figure 4 A plot showing the conversion from the number of grains per mm squared and mean linear intercept values to G grain size units.**

There are different ways of reporting grain size, e.g. a mean intercept value or a number of grains per unit area. Therefore, in order to compare the different grain size measurement methods, it was necessary to have a common means of reporting. This was achieved by using the ASTM Grain Size Numbers, G, where

the mathematical relationships with the mean linear intercept and the number of grains per unit area were adopted from ASTM E112 [7]. The equivalent mean lineal intercept values (mli) and number of grains per mm<sup>2</sup> (#/mm<sup>2</sup>) are given in Figure 4.

Essentially the ASTM grain size number was defined in ASTM E112 as:

$$N_{AE} = 2^{G-1} \quad \text{Equation 4}$$

Where  $N_{AE}$  is the number of grains per square inch at 100X magnification.

Therefore:

$$G = \log_2 N_{AE} (+1).$$

For example, if there is 1 grain counted per square inch then the grain size number,  $G$ , is calculated as 1, if there are 2 grains counted then the  $G$  number is 2, 4 grains give  $G$  as 3 and 8 grains give  $G$  as 4, etc.

### 3.3.2. Manual Methods

The recognised industrial standards for grain size measurement were ISO 643 [6] and BS 4490 [5] and ASTM E112 [7]. Within these standards there were five methods of grain size measurement. These were the comparison chart, the planimetric, the lineal intercept, the single circle, and the three circle methods. The last three methods can be categorised together as intercept methods.

#### 3.3.2.1. Comparison Chart Method

The comparison chart method was different from all the others, as it was not quantitative. It simply required a visual, subjective comparison of a micrograph of the microstructure to be assessed against reference charts. Each set of charts represented particular microstructure types and within each set individual charts showed the microstructure to a certain ASTM grain size number, G.

### 3.3.2.2. The Planimetric Method

The planimetric method involved randomly placing a circle of a known circumference onto the microstructure. All the grains within the circle are added to half the grains that intersected the circle. This was achieved by placing a transparency with a circle drawn on it randomly over a micrograph. Using a dry wipe marker pen each grain within the circle was marked and counted, together with those that intersected the circle. The same transparency was wiped clean and then used for other fields of view.

From this the number of grains per square millimetre was calculated using the formula:

$$N_a = f(N_{\text{inside}} + N_{\text{intercepted}}/2) \quad \text{Equation 5}$$

where  $N_a$  is the number of grains per square millimetre,

$f$  is known as the Jeffries multiplier and is equal to the reciprocal of the measured area times the square of the magnification,

$N_{\text{inside}}$  is the number of grains counted completely within the measured area and

$N_{\text{intercepted}}$  is the number of grains that intercept the circle.

Thus the number of grains per unit area ( $\#/mm^2$ ) are reported.

#### 3.3.2.3. Intercept Methods

The remaining three methods all essentially follow the same principle. A line of a known length was placed randomly on the microstructure and the number of intercepts or intersections counted, an intercept being a segment of the line overlaying a grain and an intersection being the point where the line cuts a grain boundary. A mean linear intercept was then calculated by dividing the length of the line by the number of intercepts or intersections.

Measurements were undertaken on photographs of the polished and etched surfaces. Table 5 shows the microscope settings used to provide the required number of counts per field.

Measuring method	Magnification		Total Magnification	Required number of fields to satisfy ASTM E112
	Objective	Photo		
Planimetric	20	3.3	66	14
Single circle	10	4	40	12
Three circle	20	3.3	66	10
Lineal	5	4	20	8

**Table 5 The microscope settings for each manual grain size methodology**

The number of fields to satisfy E112 was derived first from selecting a magnification that would yield the stipulated number of grains per field. Thus for the intercept methods a minimum of 50 grains per field have to be intersected. The lineal method required the lowest magnification since 50 intercepts were obtained across 2 lines requiring more grains per image. The planimetric and

three circle methods required the highest magnification since, for the three circle, more grains were intercepted for a given area due to there being three circular lines, and for the planimetric more grains were counted within an area than counted across two straight lines. The single circle method required a lower magnification than the three circle method to obtain the required number of grains since only one circle was utilised.

These magnifications were set for each method and, in total, 168 fields of view from the six different specimens were characterised. As the grain size varied from specimen to specimen, the magnification could have been similarly adjusted to ensure that at least the recommended number of grains per field stated in E112 were available [10]. However, the variation in grain size from specimen to specimen was small and hence the adjustment of magnification for each specimen was not justified. Maintaining the magnification settings detailed in Table 5 allowed for a more efficient production of data.

Since the magnifications selected for the planimetric and the three circle methods were identical the same fields of view were used for both methods. The transparency used for the planimetric method also contained another two concentric circles of smaller diameters. Counting the intercepts with the three

circles was then performed immediately after counting for the planimetric method, again marking the grains with a marker pen as they were counted.

Measurements using the single circle method were performed at a lower total magnification (Table 5). The procedure used was similar to that for the three circle method except that only one circle, the largest of the three, was used.

The lineal method involved drawing two straight lines along the length of the micrograph ensuring that there was sufficient space between them so that the same grain was not intercepted by both lines. The total magnification was the lowest of those employed for all the methods; on average each field contained approximately nine times as many grains as the fields employed for the planimetric method.

For all these 'counting' methods the magnification factor was incorporated within the calculations to give absolute results.

### **3.4. Automatic Image Analysis**

The image analyser used was a Buehler Krautkramer's Omnimet system. A Hitachi Denshi KP M1 black and white CCD camera, with a 410,000 pixel

resolution, was attached to a Vanox T optical microscope allowing images from the microscope to be captured on the image analyser.

Areas of specimens were captured and the images digitised. Subsequent grain boundary reconstruction was performed allowing grain size measurements to be conducted. The results of these measurements were reported by converting area measurement of each grain to an ASTM grain size number.

Since a comparison of measurement methods was conducted it was important that images captured on the image analyser were from the same specimen condition as that used for manual measurements. Thus a like for like comparison could be conducted. This was relatively simple to achieve since the camera used for the image analyser was attached to the same microscope as that used to photograph the specimens for manual measurements.

Initially a micrometer bar was imaged at the objective magnification used for subsequent measurement and this was used to calibrate the magnification. Hence a calibrated magnification was stored with each individual image.

### 3.4.1. Pixel Resolution

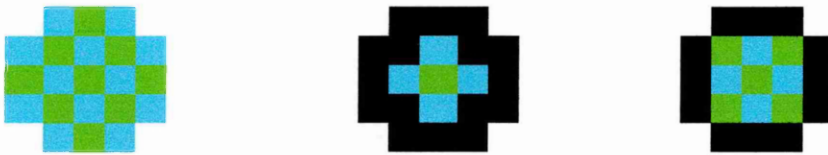


**Figure 5 Images demonstrating the error imposed from adding a boundary to an object**

A visual estimation was made to ensure that each captured image contained enough grains for each measurement method in accordance with the standards and also to ensure that there was sufficient pixel resolution for measurement of the smallest grain.

This is illustrated in Figure 5 where there are three images. These images are, from left to right, the object that requires measuring, this object and a boundary with 4 - connectivity and finally the object and a boundary with 8 -connectivity. As can be seen from this figure, if only laterally adjacent pixels (up, down, left, right) are considered to be connected this is 4 – connectivity, whereas if, in addition, the

diagonally adjacent (45 degree neighbours) pixels are also considered this is 8 – connectivity.

The boundary was required to define the grain for subsequent measurement. However, if the boundary was not considered as part of the measurement, as was the case for the automatic image analysis system used for this thesis, then an error was introduced. Again referring to Figure 5 the original image was comprised of 28 pixels, whereas there would be only 5 and 9 pixels measured for the 4 – connectivity and 8 – connectivity respectively. Therefore there was a considerable reduction in the number of pixels measured when a boundary was introduced with 4 – connectivity producing the worst case scenario, which was the situation with the automatic image analysis used for this thesis.

However, this error was reduced with increasing pixel resolution; if the boundary was always reduced to a one pixel thickness then for an increase in the number of pixels forming the object, the ratio of boundary to grain in pixels was effectively reduced.

Therefore the number of grains chosen per field of view was a compromise between the number stipulated in the standards and to ensure there was sufficient pixel resolution for the smallest grains.

### 3.4.2. Grain Boundary Reconstruction

Various approaches were investigated and used to create a complete grain boundary network. The following is a description of the image convolution processes that were generally adopted.

#### 3.4.2.1. Image Convolution Processes

Generally image convolution involves adjusting a pixel value according to the surrounding pixel values. For example, a 3 x 3 kernel (9 pixels) is passed across an image and the centre pixel is adjusted to match the average pixel value of the other 8 neighbouring pixels that fall within the domain of the kernel.

-1	-2	-1
0	0	0
1	2	2

The above is a representation of a 3 x 3 convolution kernel where the number in each element of the kernel represents its weight. Convolution is conducted on all

pixels within the domain of the kernel as it scans an image. The weights and the subsequent calculations will determine the output image. For example the product of the element weight and the original image grey level values of each pixel the element is assigned to are summed. The centre pixel would then be assigned the value of this summation. A further calculation may be applied to the summation, e.g. normalising by dividing by the sum of all the weights. The effect of such a convolution is to smooth an image by averaging out the pixel values within the kernel domain.

#### 3.4.2.2. Edge Detection

As the title suggests the function of this convolution is to detect the edge of an object. This was particularly important for grain size measurement since it was the grain boundaries that must first be detected in order to define the size of the grain.

In examining the neighbouring pixels an edge detector quantifies the slope and direction of a grey-level transition, i.e. the gradient of the grey-level. The gradient is a measure of how quickly the grey level values of pixels change when an image is scanned. If it has texture then the gradients will be large whereas if it is smooth then the gradient will be small. Therefore, a detected grain boundary has a large gradient since there is a large grey-level transition.

A convolution filter is required for each of the x and y directions and the results are computed together to provide the gradient.

$$m = \left( \left( \frac{\partial I}{\partial x} \right)^2 + \left( \frac{\partial I}{\partial y} \right)^2 \right)^{0.5}$$

**Equation 6**

$$\theta = \tan^{-1} \left( \frac{\frac{\partial I}{\partial x}}{\frac{\partial I}{\partial y}} \right)$$

**Equation 7**

Equation 6 and Equation 7 define how the magnitude and direction are related to the x and y components of an image, I, where m is the magnitude of the gradient and  $\theta$  is the direction.

For example, a convolution filter that is based on gradients is the Sobel filter.

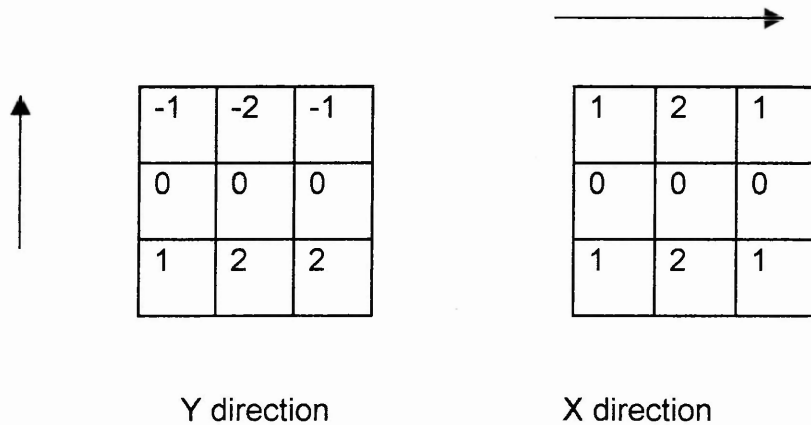


**Figure 6 The Sobel Convolution Filters**

Effectively the results of applying each convolution to the image are inputted into Equation 6, i.e. they are combined as the square root of the sums of their squares. This convolution was an effective means of detecting grain boundaries but good specimen preparation was a prerequisite, i.e. that good delineation of boundaries were required to be detected as edges.

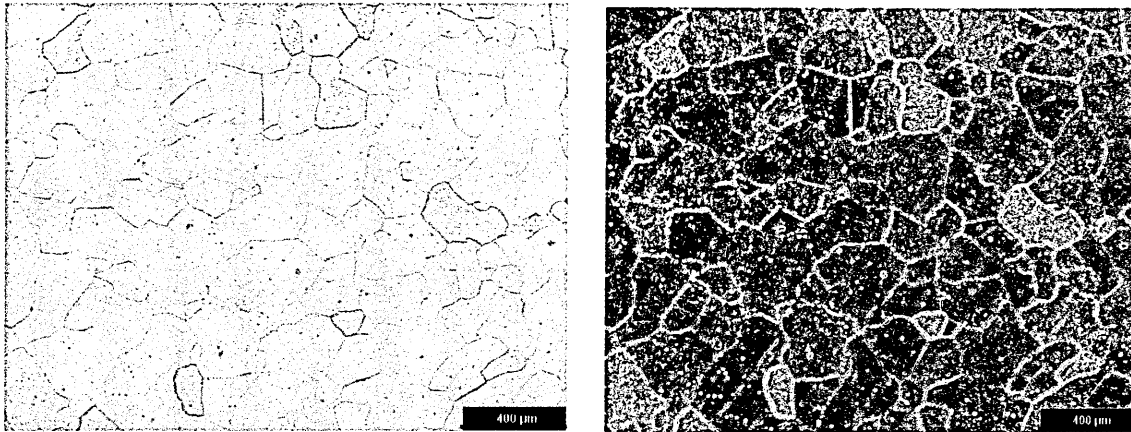


**Figure 7 A digital image of the mild steel and the same image after the Sobel filter has been passed through.**

Figure 7 represents a digital image of the mild steel (left) and the resulting digital image produced after Sobel convolution (right). As can be seen in the image of the mild steel there was good boundary delineation that corresponded with the Sobel edge detection. The Sobel image allowed for thresholding of the boundaries, as described in section 3.4.2.3, for subsequent measurement of grain size.

#### 3.4.2.3. Thresholding

Thresholding is simply image segmentation where specific objects are highlighted. This was basically achieved by selecting a grey-level range and all the parts of the

image that fall within that range are then segmented. This involves a foreground/background separation, i.e. the segmented part of the image becomes the foreground and the remainder becomes the background. The simplest example of thresholding is the formation of a binary image. Here a grey level is defined and those pixels that fall within this range are then transformed into black pixels (foreground), grey value = 1, and the remaining pixels are transformed into white (background), grey value = 0. An example of a binary image is shown in Figure 9 where the grain boundaries of the mild steel are black and the remainder of the image, i.e. the grains, is white.

The ultimate goal of segmenting images of specimens was to highlight the grain boundaries. However, often there were parts of the image that fell within a defined grey level range but did not require segmentation, e.g. objects that were not boundaries. Therefore a compromise was necessary where the thresholding level was limited to allow the maximum segmentation of grain boundaries but also to ensure the unwanted objects were maintained separated from them. By maintaining these unwanted objects separate they could then be removed by further segmenting for a size range. The pixels that formed an object, which fell within this size range, were then removed from the foreground domain. However, the consequence of this resulted in a reduction of grain boundaries thresholded.

Thresholding could be as effective if performed without edge detection provided the grain boundary delineation was good. However, edge detection could be a useful means of detecting boundaries without detecting unwanted objects if the grey level gradient of these objects was low.

Beyond this the fundamental processing to complete the boundary network is outlined below and holds for all image processing conducted.

Grain boundary reconstruction was conducted at this stage. This involved inverting the image so that the grains within the boundaries became the threshold regions and these regions were then eroded.

Erosion is a morphological operation, i.e. it is a measurement of the shape and form of object. It operates at a binary level where there are only black pixels (grey value = 1), or white pixels, (grey value = 0), which is the result after thresholding for the image analysis system described here. It was the boundaries that have the grey level value = 1 as they are the objects targeted for thresholding.

Each part of the kernel matrix were given values of one and it was passed along each of the pixel positions in the input image. If there were corresponding 1 values in all the pixel positions under the kernel then the value for the output image was 1,

whereas if any 1 pixel position did not correspond then the output value was 0. This output value was applied to the corresponding pixel position in the output image to where the centre pixel of the kernel was positioned on the input image.

By eroding the pixels in a manner determined by the kernel chosen, e.g. hexagonal, the grain area was eroded, consequently thickening grain boundaries and connecting them up.

Then a deconvolution algorithm was applied which effectively thickened the grains. This essentially involved adding pixels to the binary image, making the grain larger and the boundaries smaller. The important feature of this operation was that the thickening process stopped when there was only one pixel between each grain. Consequently thickening the grains in this way rendered the boundaries to a one pixel width whilst maintaining their connectivity.

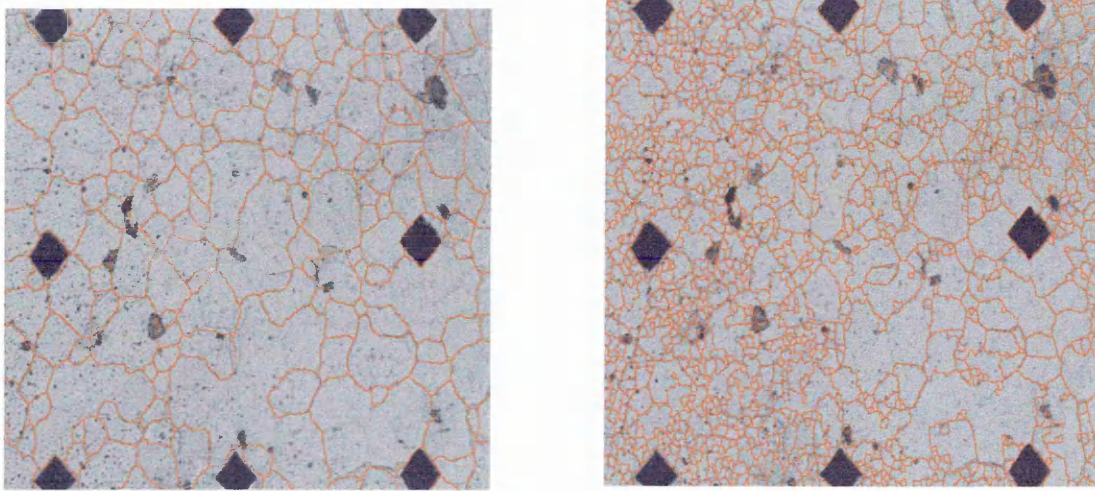


**Figure 8 Image demonstrating how grain boundary reconstruction can produce grains that are too large (left) and too small (right)**

This technique of grain boundary reconstruction depended on how well the boundaries could be thresholded initially. For example, if there were few boundaries in the foreground domain from thresholding then the subsequent boundary reconstruction process would produce grains that were too large. This is depicted in Figure 8 where the grain boundaries (shown in red in the foreground domain) have been reconstructed from an optical image of the mild steel. As can be seen from the left image the grains reconstructed are generally larger than what the optical image showed. In other words fewer boundaries in the foreground domain than there actually were resulted in a grain boundary network

domain than there actually were resulted in a grain boundary network that represented grains that were larger than what was seen from the optical image. Conversely, if there were many objects other than boundaries in the foreground domain (right image of Figure 8) then the resulting boundary network represented grains that were smaller than the perceived size.

Electronic editing of the boundary network was required at this stage. This compensated for those grains that were either too small or too large, for those boundaries that did not etch up and for the removal of unwanted artefacts. Finally a complete grain boundary network was created in the threshold region which was subsequently used for grain size measurements.

Measurements were conducted by calculating the area within each boundary and then translating that result to an ASTM grain size number. In order to eliminate the error that is introduced by having incomplete grains around the border of the image these were removed prior to measurement, leaving only complete grains.

### 3.4.3. Grain Size Measurement Methods

It was necessary to reproduce the grain size measurement methods used for manual measurements to produce the like for like comparison. Simply digital lines

of known lengths were introduced to the binary images, with straight lines for the lineal intercept method and circular for the three circle and single circle methods. Using Boolean operations intercept lengths between grain boundaries along these digital lines provided the grain size measurement. The planimetric method was not reconstructed using the image analyser as the system is designed to do measurement, e.g. area or lengths, and estimate grain size from these dimensions but not from counting a number of objects.

### **3.5. Missing Boundaries and Grain Size Measurements**

As described in section 3.4.2 electronic editing of the grain boundaries was required when the grain boundary reconstruction was conducted using the image analyser. Inherently this introduced a level of subjectivity to the reconstruction since the location of a grain boundary was subject to the discretion of the operator [90]. It was this subjectivity that was investigated in terms of grain size measurements from two perspectives, i.e. determining the impact of a missed boundary from the network, otherwise known as a missing boundary, and also the importance of the correct determination of the location of a grain boundary in the reconstruction.

### 3.5.1. The Impact of Missing Boundaries on Grain Size Measurements

The investigation involved creating binary images of the mild steel in the manner described in section 3.4.2. Five fields of view were chosen randomly and each boundary segment was manually edited to ensure that there was a seemingly complete network. There was some uncertainty in the boundary network being complete since the location of the boundaries was subject to the discretion of the operator. However, for the purposes of this specific investigation the boundary network was assumed to be complete. This assumption was valid as a comparison of grain size measurements was required from a known standard, in this case a complete network of grain boundaries. Then each boundary segment was numbered for subsequent reference. This allowed for the removal of a known percentage of boundaries, namely 5%, 10%, 15% and 20%, in a random fashion. The boundary segments to be removed were chosen by a random number generator. Once the individual boundaries had been identified they were removed using the image analyser manual editing facilities. Finally, including those images with the original complete networks (0% missing boundaries), there were a total of 25 images. Examples of 0% and 20% degradation are shown in Figure 9.

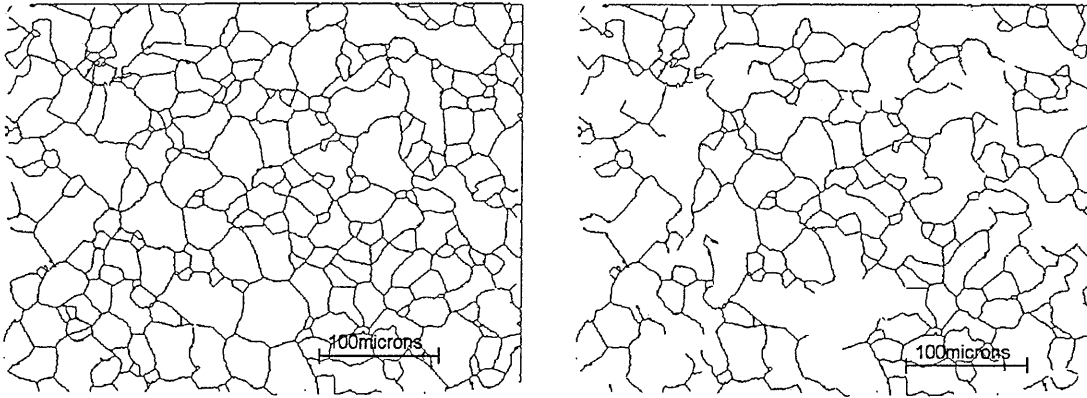


**Figure 9 Binary Images showing 0% (left) and 20% (right) missing boundaries.**

Grain size measurements were conducted on these images using the methods described in section 3.3.2. Thus an analysis of the impact of missing boundaries on grain size measurements became possible.

### 3.5.2. The Location of Missing Boundaries

#### 3.5.2.1. Magnification selection

Consideration of the grain size was given when determining the magnification that would be used to map an area of the sample using EBSD. It was important that there were sufficient grains to provide a number of missing boundaries for subsequent analysis, i.e. by comparing the optical images with the EBSD images. However, it was also important that the smallest grain could be sufficiently resolved to allow for subsequent grain size measurement using the image analyser, (see section 3.4). In order to achieve both criteria it became necessary to split the area into four segments before mapping. The resulting four maps were then reassembled providing a montage effect.

This was achieved by marking the area with eight hardness indentations as shown below.

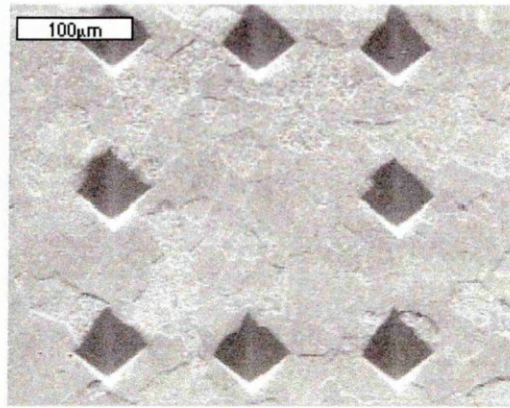


**Figure 10 The hardness indentations providing markers for four segments to be montaged.**

Each segment then had three hardness indentations making a 'L' shape. Having eight indentations allowed for there to be one common indentation between adjacent segments. They were then used as reference points for reassembling the segments, which then provided the same image as the original optical one.

**3.6. Electron Back Scatter Diffraction (EBSD)**

**3.6.1. System Set Up**

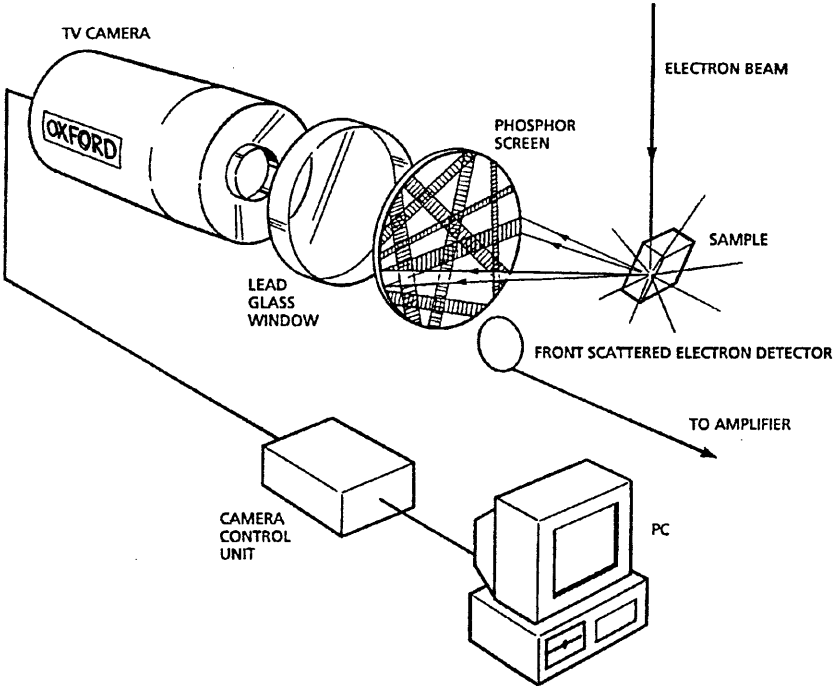


**Figure 11 Components of an EBSD system**

Figure 11 represents a typical set up for EBSD in a scanning electron microscope (SEM). The actual signal observed during EBSD is relatively low and is obtained

from the first 10 to 50 nm below the surface. A high tilt is therefore required since when the beam is incident normal to a specimen then it is channelled deep into it. The electrons therefore have further to travel before reaching the surface and are more likely to encounter additional scattering and absorption and thus further reducing the intensity of the signal [91].

The EBSD pattern is captured using a phosphor screen. This screen is normally held adjacent to the specimen, although certain geometrical constraints within the SEM might rule otherwise, allowing the BSE to interact with the phosphor causing it to fluoresce. A low light CCD camera is used to image the pattern produced on the screen. They are preferred over film primarily for their linear response thus making quantitative information directly available, and that developing photographs from the film is more time consuming [92]. Within the camera part the diffracted beam is converted into light by a scintillator which is then transferred to the CCD chip. The camera is controlled by a computer, which also enhances and displays the pattern on a monitor. The computer software digitises the image and indexes the pattern.

### 3.6.2. Formation of EBSD patterns

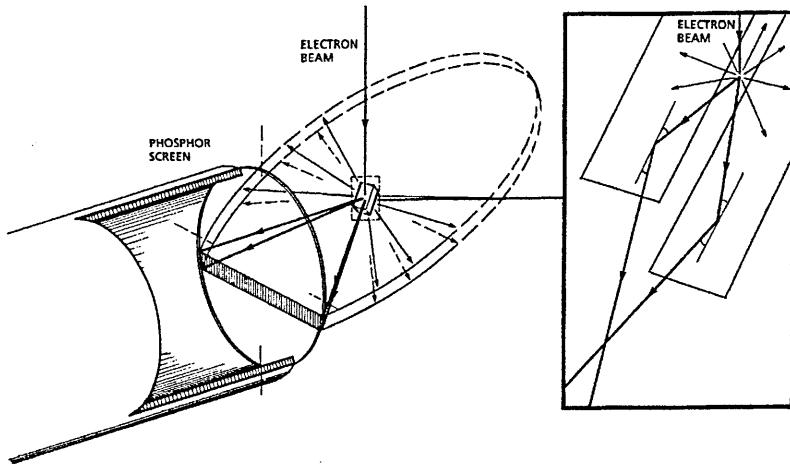
Essentially a Kikuchi pattern is a reciprocal 'map of angular relationships in a crystal' [26] and is formed through the interaction of the SEM primary beam with the specimen causing the electrons in the probe to undergo multiple scattering into a volume immediately below the sample's surface.

Some electrons impinged and scattered elastically on the lattice planes at the Bragg angle given by:

$$2d\sin\theta_B = n\lambda$$

**Equation 8**

where  $d$  is the interplanar spacing for a family of planes,  $\lambda$  is the electron wavelength,  $n$  is the order of reflection and  $\theta_B$  is the Bragg angle. Those electrons that were scattered inelastically form the diffuse background.



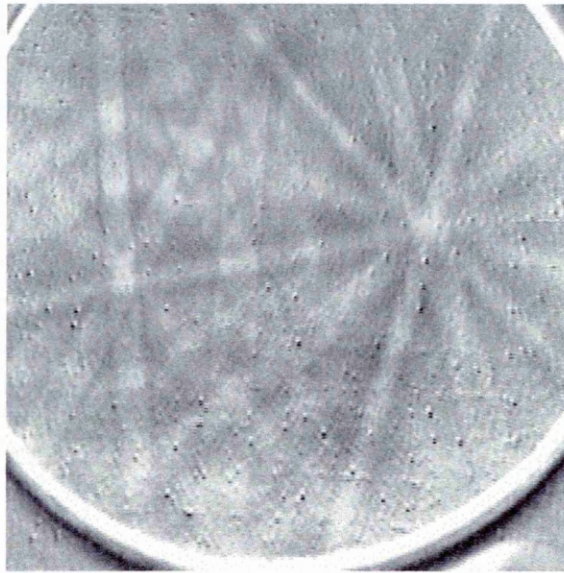
**Figure 12 A schematic showing the formation of one pair of Kikuchi lines from the diffraction of the electron beam with one family of lattice planes.**

Figure 12 is a schematic demonstrating how an EBSD pattern is formed on a phosphorous screen through the interaction of the beam with the sample. As stated previously focusing the electron probe on a single grain (crystal) causes the atomic planes within to Bragg diffract the scattered probe. Because of the multiple electron scattering, virtually all the planes in the crystal are able to diffract, and the diffraction process will give rise to many diffraction lines, which form a diffraction pattern. Since the Bragg condition can be satisfied from both sides of a lattice plane two cones of electron radiation are produced after diffraction for each plane. When a flat surface, such as the phosphorous screen, is placed within the path of this radiation the cones will appear as pairs of straight lines. Bragg angles are

relatively small for the electron source of an SEM, around  $0.5^\circ$ , and so the apex angle of the cones is so large the lines appear straight. These are Kikuchi lines and the pattern produced is equivalent to a Kikuchi map observed in the TEM. Therefore each pair of lines represents a lattice plane with the actual trace of the plane lying equidistant between the pair. From the Bragg equation the interplanar spacing is inversely proportional to the Kikuchi line spacing. Zone axes, or poles, are identified where line pairs intersected.

The total angular range of a Kikuchi pattern depends on the distance between the specimen and the phosphorous screen, in that the greater the distance the smaller the range. For EBSD about  $80^\circ$  of pattern was visible in an EBSD pattern.

### 3.6.3. Interpretation of EBSD Patterns



**Figure 13 EBSD pattern from the mild steel**

Figure 13 shows a typical EBSD pattern collected from the mild steel. It demonstrates the pairs of parallel lines that intersect at various positions within the pattern. As stated previously the EBSD pattern could be considered as a map of the angular relationships between atomic planes in a small region, which in the SEM was down to approximately  $0.5\mu\text{m}$  in size, depending on the probe size.

Analysis of an EBSD pattern can yield significant information. As stated before each line pair (band) within an EBSD pattern represents an atomic plane, the width of the band is inversely proportional to the interplanar spacing, and a point of intersection represents a zone axis. This information, in conjunction with measured angles between planes and crystal directions can be used to identify the phase producing the pattern. If the crystal structure of the phase being analysed is already known, then the EBSD pattern can be used to determine the orientation relative to a reference direction, for example the electron beam or sample normal.

#### 3.6.3.1. Automatic Pattern Indexing

Integral to automatic pattern indexing is the Hough Transform. This is essentially a image convolution process that detects straight lines such as Kikuchi lines, which are essentially straight although there is some curvature present but is undetectable due to the Bragg angles involved being so small. Therefore the Hough Transform has been designated the optimum convolution for identifying the important features of a Kikuchi pattern for subsequent indexing [30].

There are two parameters within Hough space to describe a straight line, represented by  $\rho$  and  $\theta$ , and are shown in Figure 14.

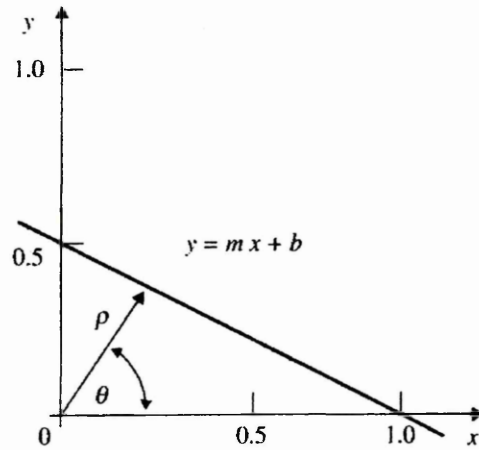


Figure 14 A plot demonstrating how lines are defined in Hough space.

$\rho$  is the nearest distance from the designated centre of the image, and thus is perpendicular to the line, and  $\theta$  is the angle this line makes with one of the axes. The line is then described as a vector,  $(\rho, \theta)$  described using polar co-ordinates thus:

$$\rho = x \cos(\theta) + y \sin(\theta)$$

Equation 9

Where  $x$  and  $y$  are co-ordinates specifying the location of the point in Cartesian parameter space.

This vector is then represented as a point within Hough space on a graph with  $\rho$  and  $\theta$  as the axes. However, the point could be on lines in all directions that pass through it. All the vectors that represent all these possible lines result in a sinusoidal line within Hough space.

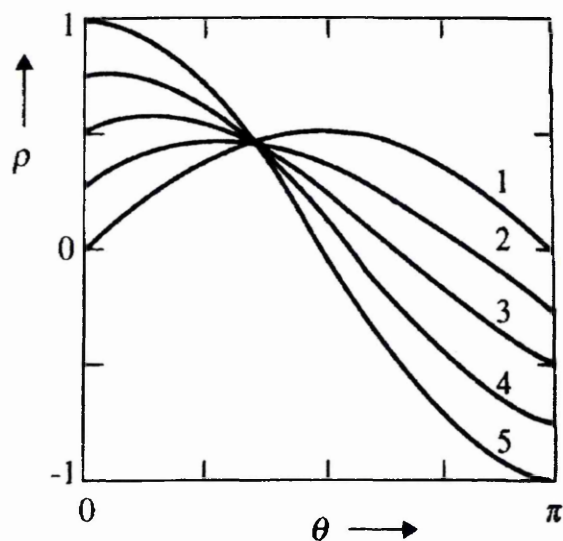


**Figure 15 A plot showing all the vectors representing a line in Hough Space**

If many points along a line within the original image, in this case the Kikuchi pattern, is then translated into Hough space in the same manner then intersections of the sinusoidal lines are then seen. This is demonstrated in Figure 15 where five

points have been translated. This is because all five points will return the same vector values for the given straight line.

In order to distinguish a straight line from the background then pixel values are introduced, e.g. the grey level, and are accumulated to each point in Hough space. A straight line is then distinguished when the intersection point of many sinusoidal lines is of a prescribed value. A straight line within the original image, i.e. a Kikuchi line, has higher grey level values than the background and is plotted within Hough space with consequently higher accumulated grey level values.

### 3.6.4. Crystal Orientations

Orientations, such as a crystal orientation to the rolling direction, are expressed using the following matrix:

$$A = \begin{matrix} & a_{11} & a_{12} & a_{13} \\ a_{21} & a_{22} & a_{23} \\ a_{31} & a_{32} & a_{33} \end{matrix} \quad \text{Equation 10}$$

where

$$a_{13} = h/C, a_{23} = k/C, a_{33} = l/C$$

$$a_{11} = u/D, a_{21} = v/D, a_{31} = w/D$$

$D = (u^2 + v^2 + w^2)^{1/2}$ ,  $C = (h^2 + k^2 + l^2)^{1/2}$  and  $(hkl)[uvw]$  describes a texture using Miller indices, i.e. (normal direction)[rolling direction]. Hence texture can be found from the third column followed by the first column. The middle column could be derived from the other two since the elements of a row or column,  $x, y, z$ , are unit vectors which are mutually perpendicular, and so

$$x^2 + y^2 + z^2 = 1.$$

**Equation 11**

#### 3.6.4.1. Misorientations

Misorientation is the orientation of one crystal to an adjacent one. It can be described by the angle/axis pair  $(\theta/l)$ , which involves three independent degrees of freedom, one for the angle and two for the axes and is derived from equation 11. The axes are essentially a direction that has the same Miller indices in both grains where if one grain was rotated about  $l$  through the misorientation angle  $\theta$  then the lattices of both grains are superimposed.

### 3.6.5. EBSD Examination Procedure

For a typical EBSD examination of a sample the following methodology would be used. First the camera and software system are calibrated using a standard single crystal presented to the camera with a predetermined orientation. This enables the systems geometry to be measured and aligned. A software specific calibration would be run to establish the geometry between the microscope, specimen, camera and diffraction pattern. This ensures that patterns collected from subsequent specimens are correctly indexed.

#### 3.6.5.1. Calibration

Calibration, as with most systems, is an integral part of ensuring that subsequent analyses produce accurate results. Within the calibration set up the working geometry, that is the working distance, the specimen tilt and consequently the distance from the source point and the pattern centre, were determined. Once these conditions were set up then all subsequent use of the EBSD system had to also use this working geometry. Essentially once calibration had been completed then the system could be optimised for orientation mapping.

Initially a germanium single crystal sample was mounted on a sample holder and placed within the microscope chamber. Once a vacuum had been obtained then the sample was tilted to  $70^\circ$  and the predetermined working distance of 10.2mm was set. This distance was predetermined by the microscope geometry and was the eucentric position. The sample was cleaved along the (100) plane and, being a single crystal, produced a readily recognisable Kikuchi pattern.

The calibration routine followed three steps:

1. Entering the crystallographic parameters of the element producing the Kikuchi pattern.
2. Finding the pattern centre.
3. Calculating the distance between the pattern centre and the source point.

Step 1 simply required inputting the element, in this case germanium, and so the system could then reference the crystallographic parameters it had stored. Step 2 involved drawing lines accurately within three Kikuchi band sets. The drawing of the lines was repeated for the same band sets but with the CCD camera position further from the specimen. The Kikuchi bands were further apart and the intersections of the bands (zones axes) were also further apart when the CCD camera was further out. The only point that should remain the same for both camera positions was the pattern centre. It was important that the lines drawn were accurately on the centre of the band sets. The accuracy in the determination of the pattern centre was dependent on the drawn lines being relatively close to one another within the band sets.

The final step involved identifying two known zone axes of a known angular separation. This was achieved by drawing two lines that intersected at the zone axes and then inputting the crystallographic angle between the zones. The distance between the two zones was measured in pixels on the pattern and this was related to the actual crystallographic parameters of the element from which the distance the pattern was projected, i.e. the distance between the source point and the pattern centre, was calculated.

By moving the camera with respect to the specimen the pattern centre co-ordinates were established. From knowledge of the pattern centre the distance from this point to the source point could be found from the location of two or more zones axes in the diffraction pattern using the product of:

$$\cos \theta = x.x1 + y.y1 + z.z \quad \text{Equation 12}$$

where  $x.x1$  and  $y.y1$  are the co-ordinates of the two zone axes  $\theta^\circ$  apart and their  $z$  co-ordinate is the distance required, which can be determined since it is the only unknown.

#### 3.6.5.2. Collection of Electron Back Scatter Patterns

The EBSD patterns were formed using a Philips FEI, XL30 ESEM-FEG. A low light CCD camera was used to collect the patterns from the phosphorous screen detector. The diffraction patterns were stored and analysed on a computer using Oxford Instruments OPAL software system running on an ISIS 300 system.

The specimen was located on a holder and then tilted to approximately  $70^\circ$  to the beam. A tilt correction was applied to the image to remove the contraction of the image. The beam was accelerated using 20KeV and the specimen was held at a working distance of 10.2 mm. Occasion was found where the accelerating voltage was increased to 25KeV to improve the pattern quality. Although an increase in accelerating voltage increased the distance between the Kikuchi lines as per the Bragg condition, this had no bearing on the misorientation results. Simply the misorientation data represented the orientation from one crystal to its neighbours and so this data was not changed if the same working conditions, e.g. accelerating voltage, were maintained throughout the mapping session.

#### 3.6.5.3. Resolution and Mapping times

The resolution factors involved in an EBSD system are categorised as spatial and angular resolution. There were various factors that had to be considered when optimising for either spatial or angular resolution and these included the probe current and accelerating voltage, the specimen tilt, the element under investigation and the working distance. Each of these factors was considered in terms of obtaining misorientation and grain sizes, that is from the perspective of the work described in this thesis.

The time required to collect a data point from a scan depends on the slowest of either the time to acquire an analysable pattern, the time required to analyse the pattern and the time to reposition to beam or stage. The first factor depends ultimately on the material and microscope operating conditions, the second on the processing speed of the computer and the third is faster for a beam scan than for a stage scan [21].

Since an accurate grain size was sought using EBSD then the optimum spatial resolution had priority. The importance of the spatial resolution to grain size was described in section 3.4 whereas in this section the conditions to reach this optimum are described. This resolution is defined as the overlapping distance between two diffraction patterns and is a function of the specimen tilt, probe current and accelerating voltage [93]. Generally the lower the value of the accelerating voltage, probe current, specimen tilt, and working distance the greater the resolution. However, there were compromising factors that also had to be considered, for example a decrease in specimen tilt resulted in a decrease in the back scatter yield and so the optimum was found to be around 70°. The yield was dependent on the depth of penetration where a higher accelerating voltage produced a higher depth reducing the back scatter yield since electrons that penetrate beyond a depth of around 20 to 50nm could not undergo back scattering. Also, with a decrease in probe current there was a decrease in the line definition of

the Kikuchi pattern decreasing the ability of the system to index a pattern. This situation was improved with image enhancement techniques although this increased the mapping time considerably. The use of a field emission gun also improved this situation since the spot size from this electron source was not as sensitive as a W filament. With the ability to increase the beam current without increasing the spot size significantly then line definition was increased without compromising the spatial resolution beyond the desired limit, i.e. to measure the smallest grain accurately.

Another important factor concerning resolution was the specimen preparation since lattice strain played an important role in pattern quality for subsequent indexing. Experience from the steels used in this thesis showed that an improved pattern quality could be obtained with a higher accelerating voltage. Also, by increasing the gain on the low light camera and utilising the background subtraction facility as an image enhancement technique then reasonable orientation maps of around 70 to 100 grains were obtained within 8 hours. In other words a map was obtained without having to increase the pattern integration time beyond what was expected for a sample without lattice strain.

### 3.6.6. Sources of error

#### 3.6.6.1. Orientation Measurement

According to Randle there were 4 sources of error that should be taken into consideration [26]. These are as follows:

1. Specimen position error: the importance of positioning the specimen within the holder relative to the microscope axes was only relevant if orientations were to be determined relative to the specimen axes. However, since all the work reported in this thesis was relevant to the orientation of one crystal to another, i.e. misorientation, then no error was induced from this.
2. Pattern interrogation errors: this was important for the calibration set up in that the location of zone axes by drawing in lines could lead to errors for subsequent automatic indexing.
3. Non-linearity errors in the TV camera: this would be apparent as a distortion in the diffraction pattern at the edges of the monitor. Any such distortion was confined to the edges of the patterns found and since it was the main central area that was clear enough for indexing this distortion did not introduce an error in the indexing.

4. Calibration errors: essentially the location of the pattern centre and the distance between the source point and this centre was crucial for accurate orientation measurement and two important factors had to be taken into consideration. The first was described above in 1 and was not significant for misorientation measurements. The second required reproducing the working distance to that of the calibration set up, which produced an associated error in orientation of approximately  $0.5^\circ$ .

Since measurement of misorientation was reported and that care was taken in setting the working distance the maximum associated error was approximately  $0.5^\circ$ .

### 3.7. Image distortion on the SEM

It was observed that the initial EBSD maps incorporated a distortion as shown below:

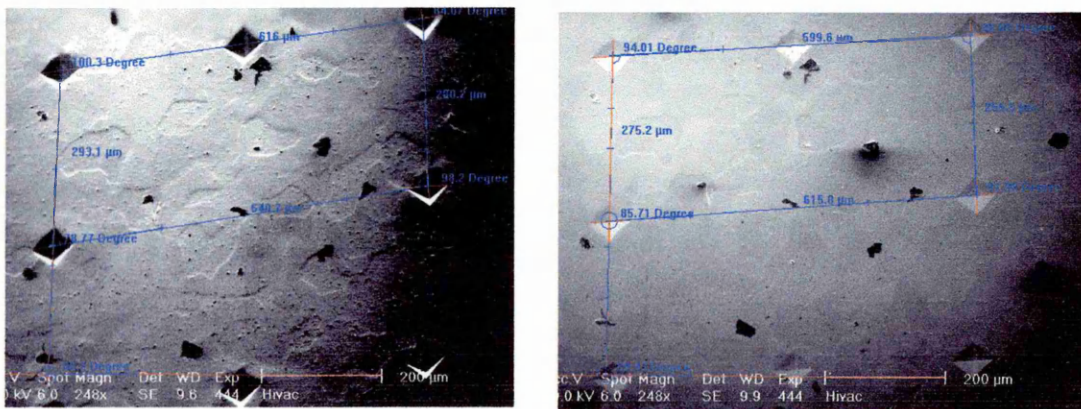


**Figure 16 A comparison of the distances between indentations between images taken at specimen at zero tilt and images at 70° tilt**

Despite a tilt correction being applied to the image after tilting to 70° there was a shearing effect, which is demonstrated by the top left angle shown in Figure 16 being larger for the tilt image (left) than the one with no tilt (right).

Such a distortion would introduce an error in grain size measurement of the EBSD map. It was assumed that this was induced by a misalignment within the ESEM chamber and that subsequent image processing would be adequate to correct this image distortion for grain size measurement.

This was achieved by comparing the measurements made of each image at no tilt and at tilt and then correcting for the shear angle and the contraction or expansion in either the horizontal or vertical directions. Consequently greater control was achieved over the tilt correction applied within the ESEM software and hence greater confidence in an accurate match between the optical image and the EBSD map. Subsequent analyses of the comparison of the grain size from measuring the EBSD images and the optical images were therefore allowed.

## **4. RESULTS**

### **4.1. Specimen preparation**

The following section details the results produced from testing various etches and suspensions, and combinations thereof in order to optimise specimen preparation for subsequent analysis using electron back scatter diffraction and automatic image analysis.

The polishing suspensions tested were:

1. Buehler's Gamma Micropolish No 3 Alumina B.
2. Struers' OP - A Acidic Alumina made up with 50% water.
3. Struers' OP - A Colloidal Silica.

The etches tested were:

Etch	Composition
Nital (2% solution)	40cm <sup>3</sup> nitric acid, 1960 cm <sup>3</sup> alcohol
Marshall's Reagent	5ml sulphuric acid, 8g oxalic acid, 100ml mixed with 30% volume hydrogen peroxide
Ferric Chloride	60g anhydrous ferric chloride, 100 cm <sup>3</sup> hydrochloric acid and making up to 2000 cm <sup>3</sup> with alcohol

**Table 6 The compositions of the etches tested for the sample preparation of the mild steel.**

The polishing cloth used throughout was Buehler's 1µm cloth.

#### 4.1.1. Results

These results refer to each preparation technique tested and reflect how the optimum was arrived at.

1. Buehler's Gamma Micropolish No 3 Alumina B (see Figure 17):

- After three minutes polishing an apparent scratch-free surface was achieved although some scratches appeared within a few grains after etching with a 2% nital solution but to a tolerable level (for the definition of a tolerable level refer to section 3.2.2.).

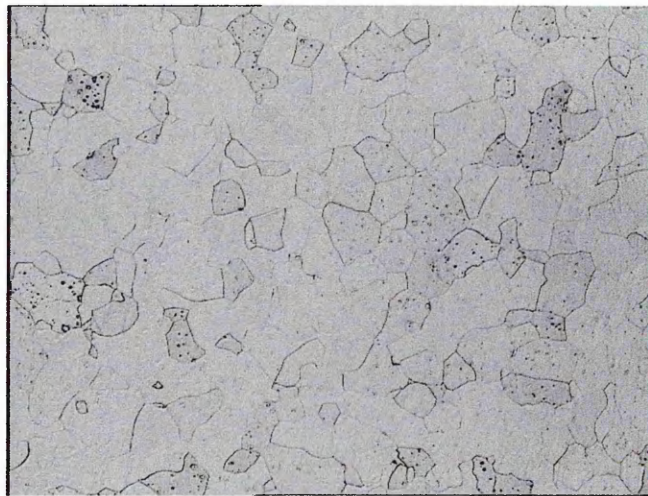


**Figure 17 An image of the specimen after polishing with Buehler's Gamma Micropolish No 3 Alumina B and etching using a 2% nital solution.**

2. Struers' OP - A Acidic Alumina made up with 50% water (see Figure 18):

- After three minutes polishing there were a significant number of scratches left although these were partially removed with a further three minutes polish although not as well as Buehler's Gamma Micropolish No 3 Alumina B. Etching with a 2% nital solution did not reveal any further scratching. It was expected that the required mirror finish would be achieved with further polishing but would also produce excessive relief.
- The specimen was subsequently re-polished to a 1 $\mu$ m diamond finish, polished using the suspension for five minutes and then etched using ferric chloride. The required mirror finish was achieved.

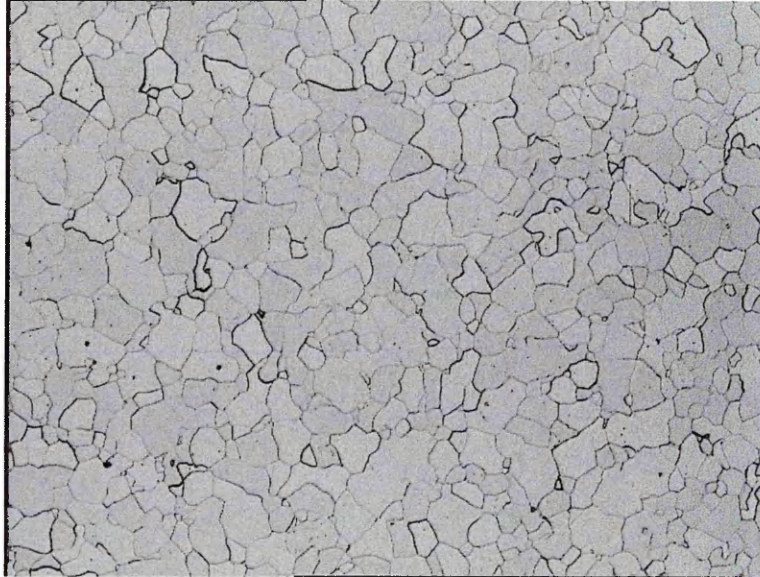


**Figure 18 An image of the specimen after polishing with Struers' OP, an Acidic Alumina, made up with 50% water and then etched with ferric chloride.**

3. Struers' OP - A Colloidal Silica (see Figure 19):

- A significant number of scratches remained after a three minutes polish although they were mostly removed after a further two minutes to a satisfactory level (as defined in section 3.2.2.).

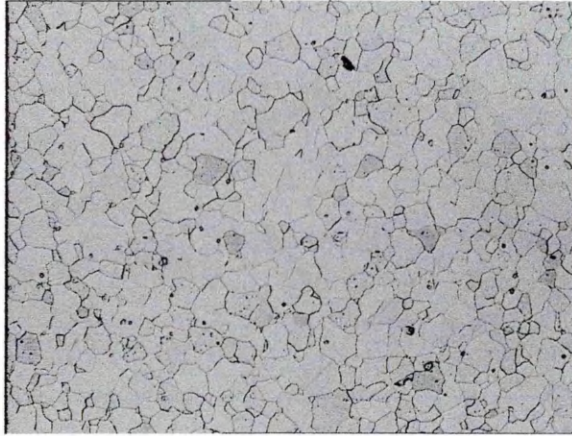


**Figure 19 An image of the specimen after polishing using Struer's Colloidal Silica and etching using a 2% nital solution**

It was also possible to polish and etch specimens simultaneously. In order to investigate an ideal combined polish/etch technique the following mixtures of etches and polishing suspensions were tested:

1. Ferric chloride with Buehler's Gamma Micropolish No 3 Alumina B.
2. Nital with Buehler's Gamma Micropolish No 3 Alumina B.
1. Buehler's Gamma Micropolish No 3 Alumina B mixed with various percentage volume concentrations of ferric chloride (see Figure 20).

1.1. 50% volume ferric chloride:

- After a two minutes preparation the specimen was over-etched with a significant number of scratches remaining. To slow down the etching effect, allowing more time for polishing, a mixture with less etch was tested.

1.2. 43% volume ferric chloride:

- After a one minute preparation the specimen was partially etched but with too many scratches remaining.
- A further one minute again produced over-etching. A further reduction in the percentage volume of etch was therefore tested.

1.3. 20% volume ferric chloride:

- After two minutes it is clear that the rate of etch attack was more controllable but there remained too many scratches even after a further two minutes.

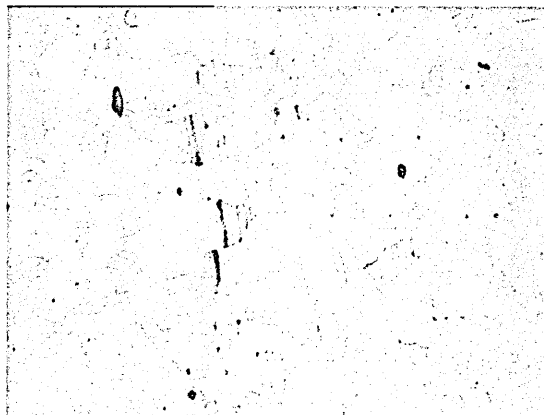


**Figure 20 An image of the specimen after using the Buehler's Gamma Micropolish No 3 Alumina B and 20% volume ferric chloride mixture.**

2. Nital with Buehler's Gamma Micropolish No 3 Alumina B with various percentage volume concentrations of nital:

2.1. 5% volume nital (see Figure 21):

- After five minutes preparation scratches were not removed sufficiently and etching was only slight. However, more polishing could induce relief, which was to be avoided. (The reasons for avoiding relief were stated in section 3.2.2.). It was concluded that increasing the percentage volume of nital in the polish/etch mixture could remove scratches more efficiently plus provide an attack allowing Marshall's reagent to be utilised subsequently. A pre-etch with nital was required for the best results using Marshall's reagent. (For the use of Marshall's reagent in the preparation of this specimen see section 3.2.2.).

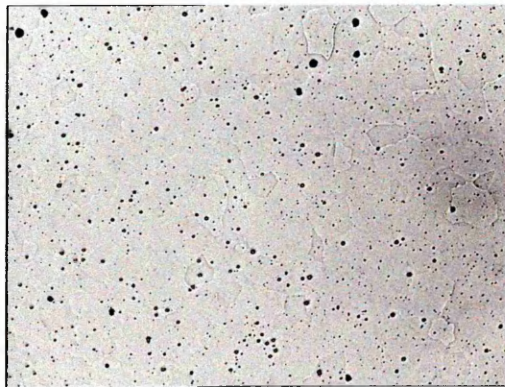


**Figure 21 An image of the specimen after using Buehler's Gamma Micropolish No 3 Alumina B and a 5% nital polish/etch mixture**

2.2. 10% volume nital (see Figure 22):

- After two minutes preparation the etch attacked much faster and hence was less controllable and over-etching occurred. However, scratches were removed to a satisfactory level, as defined in section 3.2.2.
- The above stage was repeated on another specimen to ensure that the results were consistent which they proved to be. To reduce the etch attack but continue with a similar stock removal a compromise of the last 2 stages was the next combination.

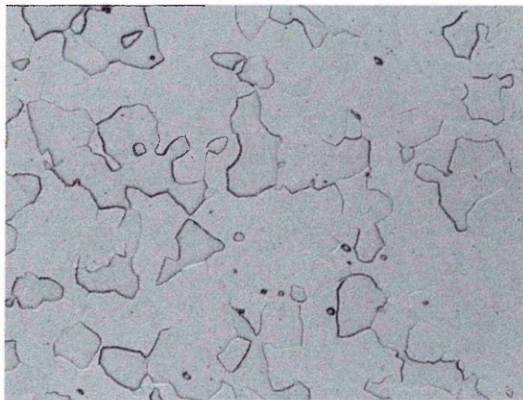


**Figure 22 An image of the specimen after using the Buehler's Gamma Micropolish No 3 Alumina B and a 10% nital polish/etch mixture**

2.3. 7% volume nital (see Figure 23):

- After nine minutes polishing there still remained a significant number of scratches although the etch attack was well controlled allowing for a subsequent etch using Marshall's reagent.

- Again this technique was tested on another specimen producing the same results. It was concluded that nine minutes was too long and relief would have been produced.

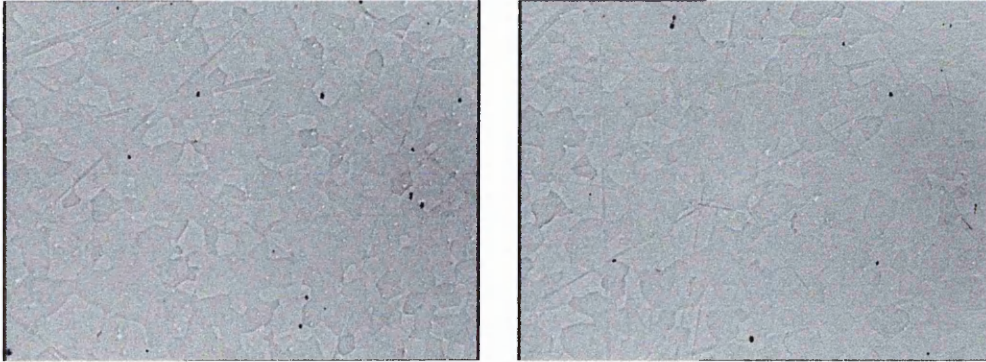


**Figure 23 An image of 2 specimens after using the Buehler's Gamma micropolish No 3 Alumina B and a 7% nital polish/etch mixture.**

## **4.2. Grain size measurements**

This section describes the results produced from characterising the mild steel for grain size using various methods. The results produced allowed for analyses to be conducted in the following areas:

- An inter-comparison of manual methods (section 4.2.1).
- The effect of sampling on the representation of the microstructure (section 4.2.2).
- The effect of missing boundaries on the measurements using manual and automatic methods (section 4.2.3).
- A comparison of the results from using optical imaging and Electron Back Scatter Diffraction (EBSD) (section 4.2.4).
- A comparison of the results from measuring using manual and automatic methods (section 4.2.5).

#### 4.2.1. Inter-comparison of manual methodologies

There were four manual grain size measurement methods utilised:

- Lineal method
- Planimetric method
- Single circle method
- Three circle method

Each method was described in section 3.3.2.

It was the purpose of this section to compare the results from using these methods to measure samples of the mild steel and then to determine the accuracy of each.

Figure 24 shows the mean results from the measurements using each of the manual methods. Around 50 grains were measured in each of the seven fields of view per specimen. This method mean value was calculated from averaging the grain size numbers from each field of view. There were a total of 6 specimens and the mean values of each across all the methods are also shown. The specimen mean was calculated from averaging the mean values from each method. This was effectively a mean of a mean, which was shown to be equivalent if the specimen mean was calculated from averaging the G

numbers from the total number of fields of view measured in each sample using all the methods.

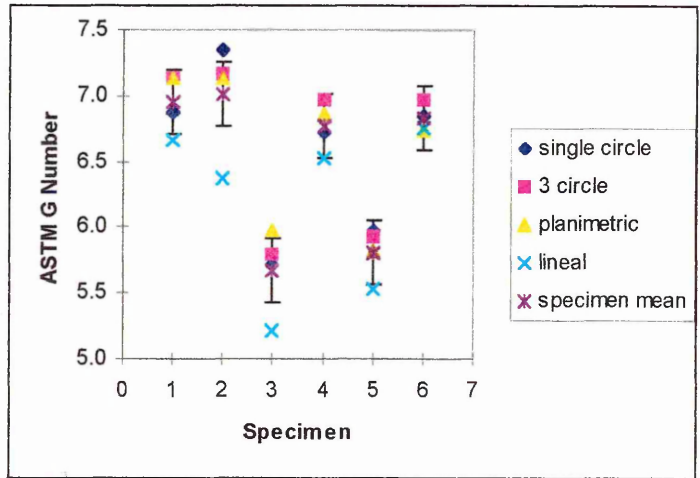


**Figure 24 A plot of the ASTM grain size numbers for each specimen and for each method**

Specimens 3 and 5 demonstrated a strong deviation from the other four specimens. The sample mean was 6.53 grain size number and was calculated from averaging the grain size numbers from all seven fields of view measured by all four methods in all six specimens, i.e. from 168 fields of view (see Table 7). Indeed, the variation in the specimen means was significantly greater than the standard errors of the individual specimen means, suggesting a real specimen to specimen variation. The correlation between the different methods also supports this since the variation in the means between individual methods for the same specimen was low, namely 6.58 (0.27), 6.66 (0.28), 6.61 (0.26), 6.18 (0.29) for the single circle, three circle, planimetric and lineal

#### 4.2.1.1. Effect of Increasing fields

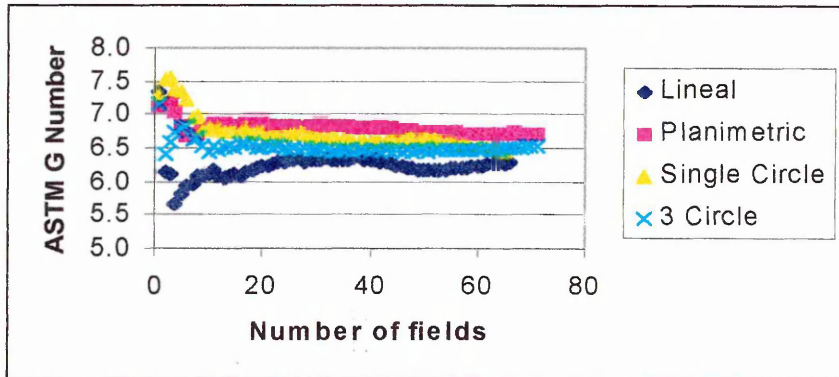


**Figure 25 A plot showing the effect of increasing the number of fields measured on the grain size number.**

The effect of increasing the number of fields on the cumulative average grain size number is shown in Figure 25. These results were produced from eight specimens, the same six specimens used for the analyses reported in section 4.2.1 plus a further two from the same reference sample. Additional fields were measured to provide a sufficient number to establish that the mean G number had converged. The G numbers produced from less than 10 fields were strongly affected by a small or large random measurement. Therefore, if the ordering of the fields was changed this would necessarily change the results in this region.

There were approximately 50 counts per field of view, and the fields were organised in a random fashion before cumulative averages were taken. It is

interesting to note that the planimetric, single circle and 3 circle were all converging to a value of between 6.7-6.8G units, whereas the lineal appeared lower at 6.3G units.

Within the standard ASTM E112 [95] a chart was shown comparing relative percentage accuracy with the number of grains counted for both the lineal and planimetric methods. Similar charts were created using the data from characterising the reference sample thus allowing a comparison with E112. Figure 26 was produced using the same equations defined in E112 to calculate the percentage relative accuracy.

This was achieved by taking the number of grains counted for each field of view, calculating either the mean lineal value or the mean number of grains per unit squared, depending on the method used, and finally calculating the percentage relative accuracy for a 95% confidence level according to the equation:

$$\%RA = \frac{95\%CI}{\bar{x}} \times 100 \qquad \text{Equation 13}$$

Where %RA is the percentage relative accuracy

CI is the confidence interval

$\bar{x}$  is the mean

It was demonstrated that a significantly larger number of grains were required for the planimetric than for the lineal, with approximately 2600 for the former and 600 for the latter, for the same 10% relative accuracy.

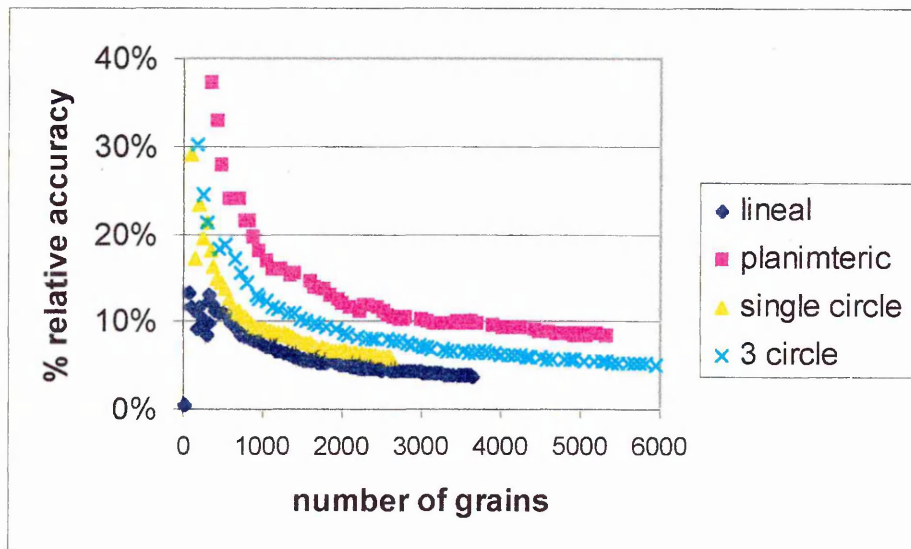


**Figure 26 A plot of the percentage relative accuracy against the number of grains measured for all methods**

The results of the other two methods was found between these two extremes with the single circle requiring approximately 1000 grains and the three circle 1400 grains for the same 10% relative accuracy.

#### 4.2.2. Sampling

The question of unbiased representation is an important one in grain size measurement. Here, “representative” was defined as ensuring that the grain size measurements incorporate the effects of the spatial variation in the grain size throughout the material [96]. The purpose of the work reported in this section was to use the database of results acquired from the measurement of 168 fields in 6 specimens. This allowed for an investigation into the relative importance of the number of specimens, the number of fields per specimen, and the number of grains per field to the final grain size number. This investigation was conducted using both the planimetric and lineal methods as these were stated to be the most accurate in ASTM E112.

##### 4.2.2.1. The number of specimens

The mean grain size number for each specimen was calculated by summing the grain size numbers for each field in that specimen and then by dividing by the number of fields.

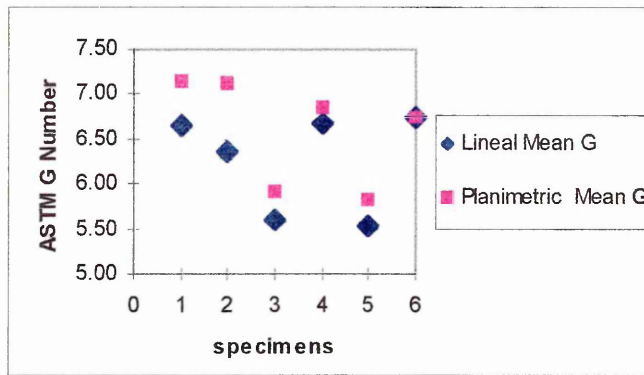


**Figure 27 A plot of the ASTM G number from each specimen from using the lineal and planimetric methods**

Figure 27 demonstrates that there was a significant variation from specimen to specimen of 1.2 grain size units for the lineal and 1.3 grain size units for the planimetric. Comparing these results with the sample mean, (see Table 7), namely 6.53 grain size number, the specimen to specimen variation was again significant with a maximum of 1.0 grain size unit for the lineal and 0.6 grain size unit for the planimetric.

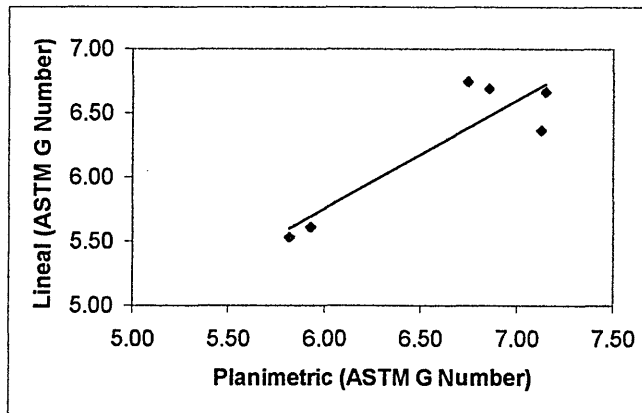


**Figure 28 A plot of the ASTM G numbers of the lineal method against the planimetric method**

Figure 28 correlates the results from each specimen given in Figure 27. The linear trend line was calculated using the least squares method [94]. The clustering effect was due to the variation from specimen to specimen. The trend-line demonstrated that the correlation between the methods was reasonable as the results produced by both methods were approximately within  $\pm 0.5$  grain size unit of each other. The equations used for converting from a mean linear intercept and a number of grains per  $\text{mm}^2$  will contribute to the scatter [95]. The conversions from mean linear intercept values to the ASTM G number were exact for circles but not for equi-axed grains. However, they were exact when converting from the number of grain per  $\text{mm}^2$  and converting from both methods produced an ASTM G number within approximately 0.01G units.

#### 4.2.2.2. The number of fields per specimen

In Figure 29 and Figure 30 the grain size numbers measured using the lineal and planimetric methods are given for each field of view. The results from each specimen are also given. Most interestingly, the variation within a given specimen was approximately 0.4-0.6 G units for both the planimetric and lineal methods in all specimens except for two. Specimen 5 varied by 1 grain size unit for both methods and specimen 3 also varied by 1 grain size unit but only with the lineal method.

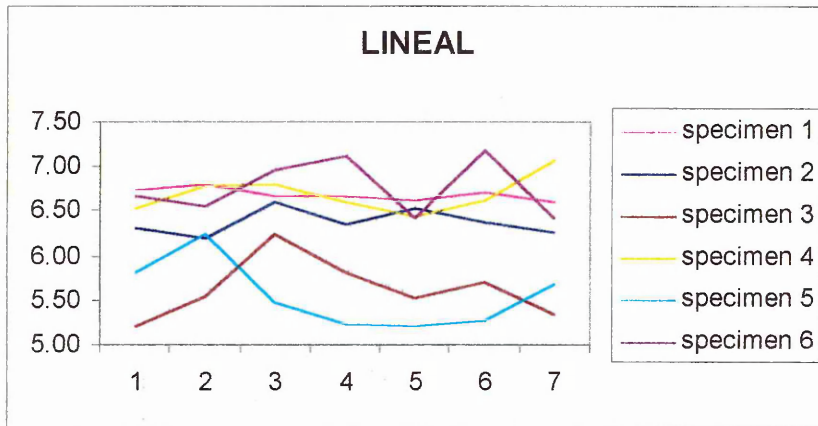


**Figure 29 A plot of the individual ASTM G numbers from each field of view in each specimen using the lineal method**

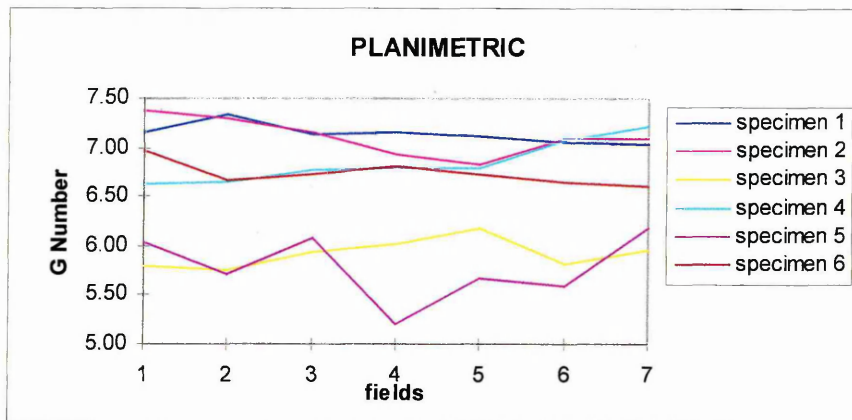


**Figure 30 A plot of the individual ASTM G numbers from each field of view in each specimen using the planimetric method**

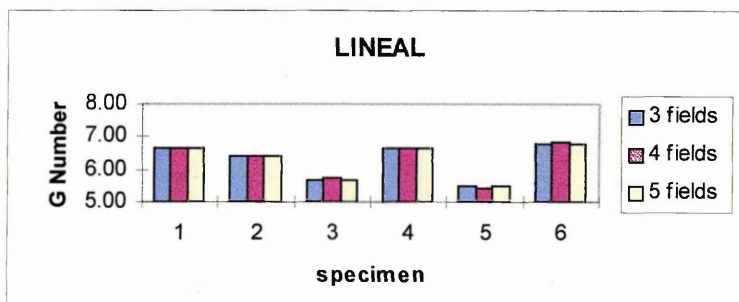


**Figure 31 A histogram of the mean ASTM G numbers from measuring fields of view 3,4 and 5 using the lineal method**

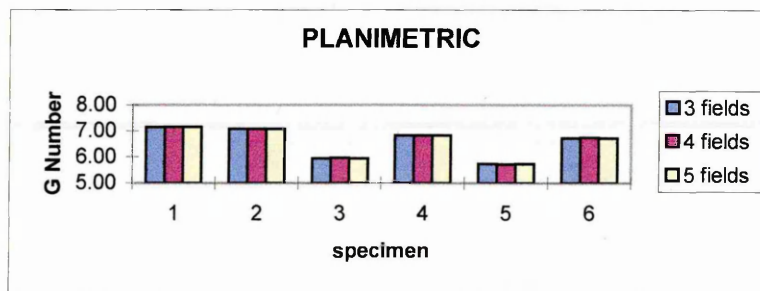


**Figure 32 A histogram of the mean ASTM G numbers from measuring fields of view 3,4, and 5 using the planimetric method**

The effect of varying the number of fields per specimen is illustrated in figure 31 and figure 32. Here the mean from measuring 3, 4 and 5 fields of view was established using the lineal and planimetric methods. This mean was measured by calculating the average G number of the first three fields of view, then the second three and so on until all seven fields of view were measured. Thus five G numbers were established from these averages and the mean of these are reported in these figures. This was repeated for 4 and 5 fields of view. It can be seen that the effect of moving from 3 to 5 fields was small in each specimen, the difference was less than 0.01 to 0.03 grain size unit using the planimetric method and 0.2 grain size unit using the lineal method. The effect on the field mean was also small in the cases of three or four fields. ASTM E112 stipulated that between 3 and 5 fields per specimen should be used for measurement by the lineal method. The final measurement was relatively insensitive to the number of fields measured. Indeed the data reported in figure 31 and figure 32 on the grain size measurements of the mild steel suggested that even with one field per specimen a reasonably accurate average grain size number could be obtained.

4.2.2.3. Number of counts per field

LINEAL				
Specimen	1 line		2 lines	
	G	mli	G	mli
1	6.79	30.42	6.72	31.93
2	6.38	35.06	6.38	35.06
3	5.78	43.16	5.73	44.69
4	7.00	28.28	6.90	30.31
5	5.76	43.47	5.66	46.58
6	6.77	30.63	6.77	30.73
Line mean	6.41	34.66	6.36	35.98
Standard error	0.24		0.25	

**Table 8 Showing the mean linear intercept values and the equivalent ASTM G numbers from measuring along 1 and 2 lines using the lineal method**

For the lineal method two intercept lines were drawn on each field and mean linear intercept values were obtained from each. An investigation was carried out on the effect of using one or two lines per field. From comparing the means

from measuring one and two lines, given in Table 8, it can be seen that the difference produced was very small at only 0.05 grain size unit.

#### 4.2.3. The impact of missing boundaries on grain size measurements

This section reports the results from grain size measurements, using both manual and automatic techniques, on digital images that have been 'doctored' to remove known percentages of grain boundaries. Knowing the percentage of missing boundaries allowed for their impact on grain size measurements to be reported in a quantifiable manner.

#### 4.2.3.1. Manual measurements

Measurements on each digitised image were undertaken using the planimetric, lineal, single circle and three circle manual methods.

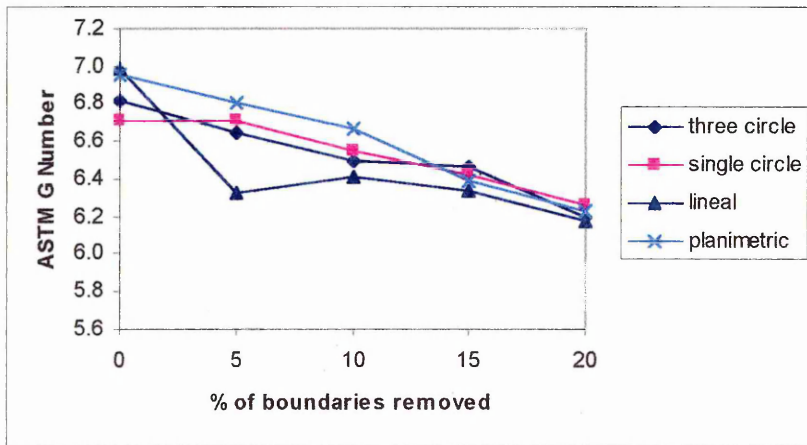


**Figure 33 A plot of the ASTM G number measured on images with 0,5,10,15 and 20% boundaries removed using all the manual methods**

The mean G numbers of the measurements on fields of view with 0,5,10 and 20% missing boundaries using each manual method are shown in Figure 33. The general trend showed that the grain size number decreased as the percentage degradation increased for each of the measuring method. (A decreasing grain size number corresponds to an increasing average grain size, as would be expected with fewer boundaries).

It is important to point out that the results produced in Figures 33 - 36 were independent of the average grain size for a given material. In other words a similar decrease in grain size number would be found with a lower or higher average grain size. This is because the effect of missing boundaries were on the mean intercept or the number of grains per unit area which were calculated from linear equations and then translated into G units.

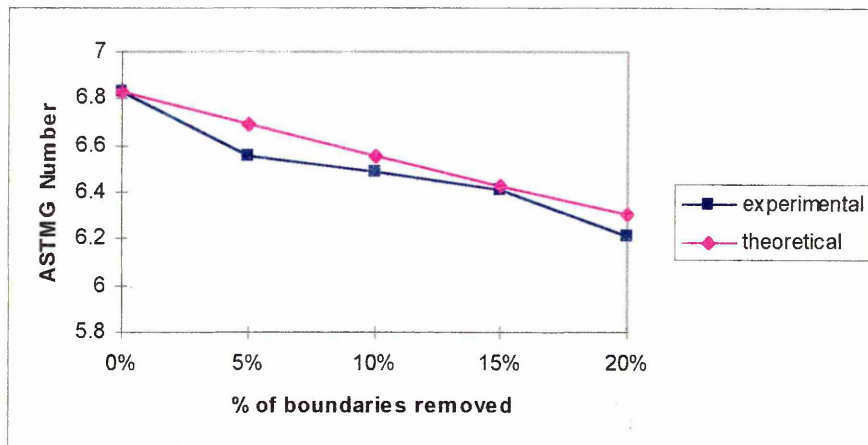


**Figure 34 A plot of the mean of the manual methods measuring the ASTM G number on images with 0,5,10,15 and 20% boundaries removed**

The combination of all the results across each method and each percentage of missing boundaries are presented in Figure 34. From 0% to 20% the change in grain size number was 0.69. The theoretical curve represented in this figure was calculated by using the same value for 0% missing boundaries used for experimental measurements and then decreasing this value by the corresponding 5,10,15 and 20%. This decrease was done on the mean lineal intercept values, not the ASTM grain size number, since it was the intercept values that were directly subject to change due to missing boundaries. The change in the mean lineal intercept values were then converted into G numbers. The predictions of the theoretical curve were confirmed by experiment.

#### 4.2.3.2. Automatic image analysis

A similar investigation into the effect of missing boundaries was conducted using the automatic image analysis system for measuring grain size. The grain size measurement techniques applied here were the single circle, three circle and the lineal methods.

The advantage of using automatic image analysis was that a large amount of data could be produced relatively quickly, thus providing a more statistically significant basis for the investigation [8,10,13].

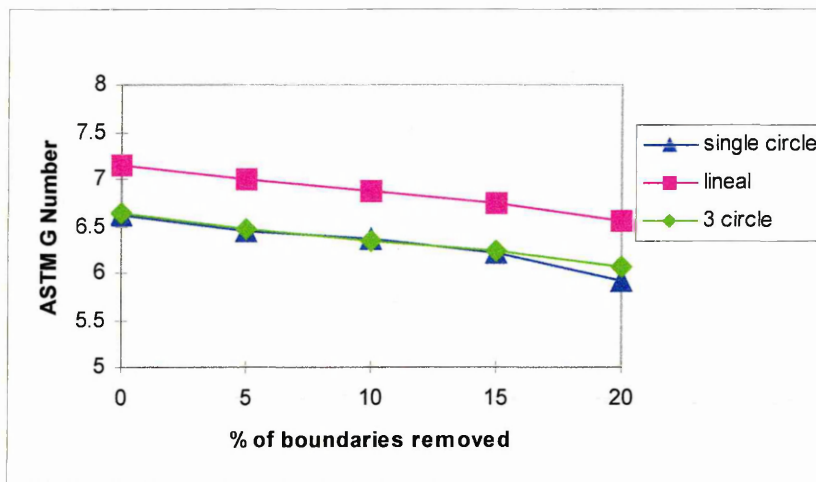


**Figure 35 A plot of the ASTM G number measured on images with 0,5,10,15 and 20% boundaries removed measuring with the single circle, lineal and 3 circle method using the automatic image analysis system**

The results from the three methods are shown in Figure 35, where it can be seen that there was an approximately linear dependence of grain size number with % missing boundaries for each method within the limits of these results. The lineal method data was yielding a higher grain size number than the three circle or single circle methods.

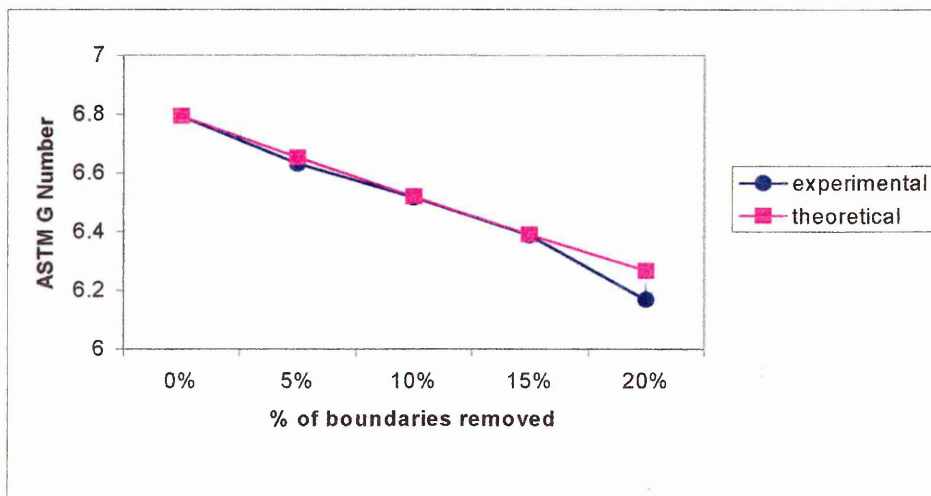


Figure 36 A plot of the mean ASTM G number from measuring with the single circle, three circle and lineal methods using the automatic image analysis system on images with 0,5,10,15 and 20% boundaries removed

Figure 36 shows the results averaged across the different methods as a function of the percentage of missing boundaries. The trend was a decrease in grain size number with the increase in percentage missing boundaries. The results showed that with 20% missing boundaries there was only a change of 0.62 in the grain size number. Again the theoretical curve was confirmed by experiment.

#### 4.2.4. Comparison of automatic image analysis grain size measurements with EBSD

All the results reported in this section were from measuring grain size using an automatic image analysis system on images created from optical microscopy and from EBSD mapping. In this instance the grain areas were measured and reported as  $\mu\text{m}^2$ . The same reference sample as reported previously in this chapter was used, i.e. the mild steel, and one field of view from each of four specimens was measured. Each field of view was indented so that images using both optical microscopy and EBSD could be created on the exact same fields. The measurements using the automatic image analysis system were also compared with manual measurements on the same fields of view.

It was assumed that the grain boundary network reconstructed in the EBSD images represented the true location of these boundaries. The EBSD system colour coded the images according to the orientation of the grains. Therefore, a boundary was located from a change in colour in the image. Locating the boundaries in this manner was deemed to be accurate, and certainly more accurate than locating boundaries from a chemical etch. Therefore, an assessment of how representative grain size measurements and grain size distributions were using optical imaging could then be conducted.

Specimen	Images		
	Optical (pixels)	Lower pixel resolution	Higher pixel resolution
1	755 × 570	255 × 200	875 × 955
2	755 × 570	510 × 335	1530 × 1000
3	755 × 570	255 × 280	641 × 740
4	755 × 570	255 × 385	445 × 660

**Table 9 The image pixel sizes of the optical and the two EBSD images for all four specimens**

Two EBSD images of different pixel resolutions were also created. The lower resolution EBSD images were the original image, as created using the EBSD system. These images were enlarged in both the x and y directions using interpolation, that is more pixels were added to form the grains whilst retaining their shape. Thus EBSD images of a higher pixel resolution were created. This allowed for a comparison of automatic image analysis measurements of grains formed of different pixel resolutions. The actual pixel sizes of the two EBSD images and the optical images are shown in Table 9 for all specimens.

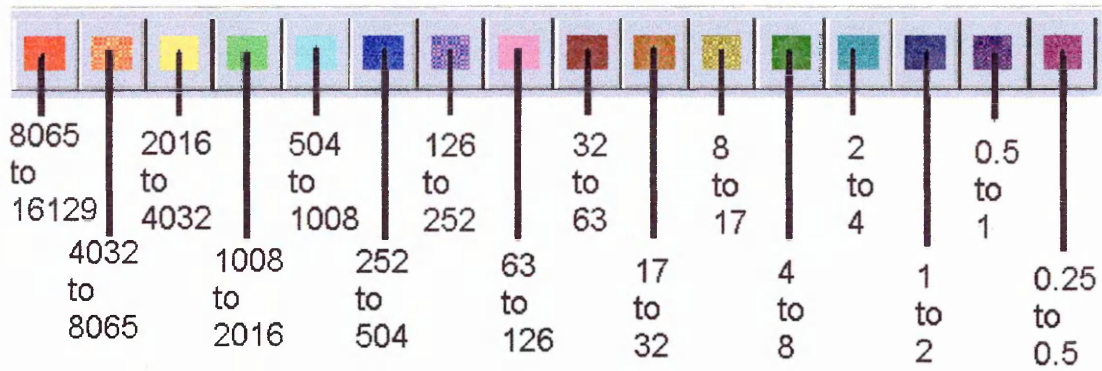


**Figure 37 Colour Code for Grain Sizes**

Colour coding was used to represent the ASTM grain size of each grain measured and the size range assigned to each colour is shown in Figure 37. This allowed for a visual comparison of grain size across the various measurement techniques employed.

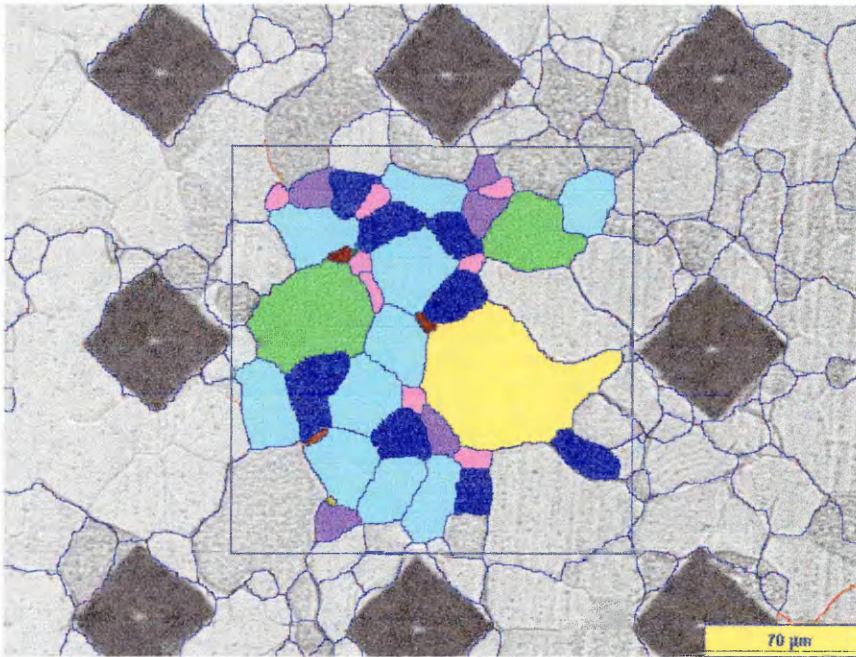


Figure 38 An Optical image of specimen 1 with the measured grains colour coded according to their size

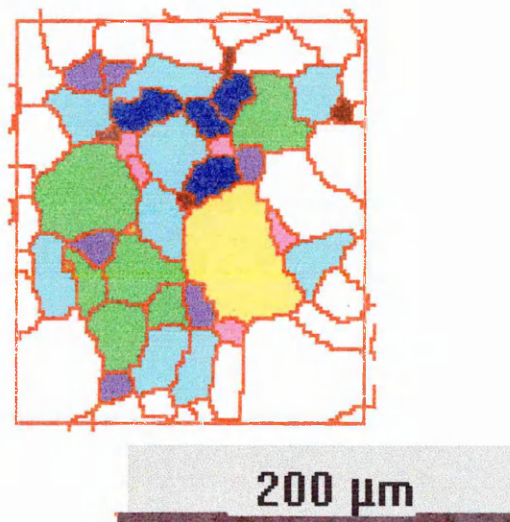
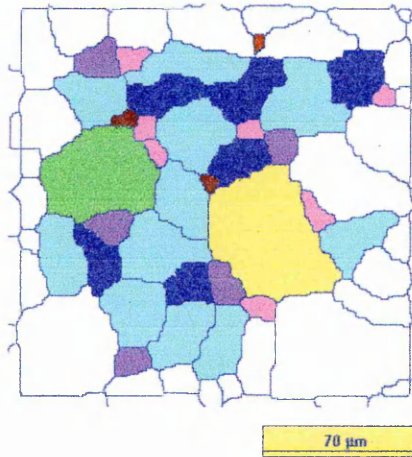
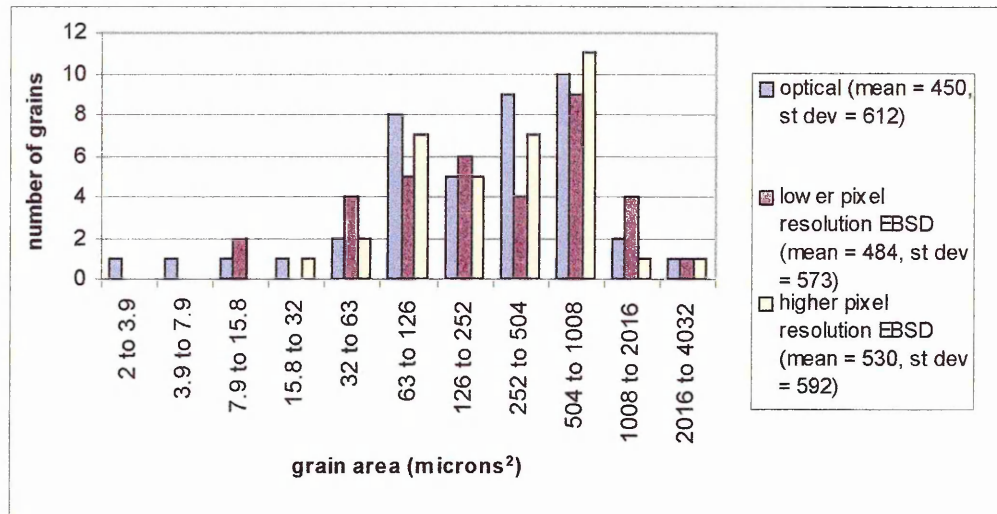


Figure 39 An EBSD image of the lower pixel resolution of specimen 1 with the grains measured colour coded according to their size



**Figure 40 An EBSD image of the higher pixel resolution of specimen 1 with the grains measured colour coded according to their size**



**Figure 41 A histogram of the grain area distributions measured on the optical and EBSD images of both pixel resolutions using the automatic image analysis system for specimen 1**

Figure 41 shows the grain size distributions for specimen 1 using the optical image and both the EBSD images of different pixel resolutions. Figure 38 shows the optical image with the grain size colour code and similarly Figure 39 and Figure 40 are the lower and higher pixel resolution EBSD images respectively.

All the mean values and standard deviation were quoted within the grain size distribution histogram. The difference in the mean grain areas of the EBSD images for both pixel resolutions was  $46\mu\text{m}^2$ . When compared with the optical image the lower pixel resolution EBSD image had a higher mean value by  $34\mu\text{m}^2$  and the higher pixel resolution EBSD had a larger value by only  $80\mu\text{m}^2$ . It is of interest that there was one large grain, coded with light blue, measured

in the higher pixel resolution EBSD image but not in the lower pixel resolution EBSD image despite the former having the larger mean grain area. With one larger grain measured it might be expected that the mean value in the higher pixel resolution EBSD image would be higher.

When comparing the two distributions of the two EBSD images of different pixel resolutions specifically, it could be seen that they were very similar, with only a single grain difference within any one grain size bin. When comparing the optical distributions with EBSD, generally there was a closer match with the higher pixel resolution EBSD for the smaller grains but the reverse applied for the larger grains. The measurements on the optical image also returned more smaller grains than the measurements on either of the two EBSD results.

Applying a colour code representing the grain areas allowed specific grains within a certain grain size range to be identified. Therefore, by comparing the two EBSD images it could be seen that, although there were the same number of grains measured within the 252 to 504 $\mu\text{m}^2$  grain size range, the grains with the corresponding dark blue colour were located in different places within each image.

There were 41 grains measured in the optical image.

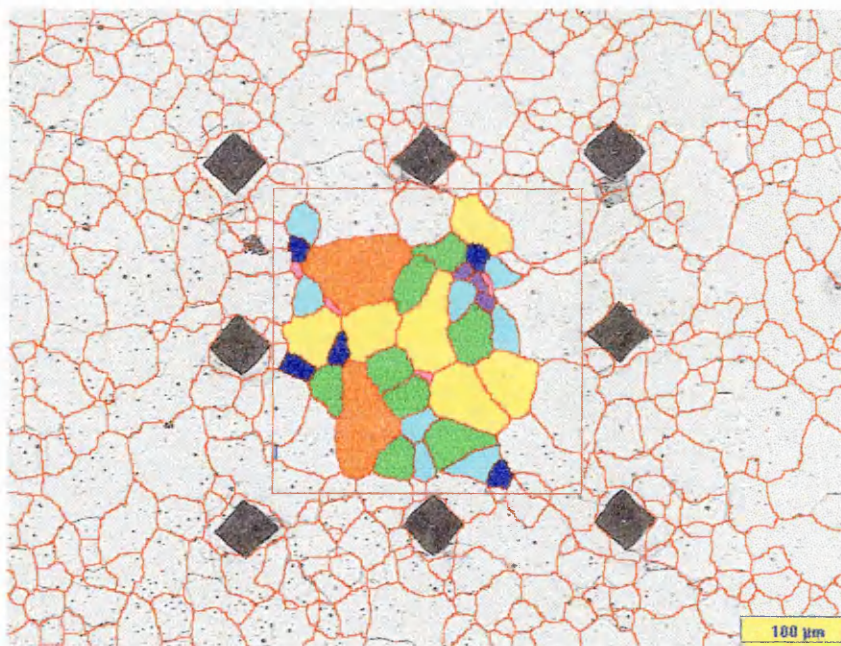


**Figure 42 An Optical image of specimen 2 with the measured grains colour coded according to their size**

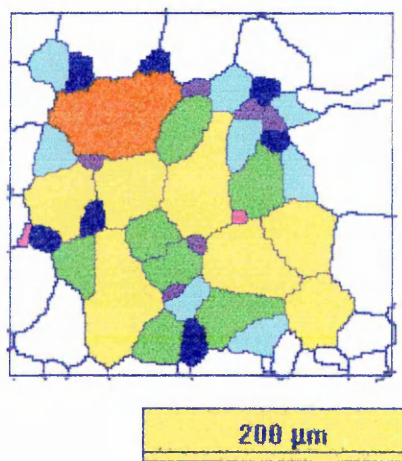


**Figure 43 An EBSD image of the lower pixel resolution of specimen 2 with the grains measured colour coded according to their size**

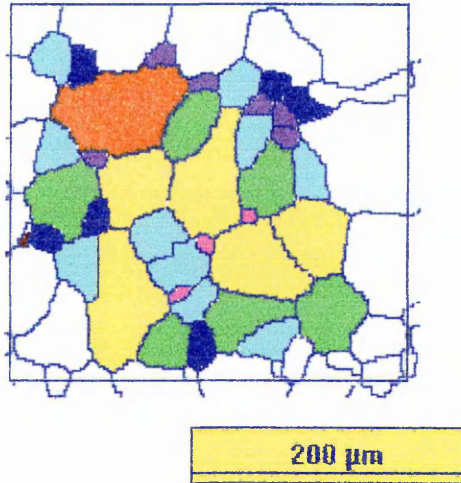
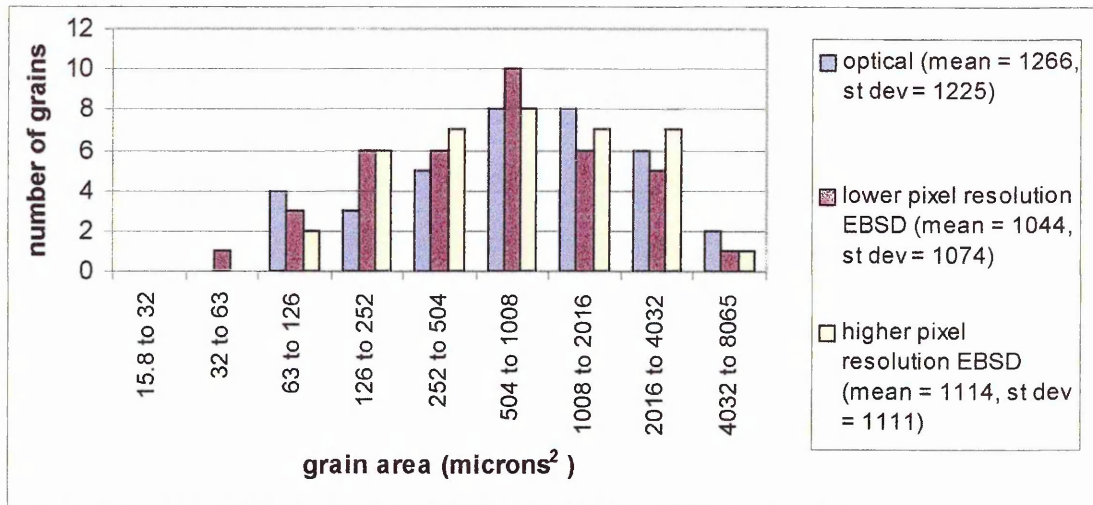


Figure 44 An EBSD image of the higher pixel resolution of specimen 2 with the grains measured colour coded according to their size



**Figure 45 A histogram of the grain area distributions measured on the optical and EBSD images of both pixel resolutions using the automatic image analysis system for specimen 2**

The same layout of the images as for specimen 1 applied to specimen 2 above and for specimens 3 and 4 below.

For specimen 2 the mean for both EBSD images were significantly lower than the optical image by  $222\mu\text{m}^2$  and  $152\mu\text{m}^2$  for the lower and higher pixel resolutions respectively. Thus the mean value of the higher pixel resolution EBSD image was  $70\mu\text{m}^2$  more than the lower pixel resolution EBSD image.

The distributions for both EBSD images showed a difference of only one grain measured for any given grain size bin, except for  $504$  to  $1008\mu\text{m}^2$  (light blue colour grains) and  $2016$  to  $4032\mu\text{m}^2$  (yellow coloured grains), where there was

a difference of two grains. Generally the lower pixel resolution EBSD image had more smaller grains than the higher pixel resolution EBSD image where more larger grains were found. The significant difference when comparing with the optical image was that both EBSD images had more smaller grains.

There were 36 grains measured in the optical image.

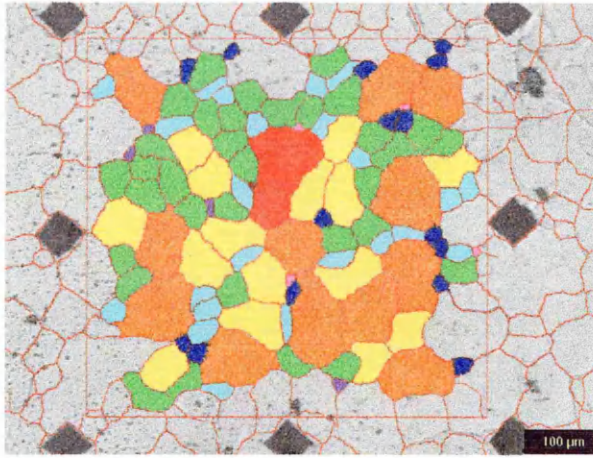


**Figure 46 An Optical image of specimen 3 with the measured grains colour coded according to their size**

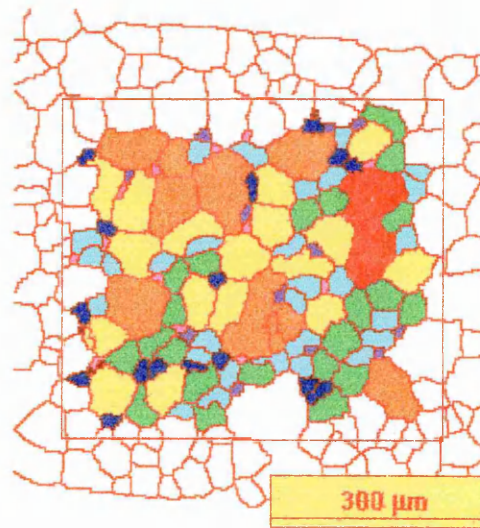


**Figure 47 An EBSD image of the lower pixel resolution of specimen 3 with the grains measured colour coded according to their size**

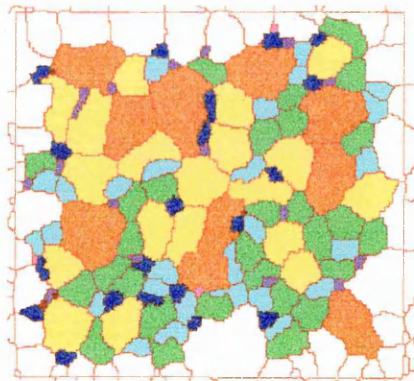
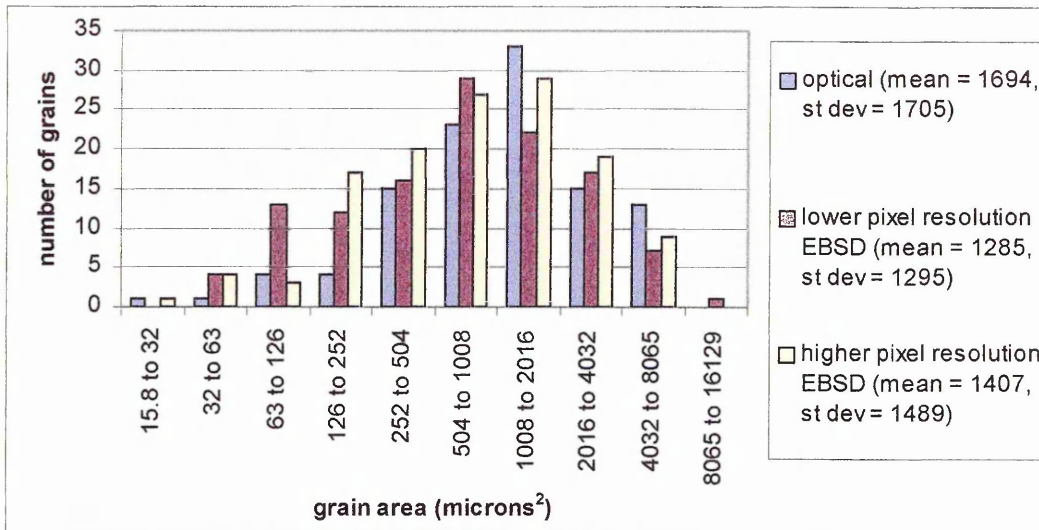


Figure 48 An EBSD image of the higher pixel resolution of specimen 3 with the grains measured colour coded according to their size



**Figure 49 A histogram of the grain area distributions measured on the optical and EBSD images of both pixel resolutions using the automatic image analysis system for specimen 3**

The mean values between the EBSD images were  $113\mu\text{m}^2$  different for specimen 3, with the higher value measured in the higher pixel resolution EBSD image. However the mean from the optical image was  $400\mu\text{m}^2$  and  $287\mu\text{m}^2$  higher than the EBSD images of the lower and higher pixel resolutions respectively.

The distributions of the EBSD images showed generally that for the lower pixel resolution there were more smaller grains whereas for the higher pixel resolution more larger grains were measured. This accounted for the mean

value being larger in the higher pixel resolution EBSD. Considering the colour coding, effectively some of those grains that were pink within the lower pixel resolution EBSD image were purple or dark blue in the higher pixel resolution EBSD. Incorporating the grain size distribution of the optical image, generally there were more smaller grains measured for both EBSD images.

There were 109 grains measured in the optical image.

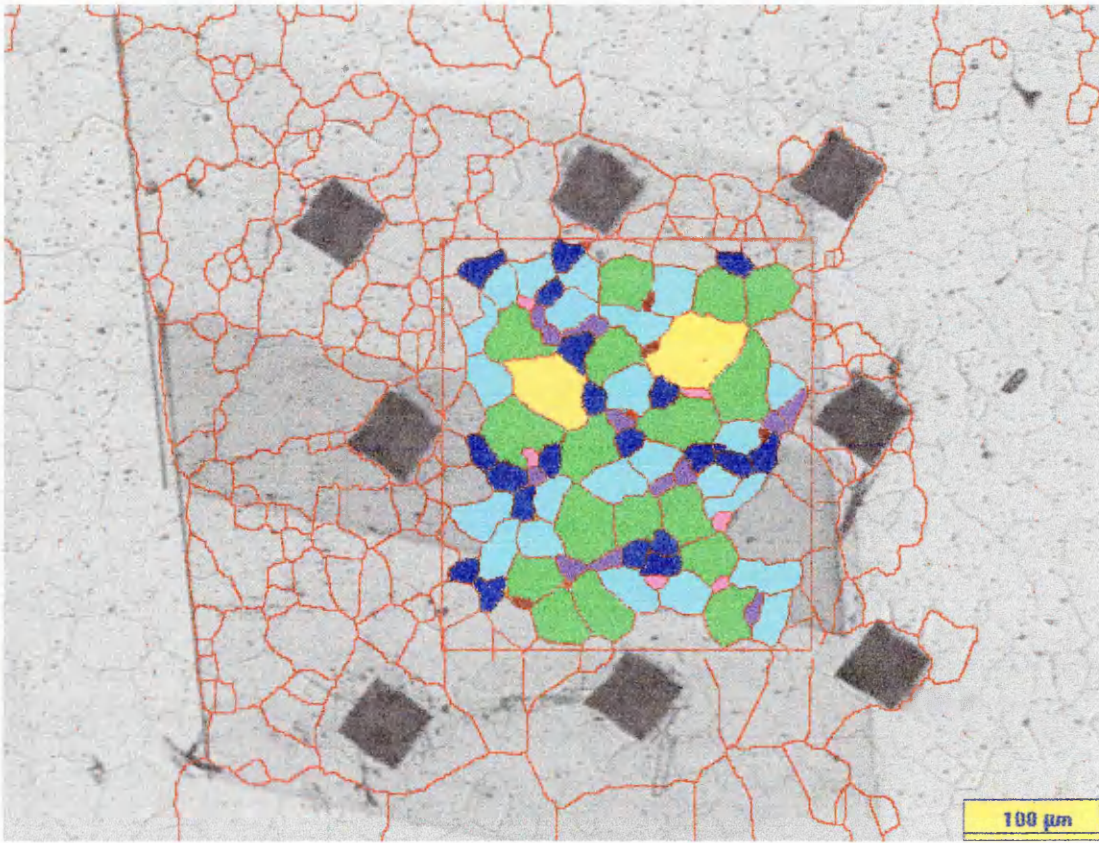
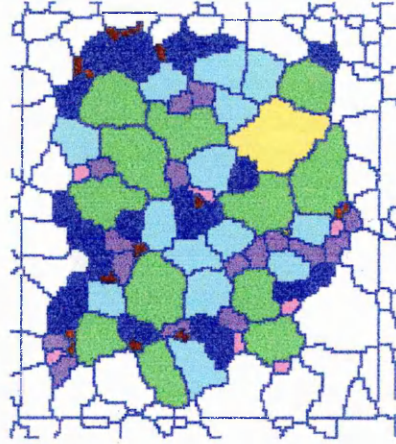


**Figure 50 An Optical image of specimen 4 with the measured grains colour coded according to their size**



200 μm

Figure 51 An EBSD image of the lower pixel resolution of specimen 4 with the grains measured colour coded according to their size

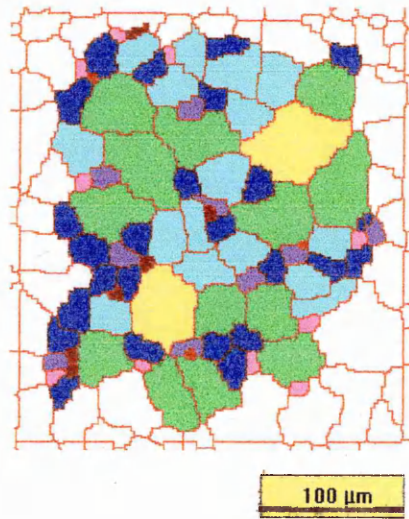


**Figure 52 An EBSD image of the higher pixel resolution of specimen 4 with the grains measured colour coded according to their size**

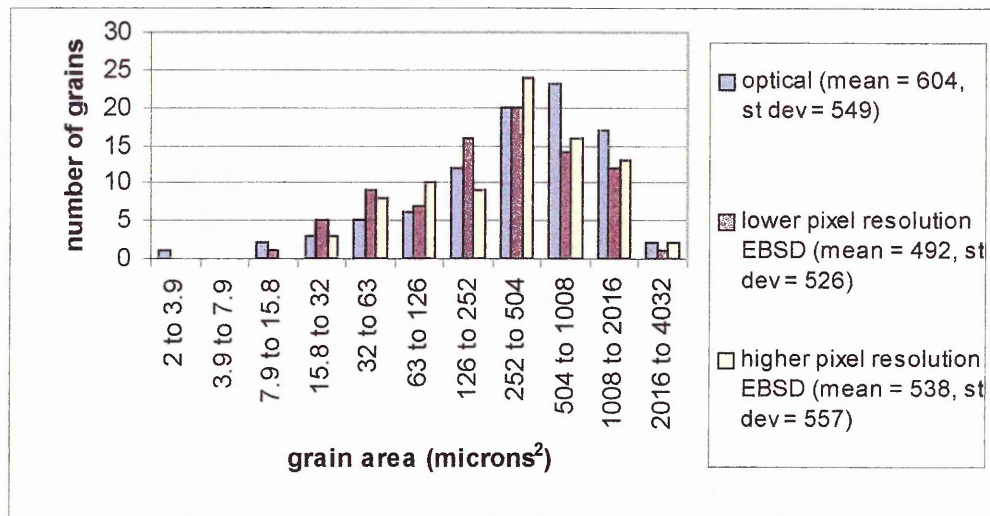


**Figure 53 A histogram of the grain area distributions measured on the optical and EBSD images of both pixel resolutions using the automatic image analysis system for specimen 4**

Measurements of specimen 4 demonstrated that the mean value was higher for the EBSD image of higher pixel resolution than that of the lower pixel resolution by  $46\mu\text{m}^2$ . The optical mean was higher than for both EBSD images, by  $112\mu\text{m}^2$  and  $66\mu\text{m}^2$  for the lower and higher pixel resolutions respectively.

The greatest difference between the distributions of both EBSD images was found in the grain size range of  $126$  to  $252\mu\text{m}^2$  (purple coloured grains), where there were seven more grains for the lower pixel resolution, and the grain size range of  $252$  to  $504\mu\text{m}^2$  (dark blue coloured grains) where there were four more grains for the higher pixel resolution. Using this point of the distributions ( $126$  to  $504\mu\text{m}^2$ ) to distinguish between both EBSD images the lower pixel resolution

generally had more of the smaller grains before this point whereas the higher pixel resolution had more of the larger grains after this point.

The optical distribution generally had more larger grains than both EBSD images for this specimen, and the reverse applied with more smaller grains in the EBSD images.

91 grains were measured in the optical image.

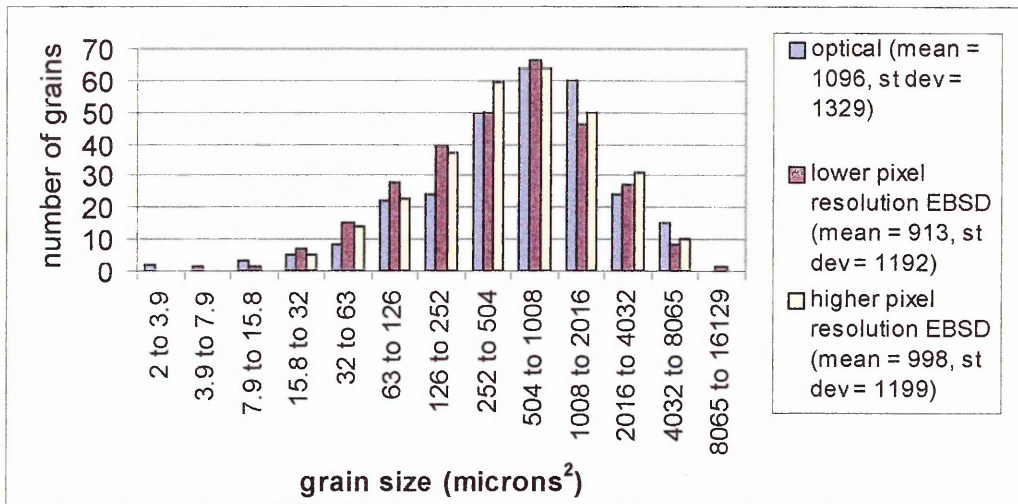


**Figure 54 A histogram of the grain area distributions measured on the optical and EBSD images of both pixel resolutions using the automatic image analysis system for all specimens**

Figure 54 represents the grain size results for all specimens and for both EBSD resolutions and optical images are represented Figure 54. A total of 277 grains were measured for the optical image. Essentially these were measurements of the reference specimen.

The mean value for the optical image was approximately  $180\mu\text{m}^2$  and  $100\mu\text{m}^2$  higher than the lower and higher pixel resolution EBSD images respectively. This trend also applied to specimens 2,3 and 4. Clearly the mean from the higher pixel resolution EBSD image was higher than the lower pixel resolution

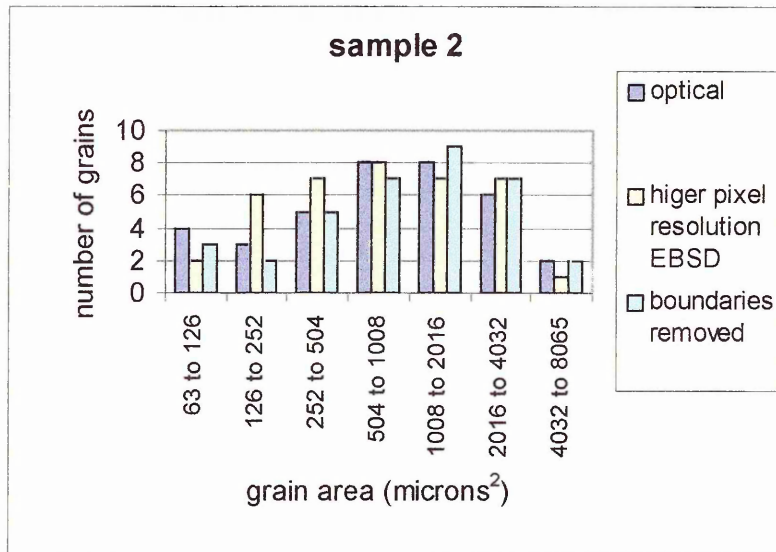
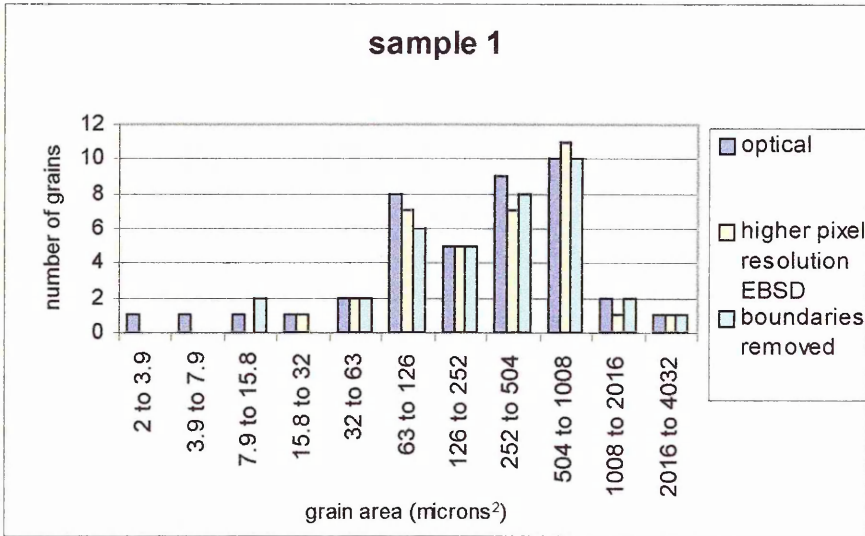
EBSD image and again this trend applied to specimens 2,3 and 4. In specimen 1 the higher mean was found in the lower pixel resolution EBSD image.

Considering the distribution of grain size, generally there were more smaller grains from the optical image than both of the EBSD images, (2 to  $15.8\mu\text{m}^2$ ). This was also found in specimen 1. This applied to the larger end of the scale, ( $15.8$  to  $1008\mu\text{m}^2$ ), as with specimen 4, whereas for those grain sizes within these two extremes there were more measured in the EBSD images.

Again in general terms, the lower pixel resolution EBSD image had more smaller grains ( $7.9$  to  $252\mu\text{m}^2$ ) than the higher pixel resolution EBSD image but fewer larger grains ( $252$  to  $8065\mu\text{m}^2$ ). This trend was also found in specimens 2,3 and 4.

Overall there were 11 more grains measured in the lower pixel resolution EBSD image than the optical, and 16 more in the higher pixel resolution EBSD image. Clearly then there were 5 more grains measured in the EBSD image of the higher pixel resolution than that of the lower pixel resolution.

4.2.4.1. Comparison of results with boundaries removed



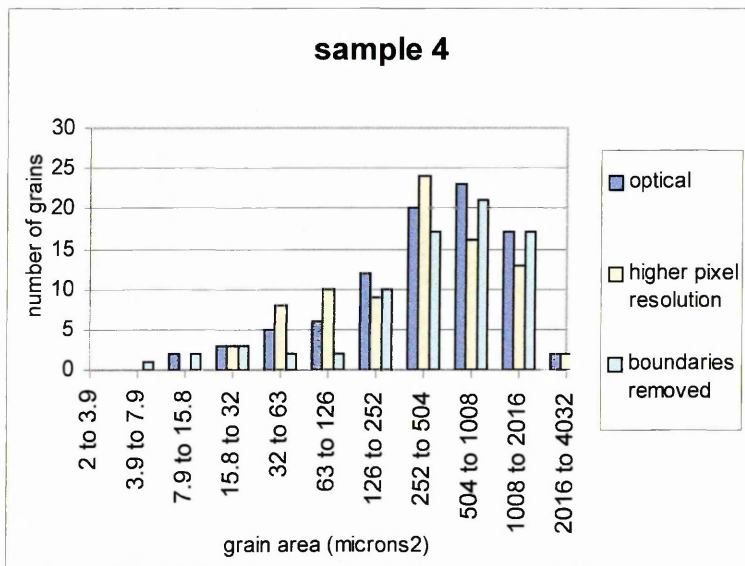
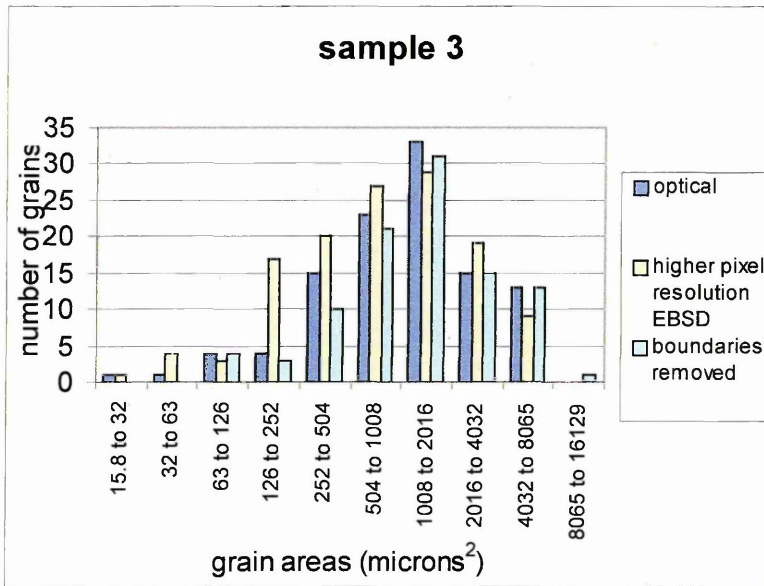


**Figure 55 Histograms of grain area distributions of each individual specimen comparing measurements on the optical images, the EBSD images of higher pixel resolution and the optical images with those boundaries not on the EBSD images removed.**

By comparing the reconstruction of grain boundaries on the optical images with that of the EBSD images those boundaries that were reconstructed but were shown not to exist on the EBSD images were identified. These boundaries were then removed from those already reconstructed and the grains were measured again. These results were compared with the EBSD results therefore allowing a direct assessment of the impact of missing boundaries. Missing boundaries were produced from an incomplete boundary delineation using chemical etching. Only the results from operator 1 were considered in this section since it was only the impact of missing boundaries that is considered and not the variation from two operators.

The distributions of the measurements conducted on the optical images with the original boundary reconstruction (optical) together with the distributions from measuring the higher pixel resolution EBSD images are also shown.

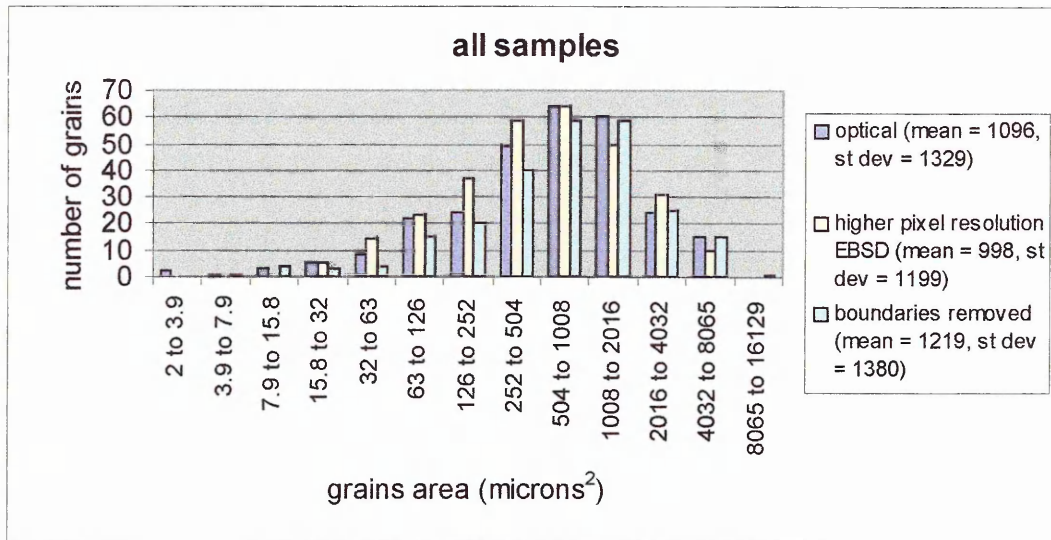


**Figure 56 Comparison of the grain size distribution from the optical image, the optical image with the boundaries that did not exist in the EBSD removed, and the higher pixel resolution EBSD images for all specimens**

The results shown in Figure 56 are of all the specimens from measuring the optical image with the original boundary reconstruction (optical), boundaries removed and the higher pixel resolution EBSD images. The difference in the mean value of the boundaries removed compared to the optical was approximately  $100\mu\text{m}^2$  but the difference was approximately  $200\mu\text{m}^2$  compared to the higher pixel resolution EBSD.

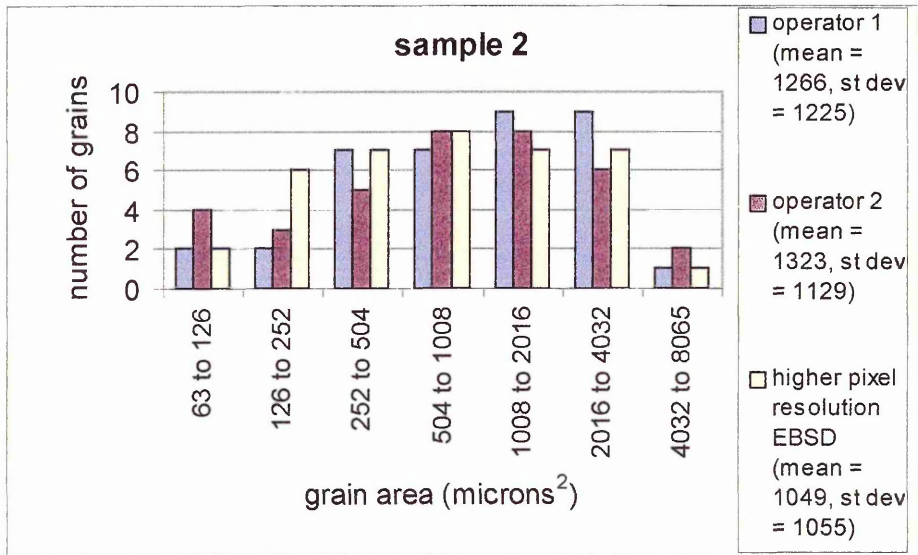
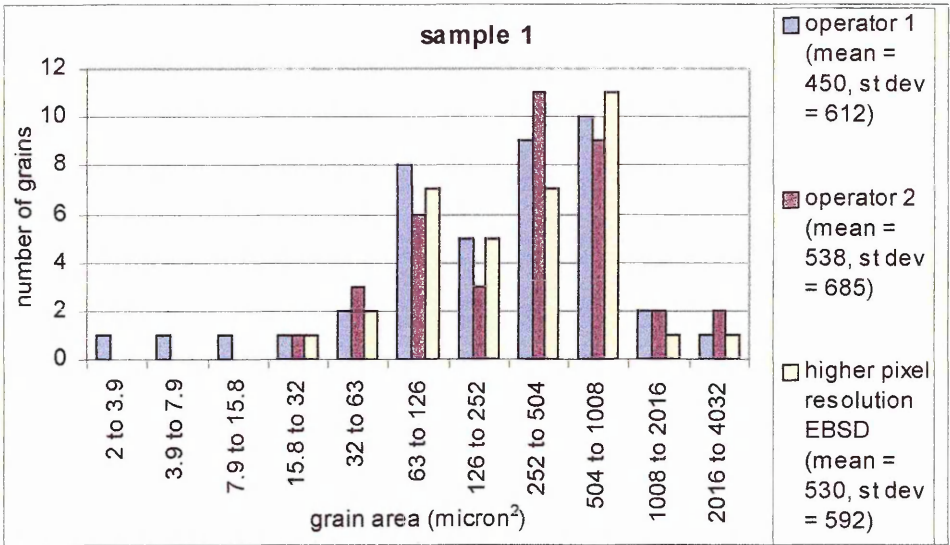
When considering the distributions, there were generally more smaller grains measured in the optical image than in the boundaries removed ( $2$  to  $1008\mu\text{m}^2$ ). Therefore, remembering that the boundaries removed were those that were shown not to exist as they did not appear on the EBSD image, the fact that the

mean value for the optical was close to that of the higher pixel resolution EBSD was accounted for by reconstructing boundaries that do not exist. This trend could also be seen to be generally true for each of the individual specimens. However, the boundaries removed mean value was closer to the higher pixel resolution EBSD than the optical for specimen 4. This was different from the other three specimens and was attributed to there being fewer incorrectly reconstructed boundaries.

When comparing the distributions of the higher pixel resolution EBSD and boundaries removed the general trend showed that the greatest difference was found in the smaller grains, from 2 to  $504\mu\text{m}^2$ . The fact there were some more grains measured for boundaries removed than for the higher pixel resolution EBSD was accounted for by there being some discrepancies in the determination of how a boundary defines a grain, for example some boundaries were only partially etched in the optical image.

#### 4.2.5. Comparison of two optical grain size measurements

To provide an analysis of the subjectivity in determining what is a grain boundary the same optical images were independently reconstructed by two operators. The results from these measurements are reported in this section and compared with those from the higher pixel resolution EBSD images.



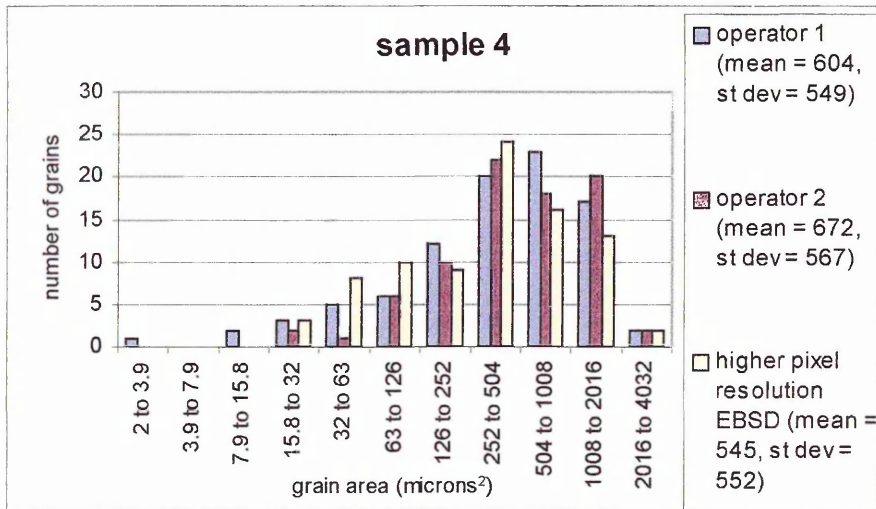
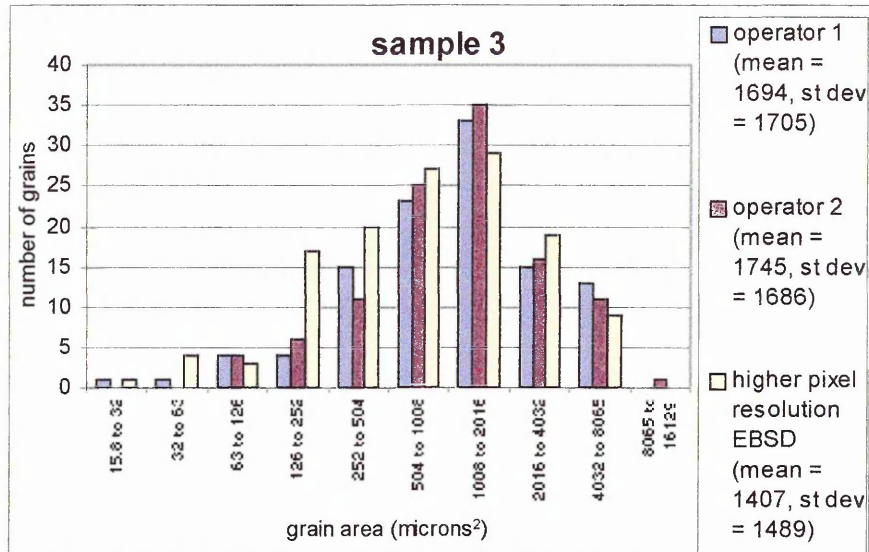


**Figure 57 Histograms of grain area distributions of each individual specimen comparing measurements on the optical images reconstructed by two operators (operator 1 & operator 2) and the EBSD images of higher pixel resolution.**

Figure 57 shows the grain area distributions of all the individual specimens and compares the optical measurements from both operators (operator 1 and operator 2) with the higher pixel resolution EBSD images. Operator 1 results were compared with EBSD in section 4.2.4. Therefore comparison of the measurement conducted by both operators with the higher pixel resolution EBSD images were made in this section.

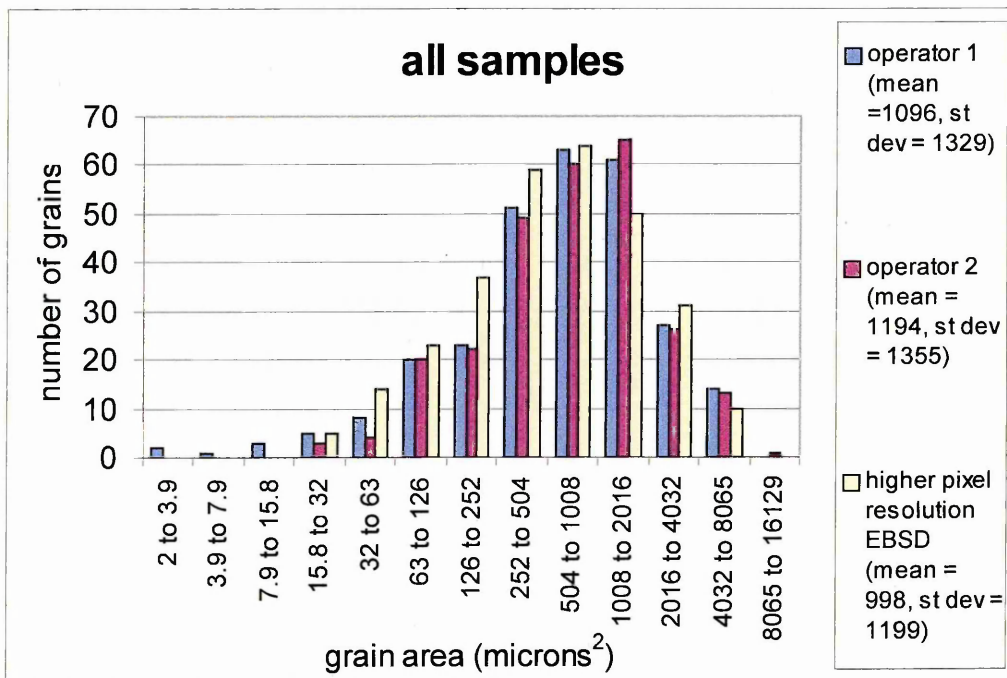


**Figure 58 Histograms of grain area distributions of all specimens comparing measurements on the optical images reconstructed by two operators (operator 1 & operator 2) and the EBSD images of higher pixel resolution.**

All the results for all four specimens are consolidated and shown in Figure 58 allowing a general comparison of both operators and EBSD to be made.

The largest mean grain size was measured by operator 2 at approximately  $100\mu\text{m}^2$  higher than operator 1 and  $200\mu\text{m}^2$  higher than the higher pixel resolution EBSD. When comparing operator 2 with the higher pixel resolution EBSD this difference in the mean was accounted for by there being many more smaller grains ( $15.8$  to  $1008\mu\text{m}^2$ ) in the higher pixel resolution EBSD image and also more larger grains in operator 2. This same trend of a higher number of smaller grains in the higher pixel resolution EBSD image than operator 2 was more prominent in specimens 3 and 4.

#### 4.2.6. The impact of not including the boundary into the measurement using the automatic image analysis system

This section deals with measurements using the automatic image analysis system. It was known that the boundaries were not included within the measurements of the grain areas using this technique. This section is concerned firstly with measurements conducted on ellipses of various aspect ratios of minor and major axes and secondly with one ellipse of a specific aspect ratio but of various areas. Therefore, the impact of not including the boundary into the measurement of objects is related to the shape and size of those objects.

## The shape of object

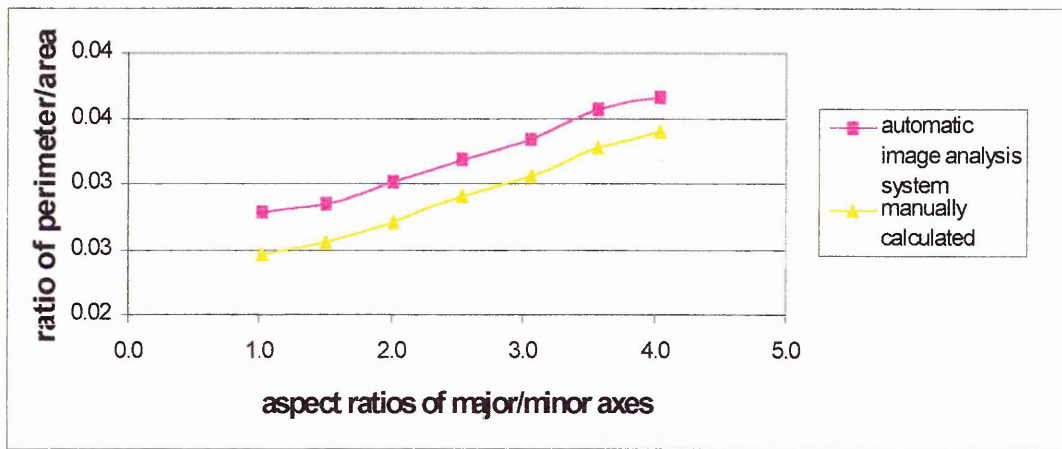


**Figure 59 The ratios of perimeter/area plotted against the aspect ratios of minor/major axes of ellipses of the same area**

Ellipses were created in digital form by first drawing a circle using an imaging package and then to stretch that circle using interpolation in the y direction by various factors. The image was then contracted by a percentage in both x and y to return the ellipse to the same area size. Thus ellipses of the same area but of various aspect ratios of the minor and major axes were produced.

The perimeter, areas and aspect ratios of the major and minor axes of the ellipses were measured using the automatic image analyser. Prior to measurement each ellipses underwent the same image process to ensure that the boundary defining the ellipses were connected and of the minimum pixel width, e.g. 1 pixel.

The area/perimeter ratios, estimated by manual calculations and by automatic image analysis are shown in Figure 59 and are plotted against the aspect ratios of the ellipses. The manual measurements effectively included the perimeter and thus allowed a measure of the impact on area measurements where the perimeter was not included. This plot demonstrated two points. The first was that the percentage of perimeter to area was the lowest for a circle, that is a minor/major aspect ratio of 1. This percentage increased with a corresponding increase in the minor/major aspect ratio. Hence an evaluation of the error introduced by not including the boundary into the measurement of grains with various shapes was provided. The second point was that there was a significant difference between the manual calculations and the automatic image analyser measurements of the perimeter/area ratios. The manual measurements were consistently lower, and this difference reduced from 11% to 7% with corresponding minor/major aspect ratios of 1 to 4.

The size of the object

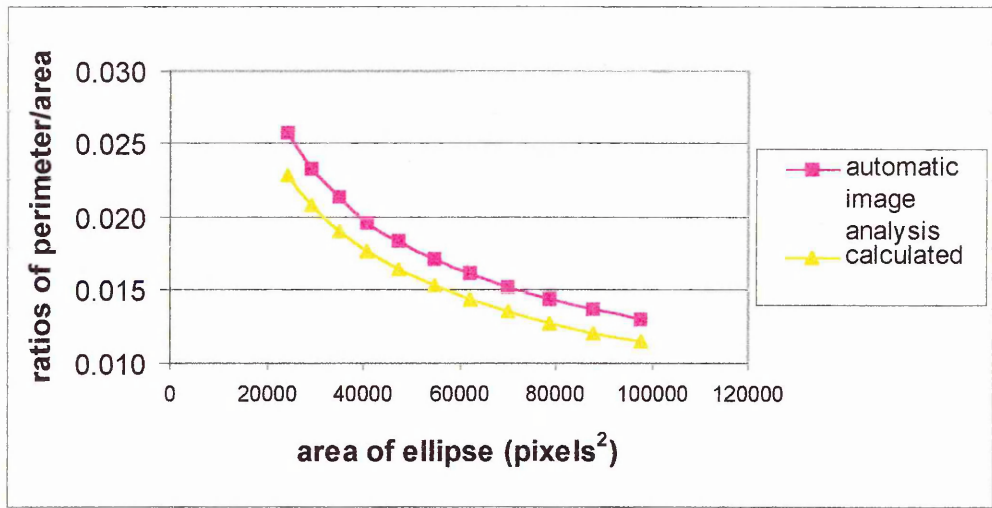


**Figure 60** The ratios of perimeter/area plotted against the area of the ellipses

The importance of the size of an object with regards to the differences introduced from image processing was provided in the results shown in Figure 60. Here an ellipse of a constant minor/major aspect ratio, namely 1.38, was enlarged to various area sizes. Again each ellipse underwent the same image processing to reduce the perimeter to a one pixel thickness. The areas and the perimeters were measured using the automatic image analysis system. The plot shown in this figure was of the area against the ratio of perimeter/area. The important point raised by this analysis was that as the area increased the ratio of perimeter/area decreased exponentially.

The perimeters and areas were also measured manually and the plot of the areas against the ratios of perimeter/area was also shown in Figure 60. These results were consistently lower than the corresponding automatic measurements and the difference between the two ranged from 10 to 12%.

4.2.7. The grain shape and misorientation of missing boundaries

Operator 1						
specimen	reason for being missing	Optical		EBSD		misorientation angle
		aspect ratio	sphericity	aspect ratio	sphericity	
1	unetched, small	1.28	0.56	1.29	0.64	58.88
				1.43	0.54	
	all unetched	1.40	0.53	1.40	0.61	27.22
				1.86	0.46	
	Unetched	2.11	0.49	1.22	0.74	51.49
				1.84	0.53	
2	unetched, small	1.49	0.51	1.34	0.69	19.36
				1.82	0.62	
3	small	1.52	0.61	1.46	0.58	48.68
				2.12	0.51	
	small, partial boundary	1.40	0.60	1.35	0.65	14.09
				1.32	0.65	
	Unetched	1.74	0.44	1.45	0.62	51.01
				1.51	0.67	
	small, unetched	1.57	0.54	1.63	0.57	59.65
				1.87	0.41	
4		1.25	0.76			
		1.85	0.48			
		1.49	0.60			
mean		1.56	0.56	1.55	0.59	
St dev		0.245	0.082	0.258	0.088	

Table 10 Grain shape and misorientation data of boundaries in the EBSD images but not in the optical images (missing boundaries) for operator 1

Operator 2						
specimen	reason for being missing	Optical		EBSD		misorientation angle
		aspect ratio	sphericity	aspect ratio	sphericity	
1	all unetched	1.40	0.53	1.40	0.61	27.22
				1.86	0.46	5.35
				1.49	0.49	25.61
		2.11	0.49	1.22	0.74	51.49
				1.84	0.53	
2	Unetched, small	1.28	0.56	1.29	0.64	58.88
				1.43	0.54	
		1.49	0.51	1.34	0.69	19.36
				1.82	0.62	
3	Unetched, small, unetched	1.74	0.44	1.45	0.62	51.01
				1.51	0.67	
		1.57	0.54	1.63	0.57	59.65
				1.87	0.41	
	Small, partial boundary	1.40	0.60	1.35	0.65	14.09
				1.32	0.65	
		1.52	0.61	1.46	0.58	48.68
				2.12	0.51	
mean		1.56	0.54	1.55	0.59	
st dev		0.260	0.056	0.219	0.089	

**Table 11 Grain shape and misorientation data of boundaries in the EBSD images but not in the optical images (missing boundaries) for operator 2**

The shape of a grain was important to their measurement using automatic image analysis systems. To further understand the differences between the results from measuring optical and EBSD images using such automatic systems aspect ratio and sphericity measurements were conducted on those grains that existed in the EBSD images but not in the corresponding optical images. These grains were missing from the optical images due to the chemical etching failing to etch all the boundaries. The results from such measurements are shown in Table 10, for the reconstruction of the optical image by operator 1, and Table 11 for the reconstruction by operator 2.

The aspect ratios were of the largest possible one-dimensional length measurement within a grain and the smallest possible length. Sphericity was a measurement of the deviation of the grain shape from a circle. A single number was the result of each measurement using the following equation:

$$4 \times \pi \times \text{area}/(\text{perimeter}^2) \quad \text{Equation 14}$$

The number one represents a perfect circle and an increase in deviation from that due to irregularities in the shape reduced this number, with zero representing the maximum deviation.

The misorientation angle data for the missing boundaries were also shown in Table 10 and Table 11, the former from the reconstruction of the optical image

by operator 1 and the latter by operator 2. The reasons why these boundaries were missed were also shown in these tables. The trends of these misorientation angle data are reported in section 4.3.

		specimens mean sphericity	
specimen	optical	EBSD	
		Lower pixel	Higher pixel
1	0.61	0.60	0.61
2	0.61	0.62	0.62
3	0.62	0.60	0.60
4	0.61	0.63	0.60

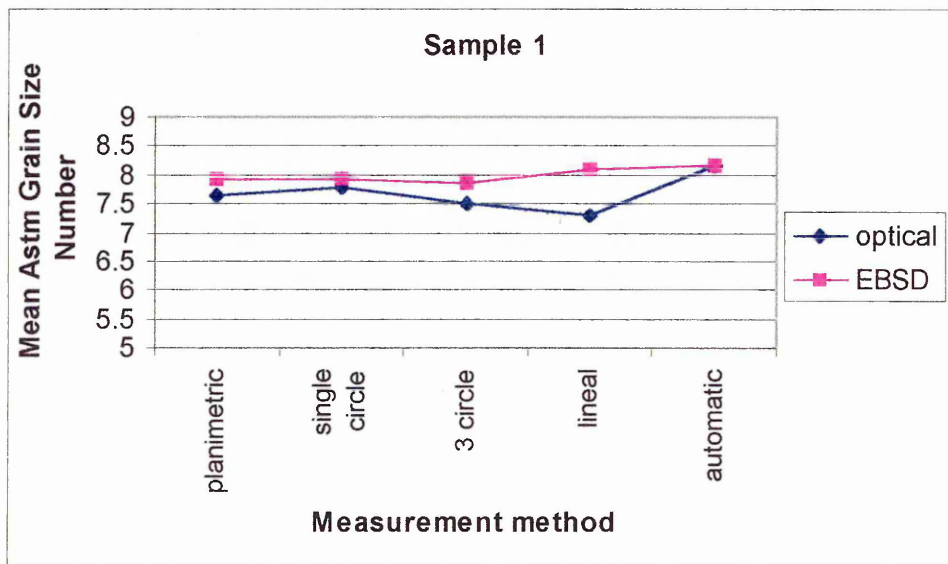
		specimens mean aspect ratios	
specimen	optical	EBSD	
		Lower pixel	Higher pixel
1	1.62	1.67	1.55
2	1.65	1.59	1.55
3	1.55	1.61	1.55
4	1.60	1.61	1.50

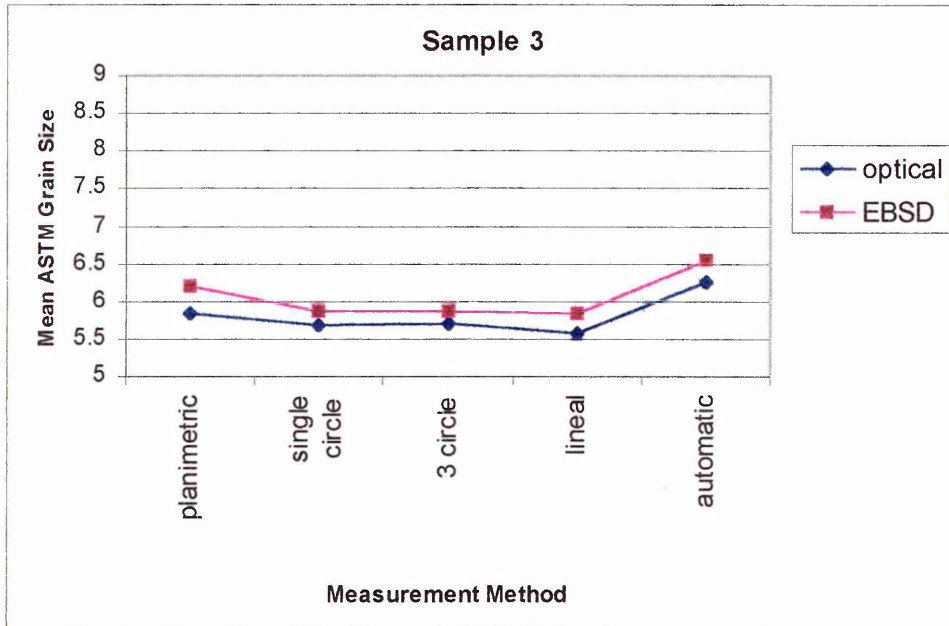
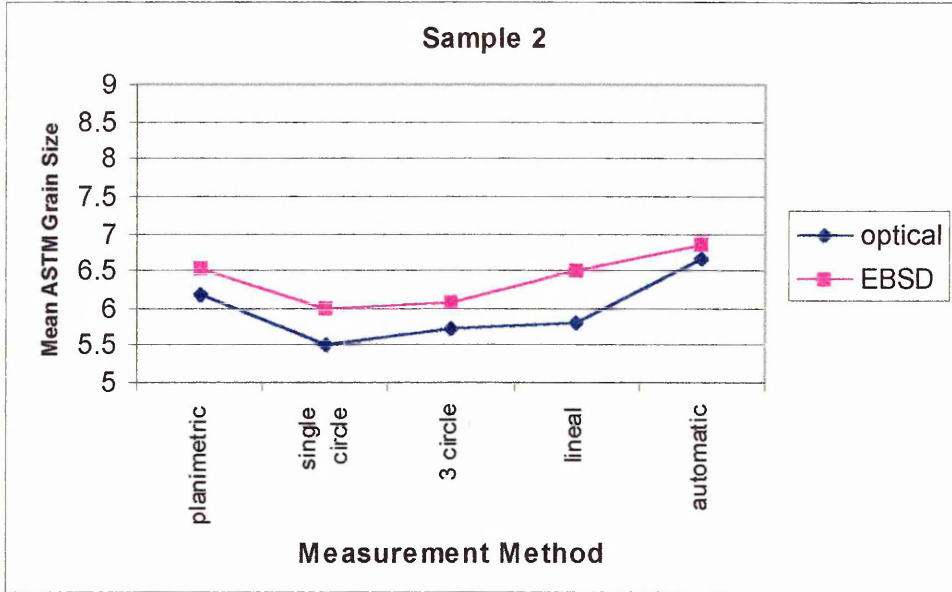
**Table 12 The mean sphericities and aspect ratios of the optical and the EBSD images of both pixel resolutions for all specimens**

The aspect ratios and sphericities of all the grains measured in the optical and the EBSD images of both pixel resolutions were measured for all four specimens. The means of each set of results are shown in Table 12. These results therefore represented the general grain shape information of each image form and each specimen.

4.2.8. Comparison of manual and automatic grain size measurements with optical and EBSD imaging

The optical and EBSD images were measured using manual techniques. The results from these measurements are reported here and were compared with the results produced from using the automatic image analyser (automatic).





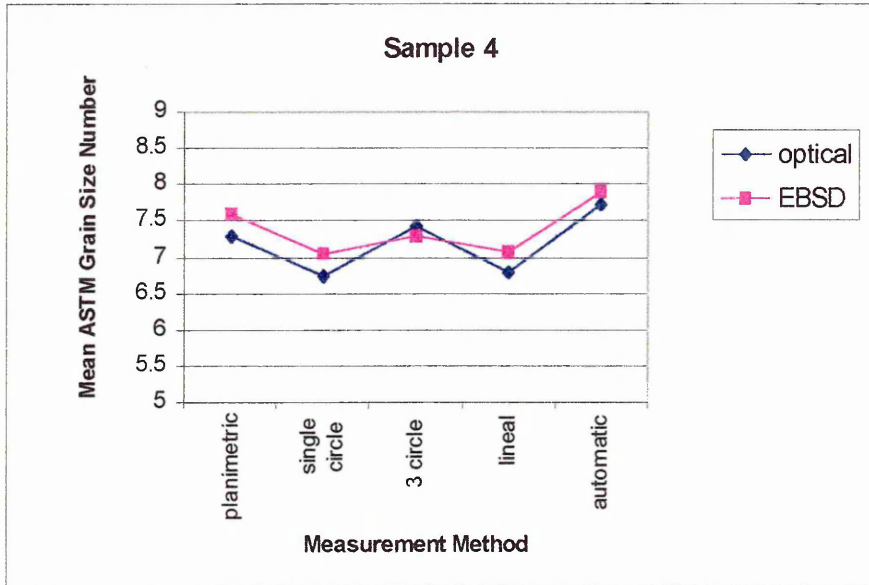


**Figure 61 A plot of the ASTM grain sizes measured on the optical and the higher pixel resolution EBSD images of each specimen using the planimetric, single circle, three circle and lineal manual methods and also by automatic image analysis**

Figure 61 shows all the mean ASTM grain size values for all manual measurement methods and were compared with the automatic methods reported in the previous sections. Manual measurements were conducted using the same optical and EBSD images as those reported in previous sections and automatic refers to the measurements conducted using the image analysis system. All the results were translated in the ASTM G number systems to allow a comparison across all methods. All manual measurements were conducted on optical images reconstructed by only one operator in this instance. A comparison could then be achieved of manual methods for grain

boundary networks produced from the optical and the EBSD images and also of automatic and manual methods.

4.2.8.1. A comparison of results from optical and EBSD imaging using manual methods

Generally the results for all methods produced a higher mean value from the EBSD images than the optical images except for the three circle method in specimen 4. The lineal method consistently returned the greatest difference between the two image sources for specimens 1 and 2. Furthermore, the overall greatest difference across the manual methods was found in specimen 1 with 0.81G units and the second greatest was in specimen 2 with 0.70G units. The greatest difference across the manual methods was found in the planimetric (0.37G units) and both the planimetric and single circle (0.30G units) for specimens 3 and 4 respectively. Any consistency in the smallest difference was only found in specimens 3 and 4 with the three circle method. Here the difference was 0.15G units for specimen 3 and 0.13G units for specimen 4. The smallest difference of 0.12G units for specimen 1 was produced by the single circle method and 0.33G units for specimen 2. Again it is significant to note that both specimens 3 and 4 had the highest number of grains measured.

#### 4.2.8.2. A comparison of results from using manual and automatic methods

When the results from using the manual methods were compared to those from the automatic it was found that the automatic consistently returned a G number that was higher than all the manual results, for all specimens and both the optical and EBSD images. This can be seen with reference to Figure 61. The maximum difference across the manual methods measuring the optical images was in the range of 0.6 to 1.2G units and the minimum was 0.3 to 0.5G. The equivalent for the EBSD images was 0.3 to 0.9G units and 0.1 to 0.4G units.

### **4.3. Assessment of boundaries with misorientation**

#### **4.3.1. Assessment with the location of boundaries on EBSD but not reconstructed on optical**

In furthering the understanding of why some boundaries did not etch (missing boundaries) an electron back scattered diffraction analysis was produced and is described in this section. Hence the misorientation data for those boundaries that did not appear on the optical images but existed according to the EBSD images were analysed.

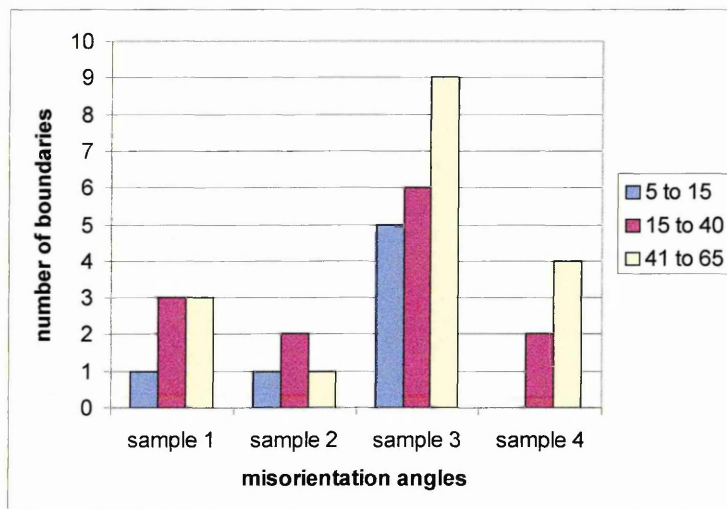


**Figure 62 A histogram of the boundaries not reconstructed by Operator 1 categorised according to their misorientation angles**

Figure 62 represents all the misorientation data from all four specimens, divided into three ranges, namely  $0^\circ$  to  $15^\circ$ ,  $15^\circ$  to  $40^\circ$  and  $40^\circ$  to  $60^\circ$ . This set of data was exclusive to operator 1 and therefore those boundaries not reconstructed by this operator on the optical images.

From examining this data it was clear that the general trend for the misorientation of missing boundaries were of the higher angles,  $15^\circ$  to  $60^\circ$ . Indeed there were no  $0^\circ$  to  $15^\circ$  misorientations for specimen 4 and only 1 each for specimens 1 and 2, where specimen 2 was the only specimen where this range did not have the lowest number of missing boundaries. However, specimens 1, 2 and 4 returned the lowest number of missing boundaries which corresponded approximately to the number of grains measured, e.g. specimen 3 the highest number of grain measured.

When comparing the  $15^\circ$  to  $40^\circ$  misorientation range with the  $40^\circ$  to  $60^\circ$  range specimens 3 and 4 had a significantly higher number of missing boundaries for the latter, there were more in the former for specimen 2 and the number of missing boundaries equalled for specimen 4.

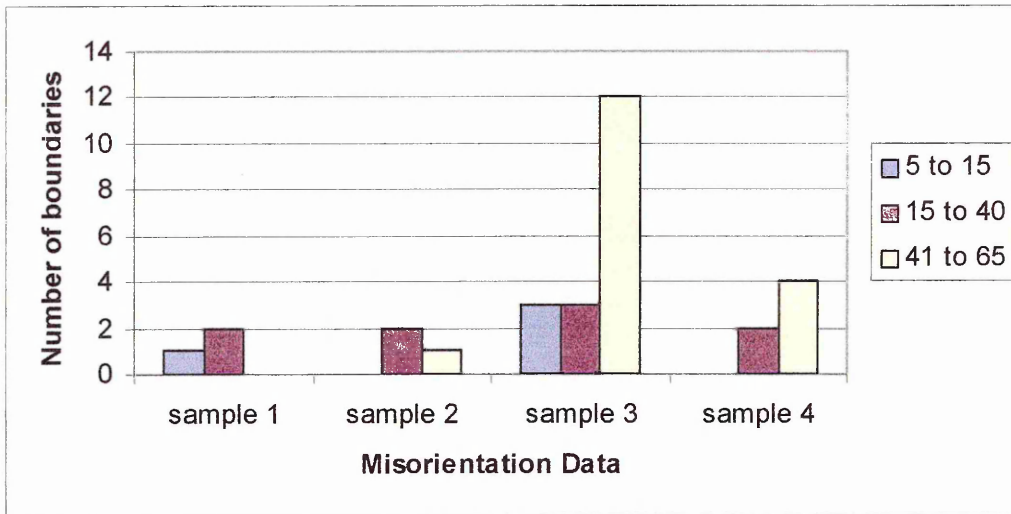


**Figure 63 A histogram of the boundaries not reconstructed by Operator 2 categorised according to their misorientation angles**

Figure 63 demonstrates the misorientation data for those boundaries not reconstructed by operator 2. Since it was the same grain boundaries from the same optical images for operator 1 and 2 then it could be expected that the same missing boundaries would be analysed for both operators. From examination of Figure 62 and Figure 63 it was clear that there were different numbers of missing boundaries. Therefore, there were reconstructed boundaries by operator 1 that were not reconstructed by operator 2 and vice versa. This was due to the subjective determination of each operator as to the locations of a boundary that was not visible on the optical images.

#### **4.4. The misorientation of grains and grain size**

This section describes the data produced from a ferrite/pearlite reference specimen. The ferrite phase was analysed exclusively wherein the grain boundary misorientation between small/small, small/large and large/large grains was considered. Small and large grains are defined below.

The analysis was conducted on four specimens, giving a total of 20 EBSD maps, that in turn constituted an analysis of over 1600 grain boundaries. Three EBSD maps were each produced for specimens 1 and 2, and 7 each for specimens 3 and 4. There were 461 small to small boundaries, 628 small to large and 554 large to large. More maps were produced for the specimens 3 and 4 to provide sufficient data to analysis the misorientation of the small/small, small/large and large/large grains for each specimen individually.

The EBSD maps were refined to show only misorientations of greater than 5° and colour coded to show where such misorientations existed. They were colour coded such that no 2 same colours were found adjacent to one another. Therefore the colours in this map then represented the grains allowing a clearer definition of where a boundary existed. Such maps were named true identification maps and an example of such a map is shown below.

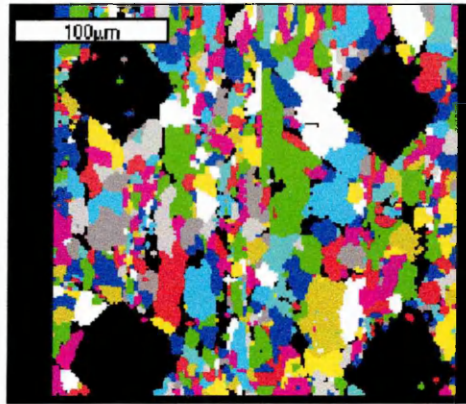


**Figure 64 An example of a true grain identification map showing a more refined grain structure**

By imposing a threshold of  $5^\circ$  any subgrains were effectively removed from the analysis.

From using the automatic image analysis system grain size measurements were conducted by first defining where there was a difference in colour and then to make this the location of the boundary.

Large grains were then defined as greater than  $63\mu\text{m}^2$  and small grains as smaller than  $15.8\mu\text{m}^2$  and colour coded accordingly. An example of an image with large grains, large and small grains and small grains is shown below together with the grain sizes associated with each colour.

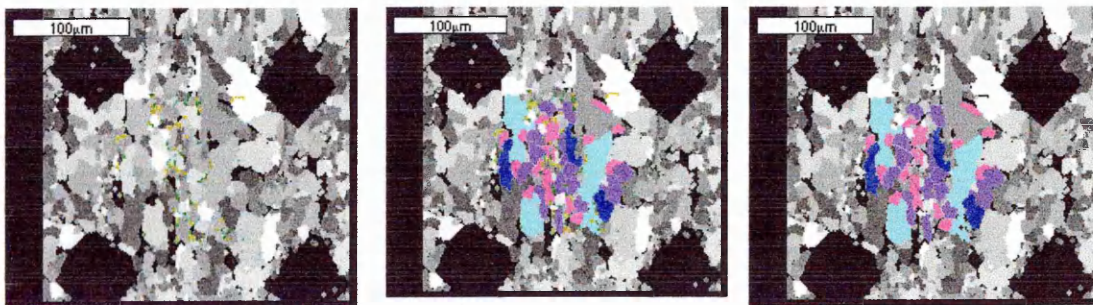
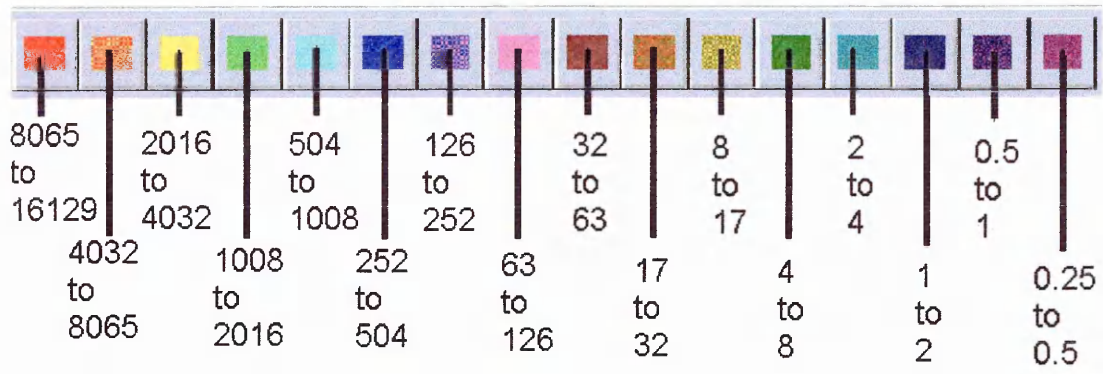
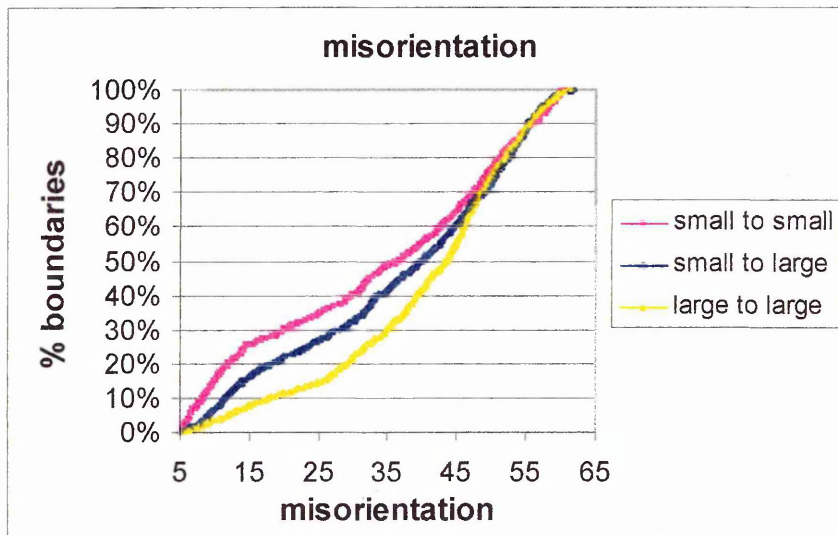


Figure 65 Examples of EBSD images with, from left to right, small grains, small and large grains and large grains colour coded according to the scale shown above.

4.4.1. Misorientation data for grain boundaries between large/large,  
large/small and small/small grains

All the misorientation data was arranged in ascending order within each category of small/small, small/large and large/large grain boundaries. Since the number of boundaries from each category were different the data was first normalised to a percentage of the total number of boundaries.



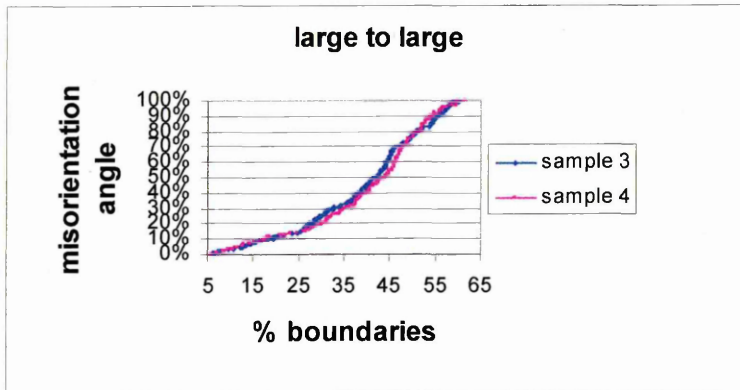
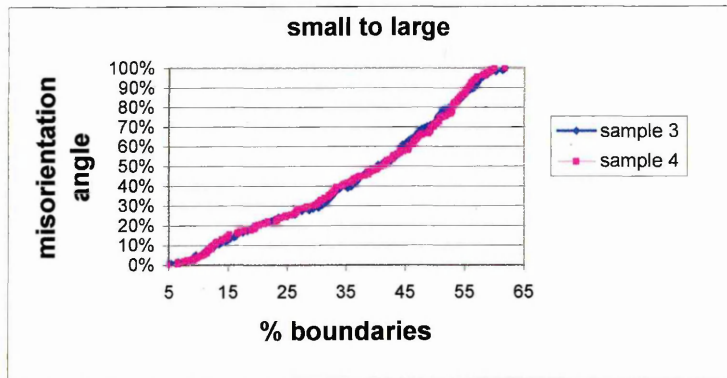
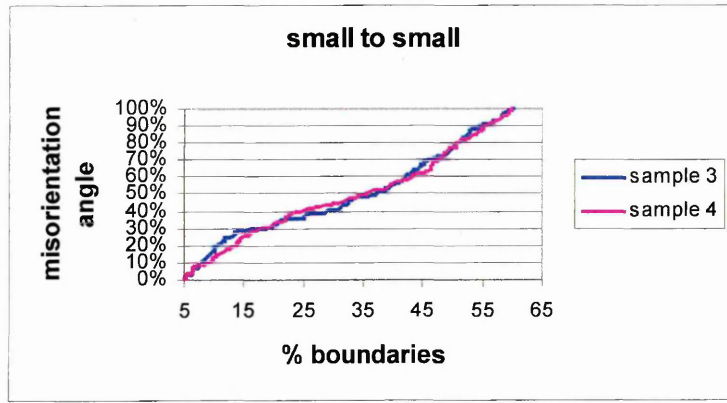
**Figure 66 A plot of the misorientation data for grain boundaries between small/small, small/large and large/large grains**

Figure 66 compares all the small/small, small/large and large/large boundaries from all the specimens. From 45° and above all misorientation categories were converging demonstrating that there was a similar percentage of these boundaries. However, below 45° misorientation it could be seen that the

large/large boundaries had the smallest incidence, followed by large/small and finally small/small. This demonstrated that large/large had the greatest percentage of larger misorientation angles, followed by large/small then small/small.

#### 4.4.2. Misorientation and grain size for Specimen 3 and 4

The misorientation for specimens 3 and 4 were compared in terms of small/small, small/large and large/large grain boundaries. For specimen 3 boundaries between 139 small/small, 169 small/large and 157 large/large grains were analysed with 138, 200 and 207 respectively analysed for specimen 4. Again the data was put into ascending order and normalised for the percentage of boundaries.



**Figure 67 Plots of the percentage of grain boundaries between small/small, small/large and large/large grains with misorientation angles for specimens 3 and 4.**

Specimen	small/small boundary		small/large boundary		large/large boundary	
	3	4	3	4	3	4
<15° misorientation	29%	25%	12%	15%	7%	7%
≥15° misorientation	71%	75%	88%	85%	93%	93%

**Table 13 showing the percentages of the total number of boundaries measured in specimens 3 and 4 that are smaller than 15° and greater/equal to 15° misorientation for each grain size category**

Specimen	3	4
<15° misorientation	16%	14%
≥15° misorientation	84%	86%

**Table 14 showing the percentages of the total number of boundaries measured in specimens 3 and 4 that are smaller than 15° and greater/equal to 15° misorientation**

Figure 67 compares the misorientation data of all three grain boundary categories for specimens 3 and 4 and Table 13 and Table 14 shows the percentages of the total number of boundaries that are low angle ( $<15^\circ$ ) and high angle ( $\geq 15^\circ$ ). These results showed that there was no significant difference in the percentages of the total number boundaries that were either low angle or high angle between the two specimens. The only notable difference was in the small/small category where specimen 3 had 29% low angle boundaries whereas specimen 4 had 25% and also was within the misorientation range  $20^\circ$  and  $50^\circ$  for large to large boundaries where specimen 3 had a slightly lower inclination than specimen 4. This suggests that specimen 3 had generally lower misorientation angles than specimen 4. Also, when the grain sizes were considered for each specimen, it was found that specimen 3 had 30% small grains whereas specimen 4 had 25%.

## **5. DISCUSSION**

### **5.1. Introduction**

This chapter will firstly discuss the contribution to the knowledge of grain size measurement practice. In order to achieve this various aspects of grain size measurement techniques are discussed including manual and automatic methods and the issue of traditional specimen preparation in order to reveal a microstructure that is representative of the bulk material. The electron back scatter diffraction (EBSD) technique is also incorporated, introducing a means to determine the presence of grain boundaries due to orientation differences rather than the visual methods of chemically revealing a grain boundary, thus providing greater confidence in what the revealed microstructure represents. Through the use of EBSD the crystallographic grain misorientation can also be determined.

Secondly this chapter will discuss the relationship between grain misorientation and grain size through the use of the EBSD technique.

## **5.2. Grain size methodology**

Grain size measurement, in conjunction with other material parameters, is a means of estimating certain properties of a material such as its yield strength, and also provides an important quality control parameter [100,3]. It is important therefore that measurements are representative of the material and this involves firstly revealing the true microstructure and secondly ensuring that an accurate set of measurements are taken [14,15]. Two important sources of errors in grain size measurement have been identified [101]. First, those arising from experimental limitations, for example poor grain boundary delineation, over-etching, miscounting, etc. The second set of errors occur through improper sampling, where fields should be chosen blindly to avoid operator bias, or recording insufficient readings. The discussion below considers these two sources of error with the aim of further understanding their impact on grain size measurements.

### **5.2.1. Inter-comparison of manual methodologies**

This section discusses a comparison of the four quantitative methodologies described in the ASTM standard, E112, in terms of accuracy, efficiency and application to equi-axed microstructures. All the results reported in section 4.2.1 are discussed here. These results referred to measurements conducted

on six specimens of a single phase, fully ferritic, mild steel. Each specimen was measured individually using all the quantitative methods and the differences produced thereof are discussed.

The ASTM standard, E112, quoted the greatest level of accuracy as  $\pm 0.5G$  grain size units for any of the four quantitative methods quoted. The material used in this investigation (a relatively equi-axed mild steel, see section 3.2.1) was characterised for grain size using these manual methods. It was found that the variation in the grain size number for values taken across six specimens for each of the lineal, planimetric, single circle and three circle methods was found to be less than  $\pm 0.5G$ . Thus the choice in method was not important for a given accuracy of  $\pm 0.5G$  as stated in E112.

When considering the average grain size as the number of fields increased the lineal method was found to stabilise at a lower value than the other three methods. This may be due either to the specimen not being the same grain size throughout, as was found with this material or truly reflects a difference in the methods. Data recorded during the initial characterisation of the specimen demonstrated that the aspect ratio of measurements along the radial and axial directions along the centre of the diametric plane, by the lineal intercept method, was 0.87 (see section 3.2.1 and Figure 68). This would correspond to a smaller G number. (e.g. fewer intercepts giving a higher mean intercept value corresponding to a lower G number). In the current work measurements by the lineal method were only taken along the axial direction of the diametric plane

and thus a smaller G number would be expected when compared to the other methods that sample in all directions. Indeed, for a change in mean linear intercept of 13%, corresponding to the aspect ratio of 0.87, the equivalent difference in G number is 0.4G units. Also, measurements using the lineal method were conducted on different parts of the samples in various orientations relative to the diametric plane, as discussed in section 5.7. When the differences between the results produced from the lineal method and the single circle, three circle and planimetric methods were considered it was found that differences ranged within  $\pm 0.5G$  units. In other words the differences were not consistently smaller, as was the case discussed in this section, since the measurements were conducted in directions other than along the diametric plane.

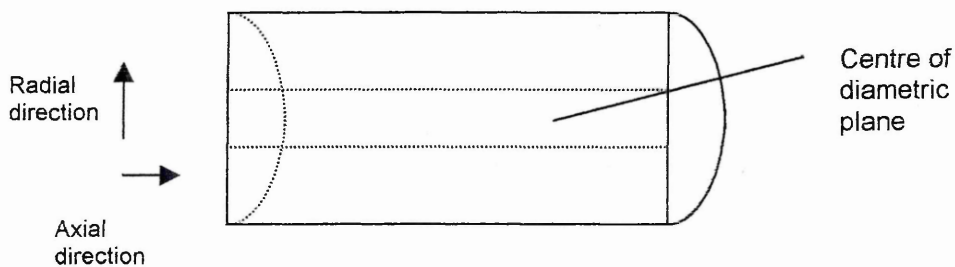


**Figure 68 A schematic demonstrating the location and directions grain size measurements were conducted during the initial characterisation of the mild steel sample.**

However, the maximum difference in the stabilising values was approximately 0.5G grain size units suggesting again that the choice of method was not significant in terms of accuracy.

E112 states that for a relative accuracy of 10% or less about 700 grains and 400 grains are required for the planimetric and the lineal methods, respectively. For the mild steel used in this work it was demonstrated that more grains were required for planimetric method than for the lineal method for a given relative accuracy, as was found in E112. However, a greater number of grains were required to achieve this relative accuracy of 10%, i.e. 600 and 2600 for the respective methods. Counting has been identified as an important factor in grain sizing. Wyman stated that although it was important to have a sufficient number of grains counted to acquire a statistical level of confidence it was also suggested that a high level of counting incurred greater errors from miscounting [102]. From this perspective it was shown that the lineal method was therefore the better method than the planimetric method with fewer grains requiring counting for a given relative accuracy.

This assessment of relative accuracy against the number of grains was extended to all methods. It was found that, to achieve a 10% relative accuracy, the planimetric method still required the highest number of grains and the lineal method the lowest. However, the requirement of more grains for a given relative accuracy was explained from a statistical perspective. The fundamental difference between using the lineal method and the planimetric

method was that the former was a one-dimensional measurement, i.e. a mean length, and the other a two-dimensional measurement, i.e. area. Thus the standard deviation of the measurements conducted using the planimetric method, measured at the corresponding number of grains for a 10% relative accuracy, was relatively higher than that of the lineal method. That is, the ratio of the standard deviation against the mean was relatively lower for the lineal method than for the planimetric method. This translated through to a higher relative accuracy using the given equations as used in E112. Indeed, when the same ratio was considered for the single circle and three circle methods they were also lower than that of the planimetric and similar to that of the lineal.

This suggested that the planimetric was the most inefficient method of all four to employ. Vander Voort corroborated this view by stating that for equal measurement accuracy, about 60% more time was required for the planimetric method than the intercept methods, i.e. single circle, three circle and lineal methods. Consequently the intercept methods were more efficient than the planimetric method [101]. With fewer grains required for a given level of accuracy then the error associated with counting a high number of grains was also effectively reduced.

However, since the lineal method was more sensitive to directionality, for a mean grain size, either the single circle or three circle method would therefore be the better choice. Each required a considerably lower number of grains measured than the planimetric method and gave a grain size that was within

$\pm 0.5G$  grain size error for all methods. This was in agreement with the findings of Vander Voort where it was found that the three-circle intercept method provided a more precise estimate of grain size in considerably less time than required by the planimetric method [80]. Furthermore, it was shown that, for a relative accuracy better than 10%, the planimetric method required a larger number of grains when compared to the other methods.

### 5.2.2. Sampling

The importance of sampling in terms of producing a measurement that is representative of the material is considered. Specifically the number of grains per field of view, the number of fields of view and finally the number of specimens are considered.

From the characterisation of the mild steel it was clear that the number of specimens used for measurement was the most important factor regarding microstructural representation.

From specimen to specimen the maximum deviation from the mean of all fields of views, 6.53 grain size number, was 1.00 grain size unit for the lineal method and 0.71 grain size unit for the planimetric method. However, the difference between the mean taken from measuring 3 fields of view and the mean from measuring 5 fields of view was 0.20G units for the lineal method and 0.03G units for the planimetric method. The final grain size measurement was

therefore relatively insensitive to the number of fields measured. Indeed the data demonstrated that a reasonably accurate measurement of grain size could be obtained by analysing one field only. Therefore for an equi-axed, ferritic steel, the number of fields per specimen measured did not play as important a role in representation as did the number of specimens.

The final part of this analysis looked at the number of grains measured per field compared to the number of fields of view. The difference in the means from using one line per field and two lines was only 0.05G units suggesting that halving the number of grains measured per field did not produce a significant effect. Therefore measuring more grains in a field of view may have provided greater statistical confidence in the measurements confined to that field, but played a less important role in the representation of the whole material.

#### 5.2.2.1. Summary

The ASTM standard, E112, provides the statistical formulae necessary to estimate a required level of confidence in the measurements. However, this is based on the number of fields used and not on the number of specimens. Therefore, it is argued that the formulae should be changed to incorporate the spatial distribution of grain size within the material, that is from specimen to specimen.

In practical terms it was accepted that it is more economical to perform grain size measurements on fewer specimens. Cutting and preparing specimens is time consuming and can be costly. However, if grain size measurement is important, perhaps for quality assurance purposes, it is recommended that an appreciation be first gained of the spatial distribution of the grain size throughout the material and from there to determine how many specimens are required to reflect this distribution. It is further suggested that the confidence in the measurements should be determined from the total number of grains measured across the specimens. Finally, the three-circle method is recommended to conduct such measurements, since it measures in all directions and requires the lowest number of grains to achieve a given relative accuracy. Although fewer grains were required to be measured for a given relative accuracy using the lineal method than that of the three circle method, it did not sample in all directions and so did not incorporate grain directionality into the measurement.

### **5.3. The Impact of Missing Boundaries on Grain Size Measurements**

Missing boundaries are important examples of the feature, or rather the lack of a feature, produced by the specimen preparation techniques. Potentially they could be seen to strongly influence the final grain size measurement. Missing boundaries occur because an etch fails to delineate a complete network of grain boundaries or to provide sufficient contrast between grains to allow each one to be seen individually [101]. Therefore, it has been an important part of grain size measurement practice to identify where missing boundaries are located. However, this is not a straightforward procedure since their identification can be very subjective and is dependent on the experience of the operator.

Initially digital images of the mild steel were created and then transformed into binary images. Subsequently these binary images were altered by removing known percentages of randomly selected grain boundaries. Grain size measurements were then conducted on each of these altered images using quantitative manual methods and also from using an automatic image analysis system. By first assuming that the images with no boundaries removed had a complete grain boundary network, and from then knowing the percentage removed, it was possible to establish a correlation between the percentage of boundaries removed and the grain size. Removing the boundaries in this

manner effectively created images with missing boundaries.

It is important in terms of representation that the microstructure produced is the true microstructure of the material; that it is not simply a result of deformation from mechanical grinding and polishing. This requires a careful and dedicated specimen preparation technique. However, it was demonstrated in this thesis that up to 20% missing boundaries did not lead to significant variations in the grain size measurements. When the mean was taken from the results from the measurements using all the manual methods, 20% missing boundaries constituted a change in grain size number from approximately 6.80 to 6.30G numbers, that is 0.50G units. This effect of missing boundaries on the grain size number was independent of the grain size. In other words the same results can be expected for different grain sizes, and so for 20% missing boundaries there is a change in grain size number of 0.50G units. This magnitude of change in the grain size approximates the accuracy expected for all the quantitative methods described in ASTM E112.

When the individual methods were considered the point of interest lay in the magnitude of the decreasing grain size number. The largest difference was found with the lineal method at 0.81 grain size unit, and the lowest with the single circle method at 0.45 grain size unit. It was speculated that the difference in the results across the methods was again due to the grain elongation, as discussed in section 5.2.1, i.e. that the measurements conducted using the lineal method were uni-directional and hence was the only

method that did not take into account the grain elongation. It was also found that the magnitude of the difference in the results between the lineal and the other methods would correspond to a difference due to elongation. The fact that the G number was consistently lower as measured using the lineal method compared to the other methods also suggested that grain elongation was the contributing factor. However, for this investigation the selection of the fields of view from specimens of the mild steel were conducted in a random manner, i.e. there was no specific area from the specimens such as the diametric plane, which was the case in section 5.2.1. The reason for the results being different across the methods has not been established.

The trends in the results from across the methods used with the automatic image analysis system were found to be in contrast to the manual measurements. Here the lineal method was yielding a higher grain size number than the single and three circle methods. Again it is unclear why there was a difference between the lineal method and the other methods. However, it is speculated that since an intercept length that is an arc, e.g. from using the single and three circle methods, requires a greater number of pixels than a straight line, this contributed to the difference. A greater intercept length corresponds to a smaller G number, hence a smaller value would be expected for the single and three circle methods compared to the lineal method. This was corroborated from the automatic image analysis measurements conducted on ellipses of various ratios of major/minor axes that as this ratio decreases, that is the more circular the shape becomes, the greater the relative number of

pixels are required to form this ellipse. In other words, when the ratio of major/minor axes increased parts of the boundary forming the ellipse approached a straight line and relatively fewer pixels were required.

### 5.3.1. Summary

The location of a missing boundary is subject to an operator's interpretation and for an intercept method of grain sizing this will influence where an intercept starts and ends. From the experiment conducted by Abrams [103] it was found that there was some systematic variation associated with different observers' interpretation of what constituted an intercept. However, although these variations were statistically significant, from a practical point of view the intercept method (three circle) transcended these observer variations. This was because the large number of intercepts provided by the method minimised this effect. Beyond this it has been shown in this thesis that, for an accuracy of  $\pm 0.5G$  units, confidence could be given to a quantitative measurement of grain size although there was an incomplete network of grain boundaries, without the need to measure a large number of grains.

In practical terms the effort involved in re-preparing a specimen due to a perceived high percentage of missing boundaries can be reduced. This effort could then be redirected to preparing more specimens in order to ensure that the required level of representation is achieved as was found from the sampling

experiments discussed in section 5.2.2.

#### **5.4. Assessment of the impact of image resolution on grain size measurements using automatic image analysis.**

Images representing the microstructure of the mild steel were also produced by using an Electron Back Scatter Diffraction technique (EBSD). Essentially this technique determines the crystallographic orientation of grains relative to reference axes, or relative to adjacent grains. This latter measurement is called the misorientation. Any misorientation found in the specimens is then represented where one grain ended and another began, i.e. the location of a grain boundary. Thus from the misorientation measurements a complete network of grain boundaries could be obtained that did not rely on grain boundary imaging techniques, e.g. optical microscopy.

These results referred to the grain size measurements conducted on two forms of the same EBSD images once the grain boundary networks had been reconstructed. One form was the original images as produced by the EBSD software and the second was from enlarging these images using interpolation, that is a greater number of pixels per grain area was produced. The actual image pixel sizes were shown in table 3. This allowed for the effect of image resolution on measurements of grain areas using an automatic image analysis system to be considered.

Humphreys [21,22] stated that EBSD could overcome the problems associated with grain size measurements particularly due to all the grain boundaries being visible. A mean grain size may appear larger from measuring with an optical technique than from using EBSD since fewer boundaries visible will cause grains to be perceived as larger. Therefore again it was assumed that EBSD would provide a complete network of grains boundaries. From this premise the difference in the mean grain areas and grain area distributions between the EBSD images and the optical images are also discussed in this section. Therefore, the grain boundary reconstruction on the EBSD images was considered to be correct and any deviations from that in the optical images are discussed.

#### 5.4.1. Differences between the EBSD images of different resolutions

The software of the automatic image analysis system employed algorithms such that the area of the grain being measured was made up of only the pixels within a boundary, and so the boundary was not included in the measurement. Therefore, it would be expected that for a given grain within an image formed with a lower pixel resolution the boundary would represent a higher percentage of pixels than that of an image with a higher pixel resolution, if the boundary thickness was the same for both images. This was demonstrated in the results presented in section 4.2.6 where it was shown that for an increase in area, in this instance the area of ellipses, the percentage of pixels forming the perimeter

reduced exponentially. Prior to these measurements being undertaken the perimeters were reduced to a one pixel thickness, as were the grain boundaries reconstructed on the EBSD images. Therefore for a higher pixel resolution a given grain will have less pixels contributing to the grain boundary and hence the relatively larger mean grain areas. When the EBSD images of different pixel resolutions were considered it was found this accounted for the variation in the mean grain areas. The mean grain areas in each of the higher pixel resolution EBSD images were of higher values than that of the equivalent lower pixel resolution EBSD images for each specimen by approximately 8%.

The other factor contributing to the different mean grain areas was the aspect ratios of the grains, as presented in section 4.2.6. Presented here were the results regarding the effect of an increasing aspect ratio of an ellipse (major axis/minor axis) on the percentage of pixels forming a perimeter, for a constant ellipse area. It was shown that for an increase in aspect ratio the percentage of pixels forming the perimeter increased. It was a requirement of the automatic image analysis system that the grain boundaries were connected using 4-connectivity. This means that a join between 2 pixels was only possible with pixels immediately left, right, top or bottom so that pixels positioned diagonally adjacent would not be detected as being connected. Therefore, a greater percentage of pixels were required to form a completely connected perimeter for an increasing aspect ratio. In a similar manner there was a correlation in the percentage difference between the mean grain area of the two EBSD images of different pixel resolutions and the average aspect ratio of the grains

measured in each. This correlation was that the lower the average aspect ratio the lower the difference in mean grain areas. Therefore the effect of the pixel resolution on the mean grain area was more marked with an increase in the aspect ratios of the grains.

#### 5.4.1.1. Summary

The grains measured in each of the two EBSD image forms were the same, except for those very small grains which were not reconstructed in the lower pixel resolution EBSD images as the image resolution was too low. Specifically, after the erosion filter had been passed through the image the grain boundaries were enlarged. The erosion filter was described in section 3.3.4.3 and essentially aided connecting up the boundaries. Then the thickening process was passed through the image, rendering the grain boundaries to a one pixel width by thickening the grains. After the erosion filter had been passed, there were insufficient pixels left for the smallest grains where the thickening filter could add pixels and enlarge the grain. Otherwise the differences in the mean grains areas were created from the other image processes that were passed through the images to reconstruct the grain boundaries. Essentially the size and shape of each grain influenced the boundary reconstruction and thus determined the percentage of boundary to grain area.

#### 5.4.2. Differences between the optical and the lower pixel resolution

##### EBSD images for grain size

The differences between the mean grain areas and grain size distributions as measured on the optical and the lower pixel resolution EBSD images are discussed in this section. Since the differences produced between the two EBSD images of different pixel resolutions were discussed previously in section 5.4.1 only the differences between the results from the optical and lower pixel resolution EBSD images are discussed here. The parameters that influenced the differences between these two image forms are the grain boundary reconstruction, image resolution and the shape of the grains measured. The grain shapes were considered for those grains where there were missing boundaries in the optical images, i.e. to determine if the shape of these grains contributed to the difference in the mean grain area as well as the difference in the boundary reconstruction. Specifically the aspect ratios of these grains were compared to those of the equivalent larger grains in the optical images. The grains were larger in the optical images because of the missing boundaries.

Both sets of results produced by two operators are also considered in this section where they are compared to one another. The results from each individual specimen and operator are discussed in turn. All the results discussed here were presented in section 4.2.7.

The mean grain area measured via the EBSD technique was lower than that via the optical technique by 11% for specimen 1. However, there were 15% more grains measured in the optical. This would reduce the mean to a value lower than that of the EBSD image since the measurement area was equal for both cases and so a greater number of grains would have to be smaller to fit. Ensuring the same area was measured in each image was achieved by indenting the specimens before the images were formed. Some of these extra boundaries were reconstructed due to artefacts being mistaken for a boundary. An artefact may be an inclusion or simply dirt on the specimen surface. With the optical image being of a grey level composition there was no colour indication that this might have been something other than a grain. Reconstructing this as a grain, i.e. creating a boundary around it, appeared to be done particularly when it was assumed that it was a small grain, and formed the grains within the 2 to  $15.8\mu\text{m}^2$  range. Specifically, these features were mistaken for a grain when they appeared within a corner of a larger grain, and so were partially surrounded by grain boundaries from the larger grain, which contributed to the evidence that it was a grain. Such wrongly reconstructed grain boundaries were also found in specimens 3 and 4.

Also some of the grains in the optical image, which did not exist in the EBSD image, were within the 32 to  $126\mu\text{m}^2$  size range. These small grains were not evident from the EBSD image during the grain boundary reconstruction, as described in section 5.4.1. The fact that there were grains within this grain size range in the corresponding higher pixel resolution EBSD image confirmed this.

There were sufficient pixels in the higher pixel resolution EBSD images from which the grains could be reconstructed.

More grains measured in the optical image than the EBSD image would reduce the mean grain area in the former. However, the image pixel resolutions were determined automatically by the respective EBSD and optical systems and the number of pixels per mean grain area was lower in the EBSD image than that of the optical by a factor of 10. The reason for the mean grain area in the EBSD image being lower than that of the optical image, the reverse case than what would be expected from the number of grains measured, was attributed to the difference in the pixel resolution. The percentage of boundaries to grains was therefore significantly higher in the EBSD reducing the grain area. Also, there were three missing boundaries identified in the optical image. There were therefore six grains in the EBSD image for these three grains containing the missing boundaries. The aspect ratios of these grains were higher in 4 of the 6 grains when compared to the corresponding grains in the optical. As was demonstrated in the results produced from comparing the percentage of perimeter to the total area, in section 4.2.6. the higher the aspect ratio the greater this percentage. Therefore, this also contributed to the mean grain area in the EBSD image being smaller than that of the optical.

There were similar reasons for the EBSD image producing the lower mean grain area than the optical image reconstructed by operator 2. Here there were 5% more grains measured in the optical image but a lower mean grain area in

the EBSD image, in this instance by 3%. As with operator 1, there was a higher number of pixels per mean grain area in the optical image plus higher aspect ratios in 5 of the 7 grains measured in the EBSD image where there were missing boundaries in the optical image. This counteracted the higher percentage of grains measured in the optical.

The extra grains in the optical image by operator 1 were reconstructed due to artefacts being mistaken for grains. Such artefacts were shown to be reconstructed as small grains in the optical image. However, the small grains reconstructed by operator 2 were identified as being correct by comparing them with the corresponding higher pixel resolution EBSD image.

The closest match of the average number of pixels per mean grain area between the optical and EBSD images was found in specimen 2 although the optical had a greater value by a factor of 2. There were 5% more grains measured in the EBSD image than the optical, all found in the 32 to 1008 $\mu\text{m}^2$  size range. Thus, being relatively small grains they did not effect the mean significantly. Therefore, the higher number of pixels per mean grain area, thus a lower percentage of boundary to grain, produced the higher mean grain area in the optical image by 24%. There were 2 more grains in the EBSD image due to missing boundaries in the optical and one of these grains had a higher aspect ratio than the optical grain. Therefore the percentage of boundary to total grain area was higher in the EBSD image for this specific grain thus the

grain area was reduced. This therefore also contributed to the difference in the mean grain area between the two image forms.

The EBSD mean grain area was 21% smaller than the optical for operator 2. However, in this case there were 3% more grains in the optical image, mostly within the 1008 to 4032 $\mu\text{m}^2$  size range. Although these grains were large they did not decrease the mean relative to the EBSD image as significantly as the difference in the number of pixels per mean grain area. There was double the number of pixels per grain area in the optical compared to the EBSD. Hence the percentage of boundary to grain area was less in the optical. As with operator 1 only 1 of the 2 grains, where there were missing boundaries in the optical, had a higher aspect ratio in the EBSD image and this contributed to the lower mean area in this image form.

In specimen 3 the combined effect of a significantly greater number of pixels per mean grain area and a greater number of grains measured in the EBSD image produced the higher mean grain area in the optical. The optical had a greater number of pixels per mean grain area by a factor of 8 and there were 17% more grains measured in the EBSD image. This combined effect produced a 24% difference in mean grain areas. This was also reflected in the grain area distribution where there were more larger grains measured in the optical image within the 1008 to 8065 $\mu\text{m}^2$  size range. These larger grains increased the mean grain area. Only one of the four grains in the EBSD image, due to missing boundaries in the optical, had a higher aspect ratio. Therefore

the corresponding grains in the optical image had a higher percentage of boundary to grain area and thus a relatively smaller grain area. However, this only marginally increased the mean grain area in the EBSD image relative to the optical image.

As with operator 1 there were more grains in the EBSD image than the optical image as reconstructed by operator 2. In this instance there were 10% more grains in the EBSD image. However, the majority of these grains was relatively small, within the  $63$  to  $252\mu\text{m}^2$  size range, and so only contributed marginally to decreasing the mean grain area relative to the optical image. When the missing boundaries were considered only 3 of the 8 grains were of a higher aspect ratio in the EBSD image. This, together with the significantly higher number of pixels per mean grain area in the optical image, contributed to the highest difference between both mean areas, at 27%.

The reasons behind the higher mean grain area in the optical, by 18%, for specimen 4 were similar to those found for specimen 2. The number of grains measured were similar, with 7% more in the optical, as were the aspect ratios of those grains in the EBSD image not in the optical due to missing boundaries. The principal reason therefore for the higher mean grain area in the optical was again due to the higher number of pixels per mean grain area, in this case by a factor of 3.5.

5% fewer grains were measured in the optical image than the EBSD image by operator 2 for specimen 4. This reduced the mean grain area in the EBSD image relative to the optical image. Together with this and the higher number of pixels per mean grain area in the optical image, the mean grain area in the optical was 26% higher.

### **5.5. Comparison of the results from the two operators**

By using the EBSD images as a standard from which to compare, the differences in the reconstruction of the boundaries in the optical images by both operators could be undertaken. They were compared to the same EBSD image relative to each specimen. However, the number of grains with higher aspect ratios measured in the EBSD images that did not exist in the optical images was similar for both operators. Also, both operators measured the same optical and EBSD images and hence the image pixel sizes were equal. Therefore, the only differences between the two sets of results were due to a difference in the number of grains measured in the optical images, hence the differences in the reconstruction. Any differences referred to in the comparison of the two operators are therefore between the EBSD images and the optical images as they were reconstructed by each operator. Also, the mean grain areas measured in the EBSD images were consistently lower than the corresponding optical images since it was the lower EBSD image size that was used for the comparison.

For specimen 1 there were fewer grains reconstructed by operator 2, which increased the mean grain area. When compared to the EBSD image, this lower number of grains reconstructed rendered the difference in the mean grain area to be significantly higher for operator 2 than operator 1.

For specimen 2, operator 2 reconstructed more grains in the optical image than operator 1 did although the mean grain area from operator 2 was higher. This was explained by the location of the grains reconstructed, as compared to the EBSD image. The extra grains in the optical image reconstructed by operator 2, that is those grains that did not exist in the EBSD image, were small. Therefore, the contribution these grains made to the mean was marginal. However, the grains in the EBSD image not in the optical for operator 1 were large and so did significantly contribute to the mean grain area. The greater difference in mean grain area from the reconstruction conducted by operator 2 was therefore due to size of grains that existed in one image form but not the other.

Similarly for specimen 3 the number of grains reconstructed did not explain why one operator produced a greater mean area than the other operator. The explanation was found in the size of the grains since although operator 1 reconstructed fewer grains than operator 2, operator 2 produced the higher mean grain value by reconstructing more larger grains.

Finally, for specimen 4, the reasons why operator 2 produced the higher mean grain area were firstly due to fewer grains reconstructed in the optical image by this operator. The second contributing factor was again the size of the grains. When compared to the EBSD image it was seen that there were more larger grains reconstructed by operator 2 and this also increased the mean grain.

To summarise, the differences in the mean grain area between the optical and EBSD images for each specimen were due to the grain shape, the reconstruction of the grain boundaries and the pixel resolution of the digital images. One of the limitations of image analysis was defined by the resolution of the camera and microscope, both limiting the overall imaging resolution. Thus, according to Vander Voort image analysis was more sensitive to magnification effects than manual methods [14]. It was found in this section that the parameters that contributed most to the differences in mean grain areas measured in the optical and EBSD images were the pixel resolution of the images and the number of grains measured. Combining these two parameters produced a number of pixels per mean grain area. This was found to be higher for the optical images than for the lower pixel resolution EBSD images for all specimens. It was found that even when this was higher in the optical by a factor of two there was still a difference in the mean grain areas of 17%.

Sphericities were also considered in the differences in the results from the optical and EBSD image forms. Sphericity uses a number between 0 and 1 to describe a shape such that a 1 describes a perfect circle whereas introducing irregularities to a shape, as is found with real grains, reduces this number. When the average sphericities for the lower pixel resolution EBSD images were considered, as reported in section 4.2.7., it was found that specimens 2 and 4 had higher values compared to the optical images. The difference in the number of pixels per mean grain area and the number of grains measured

between the optical and the lower pixel resolution EBSD images were the lowest in specimens 2 and 4. With these differences being the lowest the difference in the mean grain areas might then be expected to also be the lowest. However, the lowest difference in mean grain areas was not found in either of these two specimens. Indeed it was found in specimen 1 where the difference in the number of pixels per mean grain area was highest of all specimens. In this specimen the average sphericity was less for the optical image than for the EBSD. Therefore the higher sphericities of the EBSD images in specimens 2 and 4 contributed to the difference in the mean grain areas being higher than that found in specimen 1. In other words, the general shape of the grains in the optical images for specimens 2 and 4 were more circular than those in the EBSD images. When measuring these grains using digital images, a lower percentage of pixels form the grain boundaries when the shape of the grain approaches a circle. This effectively increased the mean grain areas for specimens 2 and 4 to a value even higher compared to the lower pixel resolution EBSD images.

Also, the decisions made by each of the 2 operators in reconstructing the grain boundaries created significant differences in the mean grain areas when compared to the EBSD images, particularly when larger grains were reconstructed. The criteria behind these decisions are explored in more detail in section 5.5.1.

5.5.1. Assumptions made in the reconstructing of the optical images by two different operators

The results discussed in this section were presented in section 4.2.5. Shown in that section were the results of the grain area distributions and the mean grain areas of the optical images reconstructed independently by two operators. These results were then compared with those of the corresponding EBSD images of the larger pixel resolution. With the premise that the EBSD system provided a complete network of boundaries this could then be utilised to determine the differences in the location of grain boundaries as determined by the two operators. Specifically, this section discusses the evidence found for the assumptions made by each operator with regards to grain boundary reconstruction.

The grain area distributions and mean grain areas from all four specimens together are discussed with individual specimens referred to with regards to the specific points raised.

The mean from the optical images reconstructed by operator 1 was closer to the means of the higher pixel resolution EBSD images than that of operator 2. Therefore there was poor reproducibility between the two operators and these differences were accounted for by the subjective nature of selecting the location of a boundary. For example, it has been well established that it is

impossible for there to be more than 3 grains meeting at one boundary junction. However, in specimens 3 and 4 the reconstructed boundaries from operator 1 included junctions where there were more than 3 grains meeting, although this was not the case with operator 2.

Leithner detailed the limitations of image analysis in grain size measurement based upon the importance of specimen preparation [10]. Indeed it was stated that automatic image analysis of microstructures necessitated the most optimum specimen preparation possible. From examining the optical images of each specimen it was of interest to note that specimen 1 had the greatest contrast between grains, whereas there was good contrast in the other three specimens between grain and boundary. What was also significant was that specimen 1 showed a very little difference in the mean grain area between both optical and EBSD images, indeed there was hardly any difference for operator 1. Relatively few missing boundaries were found for operator 1. The differences in the grain area distributions were therefore accounted for mostly by the extra boundaries reconstructed in the optical image that were not on the EBSD image. However, with such good correlation between the mean grain areas the number of boundaries that existed in one image form but not the other was low. Therefore contrast between the grains aided the operator to locate boundaries better than contrast between the boundaries and the grains.

### 5.5.2. Boundaries found in one image form but not in the other

It is pertinent to discuss in more detail why some boundaries existed in either the optical or EBSD images but not in both. Since only the differences between the optical and EBSD images of the higher pixel resolution are discussed in this section the only contributing factors to the production of a difference in the mean grain areas were limited. These factors were a different number of grains measured between images, a boundary had been reconstructed in the optical image that did not exist in the EBSD image (extra boundaries), and missing boundaries. After an examination of both image forms those boundaries that did not exist in both were identified.

#### 5.5.2.1. Boundaries that existed in the optical images but not in the EBSD images

From examining the location of where a boundary had been reconstructed on the optical image, but EBSD showed that there was no boundary, it was possible to determine some of the image features that influenced each operator in making their incorrect assumptions regarding what constituted a grain. These are listed below:

- An artefact within the image assumed to be a grain.
- A line assumed to be a boundary.
- The shape and size of surrounding grains.

The instances where an artefact was mistaken for a grain, and hence boundaries were reconstructed around it, were discussed in section 5.4.1 and so only lines and the shape and size of surrounding grains are discussed in this section.

There appeared in the optical images almost straight lines that were scratches from specimen polishing and were mistaken for a boundary. The lines started and stopped within one grain when this grain was more raised from the surface than the surrounding grains, this relief being produced from polishing and was indicated by a grey level contrast in the optical images. The fact that they

started and finished at a grain boundary contributed to them seemingly being boundaries also.

Although there was no clear evidence for this, it was assumed that the general size of the grain perceived by an operator, that is in a similar way an operator assesses grain size by using the comparison chart method, influenced decision of where a boundary was located. When using the comparison chart method an average grain size is often required and for the reconstruction of a boundary it was argued that this perceived average grain size was influencing this decision. In other words a boundary was reconstructed within a grain if it was deemed to be too large. This was particularly true if there were other features, described above, involved. For example, if a scratch was mistaken for a boundary but the grain then created by this boundary was consistent with the general perceived grain size then this boundary would remain. In other words there was no indication that this grain was inconsistent with the general view.

#### 5.5.2.2. Boundaries that existed in the EBSD images but not in the optical images (missing boundaries)

Those boundaries that were reconstructed by operator 1 in the optical images but did not exist in the EBSD images were removed. Any differences in the location of boundaries were now effectively due to missing boundaries in the

optical images. The differences in the mean grain areas between the optical and EBSD images were then reconsidered and results discussed in this section were presented in section 4.2.4.1.

Certain features were identified to explain why these missing boundaries had not been created on the optical images but existed in the EBSD. These are as follows:

- No partial boundary from which to complete.
- The generally perceived grain shape.
- Grains too small to be visually clear.

Often a boundary was not completely etched but left only a partial boundary. This was a clear indication where a boundary should be reconstructed and without them a boundary could be missed. This applied to all grain sizes.

In a similar way with boundaries being reconstructed that did not exist, the perceived shape and size of the grains were influential to missing a boundary. This was particularly influential with regard to grains that were missed because they were within a large grain and at one edge. Therefore when they were not reconstructed in the optical image then the remaining large grain appeared consistent with the surrounding grains. This was found in specimens 1 and 2 and accounted for there being more grains measured by both operators of areas between 252 to 2016 $\mu\text{m}^2$ . Also, it emerged that the general shape of the

grains influenced each operator differently. For example, sphericity measurements were undertaken on the grains where there were missing boundaries in the optical images and on the equivalent grains in the EBSD images. The standard deviations on the means of these sphericities from all specimens were also calculated. It was found that the standard deviation was significantly lower for the grains in the optical images for operator 2 than those from the EBSD images for the same operator whereas they were found to be similar for operator 1. The tighter spread of the sphericities results suggested that operator 2 was more consistent in reconstructing grains that were of a similar shape.

Small grains had been missed also because they were so small the resolution of the image was such that they could not be seen as etched up boundaries. The evidence for this was found in specimen 4. This specimen had the lowest number of pixels per mean grain area of all the optical images and there were very small grains not measured in the optical images by both operators that existed in the EBSD. The determination of a grain boundary in the EBSD images did not require a boundary to be delineated as was the case with the optical images. Colour coding represented the misorientation of the grains with the EBSD system and so the location for reconstructing a boundary was determined from a change in colour. Therefore, very small boundaries were not lost due to an insufficient pixel resolution as was the case with the optical image for specimen 4.

## **5.6. Missing boundaries and misorientation**

In trying to understand further why an incomplete network of grain boundaries was found with optical imaging from nital and Marshall's reagent not etching up all the boundaries in the mild steel, the misorientation angles for the missing boundaries were analysed. This analysis was derived from the results reported in section 4.3 where, by comparing the optical images with the corresponding EBSD images of the same areas, the location of missing boundaries was found. EBSD provided the misorientation data for these missing boundaries.

There was a broad range of misorientations angles found, from 5.35 to 59.65°. However, when the boundaries were categorised as low angle, e.g.  $<15^\circ$ , and high angle,  $\geq 15^\circ$  then a trend emerged. Specifically there were more high angle boundaries than low angle boundaries with 81% and 87% of the total number of missing boundaries, for each of the two operators respectively, being high angle boundaries.

Also, each missing boundary was characterised as follows:

- Not etched up.
- Small grain.
- Partially etched up boundary.
- Small grain, partially etched up.

However, it was found that there were no obvious differences between each characterisation category, that is there were similar ranges found to that of the overall misorientation angle range for all the missing boundaries.

#### 5.6.1. A summary of the results from using automatic image analysis

As a comparison with manual image analysis Le Pennec et al set out to measure low carbon steel using automatic image analysis [13]. It was concluded that the questionable reproducibility of manual methods was overcome and in addition a relative error of the mean intercept of 1% or 2% could be gained allowing mechanical properties to be predicted with a level of accuracy never before reached. In this study the relative accuracy on the total number of grains measured in all specimens together using automatic image analysis was approximately 14%, which was considerably improved on those discussed in section 5.2.1 for the best of manual measurements for the same number of grains. This concurred with the findings of Le Pennec in this instance but it had also been demonstrated that reproducibility between two

operators was low since the mean values for all specimens was approximately 10% different. Hence automatic image analysis was not found to overcome the questionable reproducibility of manual methods significantly since the determination of the location of a boundary was still subjective in nature.

When the differences in the optical and EBSD images were considered the influencing factors were the image pixel resolution and the location of the boundaries. When those boundaries that existed in the optical images but not in the EBSD images were removed then any difference in the location of boundaries were due to missing boundaries. These were boundaries that have been missed in the optical images due to either the image resolution or a failure to chemically etch them. There was no direct correlation derived between the misorientation of the grains and partially etched or completely unetched boundaries. The optical images were then measured again for grain size and the differences in the mean grain areas when compared to the higher pixel resolution EBSD images ranged from 11 to 25%. Even for specimen 2 where there were only 3 missing boundaries, this difference was still 16%.

When the image pixel resolution was considered as the only factor influencing the differences between grain area means of the same specimen area, as was the case when both EBSD images of different pixel resolutions were compared, there was a difference of between 6 and 10%. When the subjective nature of the reconstruction of boundaries were incorporated then the differences in

mean grains areas changed the range from 3 to 27%, as was found when the optical and the lower pixel resolution EBSD images were considered.

### **5.7. Comparison of manual and automatic grain size measurements with optical and EBSD imaging**

The images created using optical and EBSD systems for specimens 1 to 4 were also measured using manual methods, e.g. planimetric, single circle, three circle and lineal. Although the same mild steel sample was used for these manual measurements as was the case for the results discussed in sections 5.2.1 to 5.3 different fields of view were used. With the variation in grain size across the specimen the results were different.

The fundamental difference between measuring manually and measuring using the automatic image analyser is that the latter required images to be digitised beforehand. Grain boundaries were considered to have no width when measurements were conducted manually whereas a one pixel width was applied to the automatic measurements. Other digital image processing effects are also considered in this section, and were also discussed in section 5.4.1. The EBSD images with the higher pixel resolution were used to minimise these effects. By using the higher pixel resolution the effects of image processing on the differences between using manual and automatic techniques became more obvious. In other words, although the effects of image processing were

minimised they were still shown to have a significant effect on the measurements. The results from these measurements were reported in section 4.2.5. where there were plots comparing manual measurements and measurements conducted using the automatic image analysis system. The ASTM G numbering system was utilised to provide a common results system to allow a comparison across all measurement techniques. On a point of clarity, when a result is described as being higher than another this effectively means that the corresponding grain area is lower. In other words a higher G number is equivalent to a lower grain area.

This section discusses the results of measuring each image form, EBSD and optical, using each of the manual methods. It also discusses the differences between measuring using automatic methods and using manual methods.

#### 5.7.1. Differences between manual measurements of the EBSD and optical images

In this section the variation between the measurements conducted using the manual methods only are considered. Specifically the reasons for the EBSD images producing different results from the optical images are discussed.

The results from measuring the EBSD images using all the manual methods were consistently higher than from measuring the optical images. Any

difference was attributed to the EBSD image showing more reconstructed boundaries than the optical due to the boundaries defining a misorientation between adjacent grains. In other words, the location of boundaries for reconstruction was more obvious using the EBSD images than the optical images where the location of the boundaries was determined from etching and from the discretion of the operator. The differences produced were within the range of 0.1G to 0.8G units.

The greatest difference in G number between the two image forms was produced in specimens 1 and 2. These specimens had the fewest grains measured of all specimens and so any differences due to missing boundaries will have a more marked effect on the grain size than would be for more grains measured, as was the case for specimens 3 and 4. The differences in grain size between the optical and EBSD images for specimens 3 and 4 were within the range 0.1 to 0.4G units whereas for specimen 1 and 2 it was between 0.1 to 0.8G units.

### 5.7.2. Differences between manual and automatic measurements of the EBSD and optical images

In this section the difference between the automatic image analysis technique (automatic) and manual methods is discussed.

There was a significant difference in the results from measuring using automatic and manual methods. The greatest difference in the G number was found measuring the optical image of specimen 2 using the single circle manual method. This difference was 1.16G units and the smallest difference was 0.09G units, from measuring the EBSD image of specimen 1, using the lineal manual method. This gives a range of difference of slightly more than 1G unit. This range was attributed to the variations in the manual methods, which were discussed in section 5.2.1. However, since the difference between the automatic and planimetric measurements was still approaching 1G in many instances and there were a similar number of grains measured in both instances, the extent of this difference was also accounted for by changes in the images from digitising for subsequent automatic measurements.

This was explained from measurements conducted on ellipses of various areas using the automatic image analysis system. The results from these measurements were presented in section 4.2.6. and showed that for an

increase in the area the percentage of perimeter to area decreased exponentially. In other words, for an increase in the number of pixels forming the area there were relatively fewer pixels forming the perimeter. This might be expected since the perimeter was reduced to a one pixel width for all ellipses. However, the percentage of perimeter to area was also calculated manually and the results of these measurements were around 11% lower than the equivalent automatic measurements. This was accounted for by the automatic measurements not including the perimeters for the area measurements but they were included for the manual calculations. The areas measured using the automatic technique were therefore relatively smaller than that of the manual for the equivalent ellipses. Thus the percentage of perimeter to area increased.

This reflected what was happening with the automatic and manual measurements on the optical and EBSD images and partly explained the differences. The perimeter was effectively the grain boundary and the ellipses represented the grains. 11% difference in the percentage of perimeter to area corresponded to 0.34G units.

When the individual methods were considered it was found that the planimetric method either produced the smallest or the second smallest difference with the automatic measurements of all the manual methods. This was found for both the optical and EBSD images. The planimetric method involved counting the number of grains within an area, thus producing the number of grains per unit area. This is effectively the mean grain area, which was how the automatic

measurements were conducted. The similarity of the two measurement methods accounted for the relatively small difference.

The largest difference between the manual methods and automatic was therefore found with intercept methods, e.g. lineal, three circle and single circle. There was no obvious trend found with the largest difference, that is no one intercept method was consistently producing the largest difference nor was there any correlation with the number of grains measured within each specimen. However, there were fewer specimens with the three circle method than each of the other intercept methods where the largest difference was produced. For any of the optical images the three circle method did not produce the largest difference for any specimen and was the second largest for two. For the EBSD images the three circle method produced the largest difference for one and the second largest for three.

This was attributed to the fact that approximately twice as many grains were measured for the three circle method compared to the lineal and single circle methods. Also, the number of grains measured using the three circle method approached the number measured using the automatic method. The lineal and single circle methods did not incorporate the large grain size distribution found in this material with too few grains measured. Conversely sufficient grains were measured using the three circle and automatic methods to incorporate this large distribution. The number of grains therefore had a significant effect on the mean values.

The individual specimens were considered when comparing the G numbers of the manual and automatic methods. For the optical images it was found that the greatest or second greatest differences were found in specimen 1 for three of the four manual methods. However, the number of pixels per mean grain area was the highest for this specimen. The results from the measurement of the ellipses showed that for a larger area the percentage of pixels forming the perimeter was lower. Thus, since specimen 1 had the highest number of pixels per mean grain area, the difference between the manual and automatic measurements would have been expected to be the lowest. Similarly the greatest difference in the EBSD images when the manual and automatic measurements were compared was found in specimen 2 for three of the four manual methods. Again this was inconsistent with the findings from measuring the ellipses since the greatest number of pixels per mean grain area was the highest for this specimen.

Therefore, the differences were not completely accounted for from the boundary not being included in the automatic measurements since this would only be around 0.3G units as was shown from the results of the measurements on the ellipses. The actual differences ranged from 0.5 to 1.2G units. However, specimens 1 and 2 had less than half the number of grains measured in specimens 3 and 4. The differences in specimens 1 and 2 were therefore also accounted for by relatively few grains intercepted or counted. As discussed previously in this section the planimetric method produced the

closest G number to the automatic measurements. The greatest differences in the G number between the planimetric method and the automatic method were found in specimens 1 and 2 for the optical and EBSD images respectively. The values of these differences were 0.5G units and 0.3G units for the optical and EBSD images respectively and was accounted for largely by the image processing. However, the differences between the G numbers between the intercept manual measurements and the automatic measurements were significantly higher for these specimens by more than double. Therefore, the combination of image processing and the relatively few grains intercepted accounted for the greatest difference between the two forms of measurement techniques.

#### 5.7.2.1. Summary

Measuring the EBSD images consistently produced a higher G value, thus a corresponding lower mean grains area, than from measuring the optical images. This was due to the EBSD system producing a boundary from a difference in misorientation between grains and hence a complete grain boundary network was the result. More boundaries were found and hence reduced the grain size, i.e. increased the G value. The highest difference in G value between the EBSD and optical images was found for specimens 1 and 2 since there were fewer grains measured in these specimens.

It was found that the differences between the automatic and manual methods were partly due to image processing. Without the boundaries being included in the measurements this effectively reduced the grain size and hence increased the G value. However, the number of grains measured also played an important role in producing the difference. It was found that the three circle method produced a lower difference as there were more grains measured. Finally the form of the manual method also contributed to the differences. The planimetric method was the closest in measurement technique to the automatic method since they both involved measuring the grain area. Indeed the differences between these two methods was accounted for by image processing where again a higher G value was found in the automatic method as the boundaries were not included in the measurements.

## **5.8. Misorientation data for grain boundaries between large/large, large/small and small/small grains**

This section discusses the trends associated with the misorientation angles of boundaries between small/small, small/large and large/large grains. The corresponding results were reported in section 4.4 where there were plots of misorientation against the percentage of boundaries, which were categorised according to the small/small, small/large and large/large grains. A different material was used for this investigation to those that have been discussed previously, namely pearlite/ferrite steel. However, only the ferrite phase of the steel was investigated since this contributed to a significantly larger proportion and simplified the investigation into the relationship between misorientation and grain size.

### **5.8.1. The association of misorientation and grain size**

This section discusses all the results produced from measuring the grain size and misorientation of all specimens. These results were categorised according to the size of the grains and the trends of misorientation and grain size are discussed. Misorientations below  $15^\circ$  were defined as low angle boundaries and thus high angle boundaries were greater than/equal to  $15^\circ$  misorientation.

It was demonstrated from the results that the highest percentage of high angle boundaries were between the large/large grains, followed by the small/large grains with small/small grains showing the lowest percentage. Therefore the lowest percentage of low angle boundaries were between the small/small grains.

Also, as there were higher misorientations found between the large/small grains than the small/small grains then these higher misorientations were associated with the large grains. Also, as the highest percentage of low angle boundaries was found between the small/small grains, with around 30%, compared to around 10% for large/large and 20% for small/large, then low angle boundaries were associated with small grains.

## **6. CONCLUSIONS**

### **6.1. Grain size methodology**

#### **6.1.1. Inter-comparison of manual methodologies**

- The variation in the mean grain size determined from the four quantitative manual methods was within the accuracy level stated in the ASTM E112. The choice of method with regards to accuracy is therefore not important.
- The planimetric method was found to be the most inefficient method because it required the highest number of grains to achieve a specific relative accuracy. Therefore it is concluded that any of the single circle, three circle or lineal methods are the better choice since they required fewer grains measured.
- It was also found that grain directionality affected the lineal method more than the other three. This was due to measurements using the lineal method being taken in one direction whereas the other three measured in all directions.

#### **6.1.2. Sampling for grain size measurements**

- Measuring more specimens is more representative than measuring more fields of view within fewer specimens.

- Varying the number of grains within a field of view had a negligible impact on the grain size measurement.
- The variation in the means calculated for each specimen was greater than the accuracy level stated in E112 although the variation in the means calculated from varying the number of fields of view and also the number of grains was within this accuracy level.

### 6.1.3. The choice of manual grain size measurement methods

It is concluded that the single circle is the best manual measurement method and the reasons for this choice is explained in the following conclusions where it is compared with the other three methods:

- Fewer grains are required to be measured in order to achieve a specific relative accuracy compared to the planimetric method.
- The mean determined using the single circle method is not sensitive to grain directionality, unlike the lineal method.
- In order to be representative of the material being measured fewer grains should be measured per field of view relative to the number of fields or specimens measured. The single circle measures fewer grains than the three circle method.
- Measuring fewer grains per field of view minimises the errors induced from counting many grains or intercepts.

## **6.2. The Impact of Missing Boundaries on Grain Size Measurements**

- A visual inspection of the images with the maximum percentage of missing boundaries (20%) could warrant re-preparation of the specimen under normal circumstances to increase confidence that the revealed microstructure was representative of the sample. However, the variation in the grain size from measuring images with the maximum percentage of missing boundaries (20%) compared to no missing boundaries was within the accuracy level stated in E112.
- This quantitative assessment of the impact of missing boundaries on a mean grain size is independent of the sample grain size, i.e. that same magnitude of difference from zero to the maximum number of missing boundaries would be found for materials of all grain sizes.

### **6.3. The impact of pixel resolution on grain size measurements using automatic image analysis**

#### **6.3.1. Grain sizes of EBSD images of different pixel resolutions**

- The differences in the mean grain size from using images of different pixel resolutions were derived from the automatic image analyser which did not include the grain boundaries within the measurement.
- The grain area measurements conducted on the lower pixel resolution images were lower than the higher pixel resolution since the ratio of boundary/grain was higher for the former, i.e. a higher percentage of pixel formed the boundaries resulting in smaller grain areas to be measured.
- The greater the grain elongation the greater the ratio of grain boundary to grain area.
- The combined effect of a low pixel resolution and a high grain elongation produced the least accurate grain size measurement since then this produced the highest percentage of pixels forming the grain boundary, which were not included in the measurement.
- The very small grains were lost to the digital image processing necessary to reconstruct the grain boundaries since the pixels required left none for the area of the grain. This effected the lower pixel resolution image more than the higher.

### 6.3.2. Grain sizes of optical images and lower pixel resolution EBSD

#### images

- The differences in the grain size measurements between the optical and EBSD images were accounted for by both grain boundary reconstruction and the pixel resolution.
- The pixel resolution played a more important role than the boundary reconstruction in determining the mean grain area.
- Since there was some variation in the percentage difference in the mean grain areas between the same optical images reconstructed independently by two operators the boundary reconstruction therefore contributed significantly to the difference in mean grain area.
- The shape of the grains also contributes to the differences in the mean grain areas.

## **6.4. The decisions regarding reconstructing grain boundaries**

### **6.4.1. Boundaries reconstructed in one image form but not in the other**

- From sphericity measurements of the reconstructed grains it was found that one operator was more consistent in producing grains of a similar shape than the other. Therefore, the perceived general grain size influenced the decisions why an operator would reconstruct a boundary when it was not clear that one existed.
- A low pixel resolution in the image failed to show where the grain boundaries of the small grains were for subsequent reconstruction.
- The reproducibility of grain size measurements of the same optical images between two operators was low due to the variations in boundary reconstruction.
- The optical images were measured again after the removal of those boundaries that were shown not to exist by a comparison with the corresponding EBSD images. This revealed that the variation in the mean grain area of the optical images and the EBSD images is greater than the E112 accuracy level.

## 6.5. Manual measurements of EBSD and optical images

- The differences between the manual measurements of optical and EBSD images were due to more delineated boundaries in the EBSD images.
- The number of grains plays an important part in the magnitude of difference between grain sizes measured in both image forms, i.e. that a lower difference between the EBSD and the optical images was found with a higher number of grains measured.
- The variation in the grain size between the two image forms was greater than the accuracy level stated in E112 for those fields of view with few grains measured but within this accuracy level for those with the higher number of grains measured.

### 6.5.1. Manual and automatic measurements of EBSD and optical images

- Automatic image analysis is still subject to the same problems of boundary determination found with manual methods since there was still some variation in the grain size from the reconstruction of the boundaries on the same optical images by two operators.

- The relative accuracy of the sample measurements by automatic image analysis, that is of all specimens together, was improved compared to manual measurements.
- The difference between measurements conducted using the planimetric methods and automatic image analysis system was completely attributed to the boundaries not being included in the automatic measurements. In other words, highly reproducible results were obtained between the planimetric method and automatic image analysis since both follow the same principle, i.e. that the whole grains are measured.
- The difference in the grain size from using the intercept methods and automatic image analysis were not accounted for completely by the boundary not being included since the magnitude of difference did not correspond.
- The number of grains measured also played a role with the smallest difference found between the automatic image analysis system and the three circle method, where there were more grains measured compared to the other intercept methods.

## **6.6. Missing boundaries and misorientation angles**

- The majority of missing boundaries were high angle, i.e. greater than  $15^\circ$ .
- It was observed that boundaries were not reconstructed due to them being either only partially chemically etched up or not at all or that the resolution of the image was too low for the boundary to be visually clear. It was found however that there was no direct correlation between these categories of missing boundaries and their misorientation angles.

**6.7. Misorientation angle of grain boundaries between large/large,  
large/small and small/small grains**

**6.7.1. The association of misorientation and grain size**

It was concluded from an analysis of the relationship between misorientation angles and grain size was that the highest percentage of high angle boundaries was between large/large grains, the second highest between large/small grains and the lowest between small/small grains.

## **7. FUTURE WORK**

### **7.1. Grain size measurements**

The work reported in this thesis was conducted on a relatively simple steel microstructure and future work would lie in improving the practice of grain size measurements of more complex structures. In doing so various aspects could be considered, some of which are listed below:

- A more descriptive means of measuring grains would be to include their shape. This has been achieved to a certain extent in this thesis by using the ratios of the longest chord length to the shortest and by sphericity measurements. However, these have been considered only in terms of their impact on the mean grain size measurement whereas more use could be made if the grain shape were related to properties. For example, cleavage planes are important to impact toughness and a useful programme could be to study the relationship of these and the shape of the grain. The use of the electron back scatter diffraction (EBSD) technique could provide the necessary orientation information.
- The measurement of grains of a structure made up of more than one phase could be achieved more effectively with the use of EBSD. Through the interpretation of EBSD patterns it is possible to define different phases effectively and to then determine the grain boundaries within each from the orientation of one grain to another. This has potential for those materials

where it is difficult to etch up boundaries in one phase and simultaneously in another using traditional chemical or electro etching techniques.

- It was shown in this work that grain size distributions can be more meaningful than a mean grain size when they are considered in terms of properties. This relationship between the grain size distribution and material properties could be investigated in other materials with other properties.

## **7.2. Automatic image analysis**

The use of automatic image analysis is becoming more prominent. However, more work is required in various aspects, including the reconstruction of the grain boundaries, pixel resolution and including the boundary into the measurement. The following are specific areas in which future work could lie:

- Current conventional image analysis systems are not able to distinguish between a grain boundary and a scratch produced from mechanical polishing as well as the human eye can. Hence specimen preparation is more important for automatic image analysis than manual. However, polishing scratches tend to be straighter than grain boundaries and the Hough Transform is particularly sensitive to detecting straight lines. The Hough Transform could therefore be adapted to detect scratches and then remove them before reconstructing the grain boundaries. Twin boundaries could also be removed when they are not to be included within a grain size

measurement since they too tend to be straighter than boundaries. Specimen preparation would then not be so crucial.

- It was shown that not incorporating the grain boundary within the measurement using digital images could invoke a significant error, especially where there is low pixel resolution. Including the boundary could then reduce the error from a low pixel resolution image but an investigation would be required to ensure that the boundaries were included in a manner proportional to the size of the individual grains. Simply applying half of the grain boundary width to both grains on either side may not result in an accurate grain size distribution. Since the width of the grain boundary represented on a digital image is extremely exaggerated, applying half the boundary width to a small grain would increase the size of this grain disproportionately relative to a large grain.
- The resulting shape of a grain, after grain boundary reconstruction, as defined from the image process algorithms may not necessarily be representative of the actual grain shape, particularly if the pixel resolution is low. Effectively there can be insufficient pixels to follow a boundary accurately or the shape of the kernels are too limited to be representative of the actual grain shape. More work into developing more sophisticated image process algorithms to define the shape of a grain or ability to only use part of a pixel to follow a boundary could lead to a more accurate digital representation of the grain shapes.

### **7.3. Electron Back Scatter Diffraction**

This technique transcends the uncertainty found in determining the location of grain boundaries that is found from using conventional optical microscopy. However, more work is required to streamline this technique in order to make it more convenient to use for grain size measurements. This could be achieved by first detecting where a boundary is located through a change of orientation and to then develop a digital algorithm that will follow that boundary by analysing surrounding pixel locations. This could effectively reduce the amount of time required to map a specimen area since only the locations of boundaries are mapped instead of the entire area.

## **8. Posters, Publications and References**

### **8.1. Posters**

Part of the results of this thesis have been presented at the following conference:

Grain size measurements and missing boundaries, incorporating EBSD by John Muirhead, Dr Jess Cawley - Congress 2000, Cirencester, England, April (2000).

### **8.2. Publications**

The following paper has been accepted for publication:

Quantitative Aspects of Grain Size Measurement

John Muirhead, Dr Jess Cawley, A. Strang, Dr Colin English and Prof. John Titchmarsh

Materials Science and Technology, Oct, Vol16, No 10, (2000) pp1160 - 1166

### **8.3. References**

1. The Effect of Low-Angle and High-Angle Grain Boundaries on Elevated Temperature Strength, M.E. Kassner, Materials Research Society, Symposium Proceedings, (1994), Vol. 362, pp 157 - 162.
2. Materials for Engineering, John Martin, published by the Institute of Materials, (1996).
3. Hall-Petch Analysis of Yield, Flow and Fracturing, R.W. Armstrong, Materials Research Society, Symposium Proceedings, (1994), Vol. 362, pp 9 - 17.
4. Hall-Petch Basis for Assessing Alloy Strengthening, R.W. Armstrong; R.M. Douthwaite, Materials Research Society, Symposium Proceedings, (1994), Vol. 362, pp 41 - 47.
5. BS4490, Micrographic Determination of the Grain Size of Steel, (1989).
6. ISO643, Micrographic Determination of the Ferritic or Austenitic Grain Size, (1983).
7. E112 Standard Test Method for Determining Average Grain Size for Manual Measurements, (1995).
8. ASTM Standard for Quantitative Metallography, G.F. Vander Voort, Hungarian Mining and Metallurgical Society (OMBKE), (1994), pp 69 - 79.
9. ASTM E1382 Standard Test methods for Determining Average Grain Size Using Semi - Automatic and Automatic Image Analysis, (1991).
10. Basics of Quantitative Image Analysis, K.A. Leithner, Advanced Materials and Processes (USA), Vol. 144, No5, (1993), pp18 - 23.
11. Grain Size Determination by Using Image Processing Based on IBM PC, I Eordogh, G Nagy, Hungarian Mining and Metallurgical Society (OMBKE), pp536 – 544
12. The Practical Use of Quantitative Metallography, Willi Pohl; Alfred Fischer, Pract. Met. 27, (1990)

13. Automatic Grain Size Measurement in Low Carbon Steels by Image Analysis, F Le Pennec, D Malewicz, Microscopy Microanalysis Microstructures (France), Vol. 7, No 5-6, (1996), pp415 - 420.
14. Statistical Aspects of Microstructural Measurements, G.F. Vander Voort, Institute of Metals and Materials Australasia Ltd, (1993), pp 1 - 6.
15. Precision and Reproducibility of Quantitative Measurements, G.F. Vander Voort, ASM International (USA), (1994), pp21 - 34
16. Practical Evaluation of Automated Measuring System for Grain Size, Y Mishima, ISIJ International, Vol. 30, No 7, (1990), pp496 - 502
17. Experimental Aspects of the Electron Back-Scatter Diffraction Technique for Grain Boundary Characterisation, Randle, V, Mater. Sci. Forum, vol. 94-96, no. 1, (1992), pp. 233-243
18. Investigation of Deformation Mechanisms of Superplastic Ti-6Al-4V Using Back Scattered Kikuchi Diffraction Patterns, Garmestani, H; Sohi, GS; Mukherjee, S; Chandra, N, The Minerals, Metals & Materials Society (USA), (1993), pp. 109-119
19. The Characterization of Grain Boundaries, Brian Ralph, Scripta Metallurgica et Materialia, Vol. 27, (1992), pp. 1509 - 1514.
20. Quantitative metallography by electron backscattered diffraction, F.J. Humphreys, Journal of Microscopy, vol 195, part 3, sep (1999)
21. A comparison of grain imaging and measurement using horizontal orientation and colour orientation contrast imaging, electron backscatter pattern and optical methods, A.P. Day and T.E. Quested, Journal of Microscopy, vol 195, part 3, sep (1999)
22. Description of Orientation Coherence in Polycrystalline Materials, B.L. Adams, P.R. Morris, T.T. Wang, K.S. Willden and S.I. Wright, Acta Metallurgica, 35, (1987)
23. Application of Microtexture Measurements in the SEM to Grain Boundary Parameters, Valerie Randle, Texture and Microstructures, Vol. 20, (1993), pp. 231 - 242
24. Overview no.115: Grain Assemblage in Polycrystals, V Randle, Acta metall. Mater. Vol.42, no. 6, (1994) , pp1769-1784

25. Book: Microtexture Determination and its Applications, V Randle, (1992)
26. Microstructural characterisation by high resolution electron backscattered diffraction in the FEGSEM - competition for the TEM, FJ Humphreys, Inst. Phys. Conf. Ser. No 161: section 9; electron microscopy and analysis group conf. EMAG99, sheffield, (1999).
27. Practical considerations in the calculation of orientation distribution functions from electron back-scattered diffraction patterns, Bowen, AW, Mater. Sci. Forum, vol. 157-162, (1994) , pp. 315-322
28. Advances in Automatic Detection of Kikuchi Bands in Electron Backscattering Patterns, NC Krieger Lassen, CHANNEL Users Meeting, Hobro, Denmark, June 8 – 10, (1998)
29. Automatic localisation of EBSP bands from Hough Transform (Hough Transform for EBSP band localisation) Kreiger Lassen, Materials Science and Technology, Oct, vol. 12, pp839 – 843, (1996)
30. An EBSD Study of Nickel Aluminde, HS Ubi, CHANNEL Users Meeting, Hobro, Denmark, June 8 – 10, (1998)
31. Microtexture and Fatigue, W Tirschler and C Blochwitz, CHANNEL Users Meeting, Hobro, Denmark, June 8 – 10, (1998)
32. Problems in determining the misorientation axes, for small angular misorientation, using electron backscatter diffraction in the SEM, D.J. Prior, Journal of Microscopy, vol 195, part 3, sep (1999)
33. Measurement of small misorientations using eletron back scatter diffraction, Angus J Wilkinson, Inst. Phys. Conf. Ser. No 161: section 3; electron microscopy and analysis group conf. EMAG99, sheffield, (1999).
34. Electron backscatter diffraction of grain and subgrain structures, F.J. Humphreys, Y Huang, I Brough and C Harris, Journal of Microscopy, vol 195, part 3, sep (1999)
35. Identification of active slip systems using electron back scatter patterns, Angus J. Wilkinson, Ins. Phys. Conf., Ser. No . 119, Section 5, EMAG, Bristol, 10-13 sep, IOP publishing, (1991).

36. A simple procedure of the assessment of plastic strain in electron back-scatter diffraction patterns, P.J. Buchanan, V Randle, P.E.J. Flewitt, *Scripta Materialia*, Vol. 37, No 10, (1997) , pp 1511 – 1518
37. Measurement of elastic strains and small lattice rotations using electron back scatter diffraction, A.J. Wilkinson, *Ultramicroscopy* 62 (1996), pp237 - 247
38. Observations of Deformation and Fracture Heterogeneities in a Nickel-base Superalloy using Electron Back Scattering Patterns, P.N. Quested, P.J. Henderson and M. McLean, *Acta Metallurgica*, 36, (1988), p2743
39. Grain Boundary Plane Crystallography and Energy in Austenitic Steel, Mark Cauk, Jörn Fiedler, Valerie Randle, *Scripta Materials*, Vol. 35, No. 7, (1996), pp831-836
40. Electron backscatter diffraction: applications for nuclear materials, A. Medevielle, I hugon and O Dugne, *Journal of Microscopy*, vol 195, part 3, sep (1999)
41. Obtaining bonding information from EELS near-edge structures: grain-boundaries in NiAl, DA Pankhurst, GA Botton, CJ Humphreys, *Inst. Phys. Conf. Ser. No 161: section 2; electron microscopy and analysis group conf. EMAG99, sheffield*, (1999).
42. Study of dislocation structures near fatigue cracks using electron channelling contrast imaging technique (ECCI), J Ahmed, A.J. Wilkinson and S.G. Roberts, *Journal of Microscopy*, vol 195, part 3, sep (1999)
43. Measurement of Boundary Plane Inclination in a Scanning Electron Microscope, V Randle, D Dingley, *Scripta Metallurgic et Materialia*, Vol. 27, (1989), pp. 1565 – 1570
44. Alternative Length Scales for Polycrystalline Materials 1 – Microstructure Evolution, CS Nichols, RF Cook, DR Clarke and DA Smith, *Acta Mater.* Vol. 39, No. 7, (1991) , pp 1657 – 1665
45. Interface science - knowing more about less, M Rühle, T Gemming, O Kienzle, R Schweinfest, *Inst. Phys. Conf. Ser. No 161: section 1; electron microscopy and analysis group conf. EMAG99, sheffield*, (1999).

46. Atomic structure of grain boundaries, Merkle, Karl L., Journal of Physics and Chemistry of Solids, Volume 55, Issue 10, October (1994) , pp 991-1005
47. The Structure and Energy of Grain Boundaries, Brian Ralph, Scripta Metallurgic et Materialia, Vol. 27, (1992), pp. 1509 – 1514.
48. Grain Boundary Plane Crystallography and Energy in Austenitic Steel, Mark Cauk, Jörn Fiedler, Valerie Randle, Scripta Materials, Vol. 35, No. 7, (1996), pp831-836
49. The Importance of Grain Boundary Character Distribution (GBCD) to Recrystallisation, Grain Growth and Texture, Tadao Watanabe, Scripta Metallurgic et Materialia, Vol. 27, (1992) , pp. 1497 – 1502 .
50. Grain Structure and Microtexture after high temperature deformation of an Al-Li(8090) alloy, M. Eddahbi, C.B. Thomson, F. Carreño, O.A. Ruano, Materials Science and Engineering A284, (2000), pp292 – 300
51. Deformation Banding, Original Grain Size and Recrystallisation in FCC Intermediate-to-High SFE Metals, BJ Duggan, CS Lee, Scripta Metallurgic et Materialia, Vol. 27, (1992) , pp. 1503 – 1507
52. On the True Dependence of Grain Boundary Migration Rate on Driving Force, G Gottstein, LS Shvindlerman, Scripta Metallurgic et Materialia, Vol. 27, (1992) , pp. 1521 – 1526
53. Effect of Recrystallisation Temperature on Texture and Grain Size of Al-SiC Composite, D Juul Jensen, H Hansen and Y.L. Liu, Materials Science and Technology, 7, (1991), p369
54. Non-Equilibrium Segregation of Solute to Grain Boundary. II. Boron Segregation on Moving Grain Boundary During Recrystallization in Fe-3% Si Zhang, S; He, X; Ko, T, Journal of Materials Science (UK), vol. 29, no. 10, 15 May (1994) , pp. 2655-2662
55. HKL EBSD System Application in Understandign the Recrystallisation Mechanisms in Steels, H petitgand, A Miroux, L Lesne, H Regle and L Chapuis, CHANNEL Users Meeting, Hobro, Denmark, June 8 – 10, (1998)
56. Characterization of local texture in a moderately deformed polycrystalline AlSi-alloy, Skjervold, SR; Ryum, N, Acta Metallurgia et Materialia (UK), vol. 43, no. 8, Aug. (1995) , pp. 3159-3176

57. The role of grain boundary character distribution in secondary recrystallization of electrical steels, Y Hayakawa and J.A. Szpunar, *Acta mater.* Vol. 45, No. 3, (1997) , pp 1285 – 1295
58. Microtexture Investigation of the Relationship Between Strain and Anomalous Grain Growth, V Randle, *Philosophical Magazine A*, Vol. 67, No. 6, (1997), pp 1301 – 1313
59. An electron back-scattered diffraction study of the annealing behaviour of cold rolled titanium, Ubhi, HS; Bowen, AW, Institute of Materials (UK), (1996), pp. 2265-2272
60. High Angle Boundaries Formed by Grain Subdivision Mechanisms, D.A. Hughes, N. Hansen, *Acta mater.* Vol. 45, No. 9, (1997), pp 3871 – 3886
61. Composition of Grain Boundaries and Interfaces: a Comparison of Modern Analytical Techniques using a 300kV FEGTEM, VJ Keast, PA Midgley, SJ Lloyd, PJ Thomas, M Weyland, CB Boothroyd, CJ Humphreys, *Inst. Phys. Conf. Ser. No 161: section 2; electron microscopy and analysis group conf. EMAG99, sheffield*, (1999).
62. Non-Equilibrium Segregation of Solute to Grain Boundary. I. Boron Segregation in Fe-3% Si during cooling. Zhang, S; He, X; Ko, T, *Journal of Materials Science (UK)*, vol. 29, no. 10, 15 May (1994) , pp. 2633-2640
63. Overview No. 127: The Role of the Grain Boundary Plane in Cubic Polycrystals, V Randle, *Acta Mater.* Vol. 46, No. 5, (1997) , pp. 1459 – 1480
64. The orientation of grain boundaries in annealed copper. D.J. Dingley, T Boa & P.J. Phillips *Ins. Phys. Conf., Ser. No . 138, Section 7, EMAG 1991, Bristol, IOP publishing, 10-13 sep*, (1991)
65. EBSD studies of Microstructure Evolution in Hot Deformed Metals, J Driver, CHANNEL Users Meeting, Hobro, Denmark, June 8 – 10, (1998)
66. Electron backscattering diffraction study of acicular ferrite, bainite, and martensite steel microstructures. AF Gourgues, HM Flower, TC Lindley, *Materials science and technology*, vol 16, Jan (2000), pp26 - 40
67. Deposition of material at grain boundaries in tension interpreted in terms of diffusional creep, P.A. Thorsen, J.B. Bilde-Sørensen, *Material Science and Engineering A265*, (1999) , pp140 – 145

68. Electron back scattered diffraction (EBSD) analysis of quasi-cleavage and hydrogen induced fractures under cyclic and dwell loading in titanium alloys, Bache, MR; Evans, WJ; Davies, HM, Journal of Materials Science (UK), vol. 32, no. 13, 1 July (1997) , pp. 3435-3442
69. Microstructurally short fatigue crack initiation and growth in Ti-6.8Mo-4.5Fe-1.5Al, Y.M. Hu, W. Floer, U Krupp, H-J. Christ, Materials Science and Engineering A278, (2000) , pp 170 – 180
70. Application of electron back-scattered diffraction patterns to the study of diffusion-bonded interfaces, H S Ubhi, C J Gilmore & A W Bowen, Ins. Phys. Conf., Ser. No . 119, Section 6, Bristol, 10-13 sep, IOP publishing, EMAG (1991)
71. Grain-boundary structure effects on intergranular stress corrosion cracking of alloy x-750, Y. Pan, B.L. Adams, T. Olson, N. Panayotou, Acta mater. Vol. 44, no. 12, (1996) , pp4685 – 4695
72. Crystallographic analysis of facets using electron backscatter diffraction, V. Randle, Journal of Microscopy, vol 195, part 3, sep (1999)
73. EBSD study of the Recrystallisation Process in NiAl, Tamm and W Skrotski, CHANNEL Users Meeting, Hobro, Denmark, June 8 – 10, (1998)
74. Grain structure and macrotexture after high temperature deformation of an Al-Li (8090) alloy, M. Eddahbi, C.B. Thomson, F. Carreño, Materials Science and Engineering A284, (2000) , pp292 – 300
75. Grain Boundary Character Distribution in Ordered FeAl, L.C.R. Lopes, Scripta Materialia, Vol. 37, No. 12, (1997) , pp1863-1868
76. A Classification of Symmetrical Grain Boundaries, V Paidar, Acta Metall, Vol. 35, No 8, (1987) , pp 2035 – 2048
77. Grain Boundaries: Phase Transitions and Critical Phenomena, Rabkin, EI; Shvindlerman, LS; Straumal, BB; Gust, W, Mater. Sci. Forum, vol. 126-128, (1993) , pp. 305-313
78. On the Orientation Dependence of Grain Boundary Migration, G Gottstein, LS Shvindlerman, Scripta Metallurgic et Materialia, Vol. 27, (1992), pp. 1515 – 1520

79. Interface Control for Resistance to Intergranular cracking. K.T. Aust, U. Erb, G. Palumbo, Materials Science and Engineering A176, (1994) , pp329 – 334
80. Grain Size Measurement, G.F. Vander Voort, Practical Applications of Quantitative Metallography, ASTM STP 839, Philadelphia, (1984) , pp85 – 131
81. Committee E-4 & grain size measurements: 75 years of progress, G.F. Vander Voort, 3 ASTM Standardization News, Vol. 19, may (1991) , pp42 - 47
82. Grain Size Measurement by the Intercept Method, H Abrams, 3 Metallography Vol. 4, (1971) , pp 59 – 78
83. Microscopic Test of Steels for Grain Size by Comparison with Standard Charts, Prüfblatt Stahl-Eisen, no12452 British Industrial and Scientific International Translation Service (BISI), Verlag Stahleisen mbH, Desseldorf, G, pp1510 – 61
84. ASTM grain size model and related random tessellation models, V Horalek, Materials Characterization, Vol. 25, No3, (1990), pp263-284
85. The New ASTM Grain Size Methods, LL Wyman, ASTM Bulletin, July, (1956), pp59-61
86. Grain Size Estimation in Anisotropic Materials, B.R. Morris; A.M. Gokhale; G.F. Vander Voort, Metallurgical and Materials Transactions A (USA), Vol. 29A, No 1, (1988) , pp237 – 244
87. Ultrasonic Discrimination of Samples With Differently Distributed Grain Sizes and Equal Average Grain Size, D Nicoletti; A Anderson, Materials Research Society, Symposium Proceedings, Vol. 362, (1994), pp 123 - 128
88. ASTM 930 'Standard Test Method for Estimating the Largest Grain Observed in a Metallographic Section (ALA Grain Size), (1992).
89. Deformation Twinning and Grain Size Aspects of Numerical Simulations of Plastic Flow, F.J. Zerilli; R.W. Armstrong, Materials Research Society, Symposium Proceedings, Vol. 362, (1994), pp 149 - 154
90. Backscattering in the scanning electron microscope, D.J. Dingley, Bristol, 10-13 sep, IOP publishing, EMAG (1991).

91. Accurate characterisation of CCD cameras for electron detection, RR Meyer, Al Kirkland, WO Saxton, Inst. Phys. Conf. Ser. No 161: section 6; electron microscopy and analysis group conf. EMAG99, sheffield, (1999).
92. Book: Microtexture and its Application, V Randle, published by the Institute of Materials, p37, (1992).
93. WD Cao, MW Lee and L Kennedy, 'Effect on Grain Size on Strength and Ductility of a Ni-Cu Alloy', Scripta Metallurgica et Materialia (USA), 28 (8), (1993), pp 955 - 960
94. The influence of polycrystal grain size on several mechanical properties of materials, R.W. Armstrong, Metallurgical Transactions, Vol. 1, May (1970), pp. 1169 – 1176